STUDY AND CHARACTERIZATION OF FLEXIBLE SUPERCAPACITOR

Thesis

Submitted for the Award of the Degree of

Doctor of Philosophy

By

Ruby Garg

Registration No: 901706022

Under the supervision of

Dr. Alpana Agarwal
Professor, ECED

Dr. Mohit Agarwal
Assistant Professor, ECED

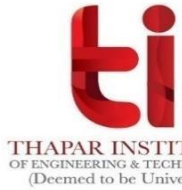

Department of Electronics & Communication Engineering

Thapar Institute of Engineering and Technology, Patial-147004

December, 2021

DECLARATION

I hereby declare that the work which is being presented in the thesis **"STUDY AND CHARACTERIZATION OF FLEXIBLE SUPERCAPACITOR"** submitted by me for the award of the degree of Doctor of Philosophy in the Department of Electronics and Communication Engineering, Thapar Institute of Engineering and Technology, Patiala, is a true and original record of my own independent and original research work carried out under the kind supervision of Dr. Alpana Agarwal, Head & Professor, Department of Electronics and Communication Engineering, Thapar Institute of Engineering and Technology (Deemed University), Patiala, India, and Dr. Mohit Agarwal, Assistant Professor, Department of Electronics and Communication Engineering. The matter embodied in this thesis has not been submitted in part or full to any other University or Institute for the award of any degree in India or abroad.

Date: 31st Dec., 2021

Ruby Garg

(Registration No. 901706022)

CERTIFICATE

It is hereby certified that the thesis "**STUDY AND CHARACTERIZATION OF FLEXIBLE SUPERCAPACITOR**" which is submitted by Ms. Ruby Garg (Regd. No. 901706022), in fulfilment of the requirement for the award of the degree of Doctor of Philosophy in theDepartment of Electronics and Communication Engineering, Thapar Institute of Engineering andTechnology (Deemed University), Patiala, Punjab, India, is a record of the candidate's own independent and original research work carried out by her under my supervision and guidance. The matter embodied in this thesis has not been submitted in part or full to any other University orInstitute for the award of any degree in India or abroad.

Supervisors

Dr. Alpana Agarwal
Professor, ECED

Dr. Mohit Agarwal
Assistant Professor, ECED

ACKNOWLEDGEMENT

I would like to express my gratitude towards my supervisors for their valuable guidance throughout the research work. The insight, observation, and quick guidance of my supervisors Dr. Alpana Agarwal and Dr. Mohit Agarwal helped me to establish the overall direction for the research and contribution immensely. Their broad knowledge, interest, enthusiasm, and constant encouragement have been essential in my development as a researcher. Foremost, I express my gratitude to my Ph.D. supervisor Dr. Mohit Agarwal. During this research, his continuous guidance nurtured me a lot. The valuable knowledge, which I gained from him, is valuable for me. I am thankful for his patient guidance and encouragement during this doctoral degree. I am grateful to the Thapar University, Patiala, Punjab, INDIA, especially to the Department of Electronics and Communication Engineering for providing me the opportunity to do this research work. I am very thankful to the Director, Thapar University for providing me university resources and facilities necessary to carry out this research work. I am also grateful to Dr. Alpana Agarwal for his continuous support, guidance, and providing me with the university resources and facilities necessary to carry out this research work. I express my gratitude to the Doctoral Committee comprising Dr. B.C. Mohanty, Associate Professor, Department of Physics, Dr. Sumit Vyas, Assistant Professor, Department of Engineering and Communication Engineering, Dr. Manu Bansal, Assistant Professor, Department of Engineering and Communication Engineering for monitoring the progress and providing valuable suggestions for the improvement of my research work. I am also thankful to the entire faculty and staff of the Department of Engineering and Communication Engineering for healthy discussions, suggestions, and necessary cooperation to complete this work. With deepest gratitude I dedicate my Ph.D. research work to my Brother Ankush Garg (IAS), my father Princepal, my mother Veena Rani, my sister Gulmehak Kaur, for the unconditional continuous support and guidance given. Without them, this would have been impossible to complete this work. I must give big thanks to my brothers Ankush Garg for their continuous motivation for completing this work. I only have come to Ph.D. because of his push. I also want to give thanks to my friends Himanshu, Ridhi Bhatla, Renu Thakur, Pragya Mishra for their understandability and motivation during the days I ignored them due to busy in this research work. Above all, I pay my reverence to the almighty God as only his blessings have made it possible who I am today.

Ruby Garg

ABSTRACT

In this era, the increase in the human population has led to an increase in energy demands. To copewith these rising energy requirements, energy storage is a major concern. The common examples of energy storage devices available are batteries and capacitors. However, the problem with batteries is that it delivers energy at a very slow rate and restrict their usage which requires fast delivery of energy such as flashlights, cameras, etc. On the other hand, the capacitor is a device that can provide fast energy delivery but its capacity to store energy is very limited. So, the motivation is to find an alternative that provides energy density greater than capacitors and power density greater than batteries. To have these benefits, the supercapacitor is a device having both qualities. The main component in the supercapacitor device is the electrode material that plays a vital role in the charge storage mechanism of supercapacitors. A large variety of electrode materials such as carbon derivatives, metal oxides, and conducting polymers are used in supercapacitors. However, in activated carbon, the uneven pore size distributions lead to low capacitance results. Moreover, studies are also carried out on carbon nanotubes and graphene. However, there is a serious limitation in graphene that its layers start getting agglomerated very easily. Further, the pseudocapacitive material such as ruthenium oxide (RuO_2) and manganese oxide (MnO_2) exhibit high cost and poor conductivity. Hence, it opens new avenues for other metal oxides to be used as electrode materials. While doing the investigations, a variety of new members of two-dimensional (2D) materials are discovered such as metal-organic frameworks (MoF), polyoxometalates (POM), MXene, and black phosphorus (BP). From all of these materials, it has been realized that MXene shows the potential application of using it as an electrode material with an excellent device performance as it is possible to systematically control the separation between their layers. Moreover, the synthesis of copper sulfide has also been carried out in this thesis as it is not widely explored in the literature for supercapacitor applications. Further, the study of doping in MXene has also been performed since doping is the best way to tune the surface activity of electrode material. It has already been studied that the method of nitrogen doping is complex which limits its application in free-standing flexible electrodes. From the available options of dopants, vanadium is considered to be the best choice for doping into the titanium carbide MXene because the atomic size of vanadium (205 pm) is similar to titanium (215 pm). Moreover, alkali metal ions have better interaction with the vanadium atom. As vanadium doping in titanium carbide is not explored much in the literature and thus is considered one of the electrode materials to be studied for this thesis. Further, the structural and electrical properties of electrode materials are highly dependent on the synthesis parameters thus, in this thesis the electrode materials are prepared and characterized by varying the process parameters.

The various process parameters during the synthesis of MXene are optimized to obtain its layered accordion-like structure since the spacing between different MXene layers plays an important role in enhancing the supercapacitor performance. The accordion-like structure in MXene is confirmed through the SEM and the presence of (110) peak in XRD at a 2-theta value of 60 degrees. It is also observed from the results that the interlayer spacing of MXene can be altered by varying the process parameters. This thesis thus represents that the process parameters play a crucial role if one has to obtain the best MXene layers structurally as well as electrically.

Moreover, the synthesis of copper sulfide as an electrode material has been carried at room temperature by reducing copper sulphate pentahydrate using ascorbic acid as a reducing agent in sodium thiosulphate with 2 hours (h) of total reaction time. The results of SEM and XRD have shown that varying the ratio of sodium thiosulphate and copper sulphate strongly affects the morphology of the copper sulfide formed. The hollow rod structure in copper sulfide helps the electrolyte ions to penetrate better into the electrode material. Thus, controlling of process parameters highly affects the electrochemical performance of the supercapacitor.

Further, to tune the properties of optimized MXene, vanadium doping has been introduced by varying the ratio of ammonium vanadate and MXene from 0.025:0.1 to 0.1:0.1 with a step size of 0.025 using a simple hydrothermal method. X-ray diffraction and scanning electron microscopy are conducted to observe the changes in structural properties of vanadium doped MXene. The doping has been incorporated into the electrode material as it will increase the conductivity as well as increase the spacing between the layers so that a greater number of electrolyte ions can interact with the electrode material.

Afterward, the electrochemical measurements of the supercapacitor device have been performed over the glass, PET, and PP substrate. The results have shown that the MXene and copper sulfide electrode materials deliver the maximum capacitance with the least arc radii on the glass substrate and as compared to PP and PET substrates because the film on the glass substrate can withstand high temperature. Whereas, the capacitive performance of vanadium doped MXene shown over the graphite substrate is greater than on the glass substrate as graphite is highly conducting in nature. Further, the energy-dispersive X-ray spectroscopy (EDS) shows that the uniform distribution of titanium, carbon, oxygen, and vanadium occurred over the entire nanosheet. The results have shown that the capacitance value of 0.025 V-MXene on the flexible conducting substrate is at par with that of the glass substrate. Further, the radius on the EIS plot of vanadium doped MXene is smaller than that of the undoped MXene which indicates that the vanadium doping made the charge transfer easier. Moreover, the

capacitance retention of 92.7% and 82.2% is obtained for 0.025 V-MXene on the graphite and glass substrate respectively after 3000 cycles.

TABLE OF CONTENTS

LIST OF FIGURES

LIST OF TABLES

LIST OF ABBREVIATIONS

XRD	X-Ray Diffractometer
SEM	Scanning Electron Microscopy
AlF_3	Aluminum Fluoride
HF	Hydrofluoric acid
PP	Polypropylene
PET	Polyethylene Terephthalate
Cu_2S	Copper sulfide
EDS	Energy Dispersive X-ray Spectroscopy
EIS	Electrochemical Impedance Spectroscopy
EDLC	Electric double-layer capacitors
IHP	Inner Helmholtz Plane
RuO_2	Ruthenium oxide
MnO_2	Manganese oxide
PANI	Polyaniline
PPy	Polypyrrole
VN	Vanadium Nitride
2D	Two dimensional
MoF	Metal-organic Frameworks
POM	Polyoxometalates
BP	Black Phosphorus
LiF	Lithium fluoride
HCl	Hydrochloric acid
NH_4HF_2	Ammonium Hydrazine
$M_{n+1}X_nT_X$	MXene
$TI_3C_2T_X$	Titanium Carbide
Ti_3AlC_2	Titanium Aluminum Carbide
DMSO	Dimethyl Sulfoxide
$CuSO_4 \cdot 5H_2O$	Copper Sulphate Pentahydrate
$Na_2S_2O_3 \cdot 5H_2O$	Sodium Thiosulphate
JCPDS	Joint Committee on Powder Diffraction Standards
TES	Thermal Energy Storage

HES	Hybrid Electrical Energy Storage
SOHIO	Standard Oil Company of Ohio
OHP	Outer Helmholtz Plane
O	Oxidised
R	Reduced
ESR	Equivalent Series Resistance
FESEM	Field Emission Scanning Electron Microscope
CV	Cyclic Voltammetry
GCD	Galvanostatic charge-discharge
OH	Hydroxyl
F	Fluorine
V	Vanadium
Ti	Titanium
C	Carbon
$S_2O_3^{2-}$	Thiosulfate Ion
Ti_2C	Titanium carbide
PVA	Polyvinyl Alcohol
PDDA	Poly-ethyl Dioxythiophene
NiO	Nickel Oxide
Ni-dMXNC	MXene/NiO nanocomposite
CNT	Carbon Nanotubes
Mn_2O_3	Manganese(III) Oxide
V_6O_{13-x}	Oxygen deficit Vanadium Oxide
N-$Ti_3C_2T_x$	Nitrogen-doped MXene
V-MXene	Vanadium doped MXene
NH_4VO_3	Ammonium Vanadate
H_2SO_4	Sulphuric acid
$MgSO_4$	Magnesium Sulphate
P-$Ti_3C_2T_x$	Phosphorus doped MXene
Ti^{+4}	Titanium Cation
Ce^{+}	Cerium cation
CuS	Covellite

$Cu_{1.75}S$	Anilite
$Cu_{1.8}S$	Digenite
$Cu_{1.95}S$	Durlite
$Cu(OH)_2$	Copper Hydroxide
RGO	Reduced Graphite Oxide
SILAR	Successive Ionic Layer Adsorption and Reaction
Na_2S	Sodium sulphate
R.T.	Room Temperature
PVDF	Polyvinylidene Fuoride
NMP	N-methyl-2-pyrrolidone
KOH	Potassium Hydroxide
Pt	Platinum
Ag/AgCl	Silver/Silver Chloride

GLOSSARY OF SYMBOLS

C_R	Rated Capacitance
F	Farads
Cs	Specific Capacitance
$\int Idv$	The area under the graph
A	Area of active material
V	Applied Voltage
v	Scan rate
$I_{discharge}$	Discharging Current
R_{ct}	Charge Transfer Resistance
R_s	Equivalent Series Resistance
I	Current
Δt	Discharging time
ΔV	Discharging Voltage
C_h	Compact layer
C_{diff}	Diffuse Layer
U_R	Rated Voltage
E	Energy density
P	Power density

CHAPTER 1

INTRODUCTION

In the past few decades, energy demands are increasing day by day because of the fast progress occurring in various fields such as industrial, domestic, strategic, and commercial fields [1]. Simultaneously, growth in the human population along with their dependence on electronic gadgets has led to extend the energy requirements. These increasing demands have blended to the locale burden on live power infrastructure and create serious indications for the future of mankind [2]. To meet these energy requirements, energy storage and energy delivery is major concern. Since the fast pace of human life has an urgent need to store energy so that it can be easily available when required. In recent years, a remarkable amount of attentiveness has been raised in developing new technologies for energy storage and delivery that will meet these energy challenges [1]. The conventional devices used were batteries, dry cells, and capacitors [3]. However, there are various challenges in their energy storage mechanisms as no device is complete in all the aspects because of one or more limitations like storage capacity, energy delivery, and operation time. Thus, it is very important to select the best energy storage device from the literature which contributes to support a particular technology [4].

1.1. ENERGY STORAGE DEVICES

Energy storage can be defined as storing energy to use in the future and thus the balance can be maintained between energy production and its demand [5]. It comes in various forms such as chemical, electrical potential, electricity, and heat. Common examples of energy storage include batteries and capacitors [6].

A battery is an active component that is a real source of energy because it continuously provides energy to the device while discharging. Battery stores the energy in the chemical form and later on converts it into an electrical form [7]. This process of storing and releasing energy is known as electrochemistry and the system which supports the battery is known as an electrochemical cell. During the chemical reactions in battery, the flow of electrons occurs from one electrode material to another electrode material via an external circuit as shown in figure 1.1. The flow of electrons produces the electric current which is used to do the work. It can be seen that for balancing the electrons flow, charged ions flow between the electrolyte solution in which the electrodes are

dipped as can be seen in figure 1.1. The process in the batteries is highly dependent on the electrode material and the electrolyte used. The number of chemical reactions

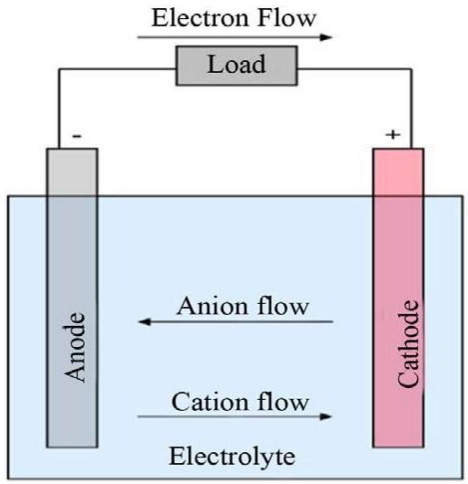

Figure 1.1: Charge storage mechanism of battery [7]

occurring in the battery decides the amount of energy a battery can store. Since the chemical reactions involved the participation of electrode material, it will affect its internal composition which in turn, reduces the life of the battery. Moreover, due to the involvement of chemical reactions the speed at which energy is delivered is very slow. However, the chemical reactions are occurring in the batteries volumetrically and thus it shows greater energy density. Thus, the batteries have poor power density with greater energy density [8].

However, on the other hand, a capacitor is a passive device because it does not produce energy. It stores energy in the form of an electric field and delivers it whenever required. In capacitor, there are two conducting plates separated by a non-conducting dielectric layer as illustrated in figure 1.2. The non-conductive layer is known as the dielectric and could be glass, air, paper, plastic, ceramics, *etc*. It can be seen that when an external supply is connected, the charge carriers on one conducting plate exerts a force on the charge carriers accumulated on another conducting plate and thus, attracting opposite polarity charges and repelling similar polarity charges [9]. This will induce opposite polarity charges on the surface of the other conducting plate. So, the two conducting plates hold equal and opposite polarity charges on their facing surfaces. This will lead to the building of an electric field in the dielectric region between the plates. The phenomena of storing charge in a capacitor is thus electrostatic unlike the batteries where storing charge is mainly because of chemical reactions. This electrostatic charge storage mechanism will thus provide fast charge delivery. The charge storing capacity in the capacitor is very less because the charge is

accumulated only at the surface of the conducting plates. Hence, the capacitors have greater power density with lower energy density [8].

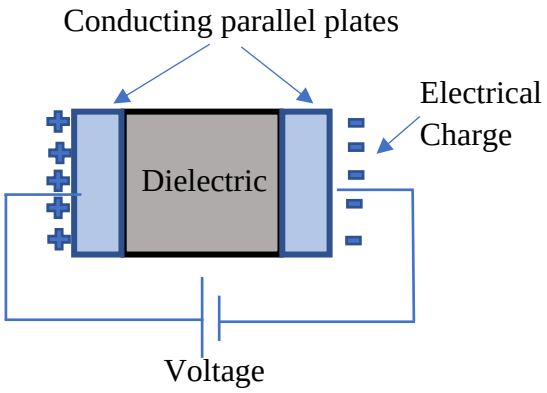

Figure 1.2: Charge storage mechanism of the capacitor

Thus, there is a need for a device that will overcome the drawbacks of both energy density and power density in capacitors and batteries. The device which overcomes these drawbacks is the supercapacitor. It is also termed electrochemical capacitors or ultracapacitors [10]. It is a passive component that comprises of two porous electrodes separated by a separator dipped in an electrolyte solution as shown in figure 1.3. These are very unique kinds of capacitors because the charge storage occurs only at the interface of electrode and electrolyte which helps in delivering the energy in a very short period. However, the layout of the supercapacitor includes porous electrodes having a greater effective surface area which will provide greater capacitance and energy as shown in figure 1.3. Moreover, the charges at electrode material and the electrolyte ions get separated by a very thin dielectric (Å) layer and thus further increase the capacitance of the device, the phenomenon called is “electric double layer”[11]. The value of capacitance and energy is increased

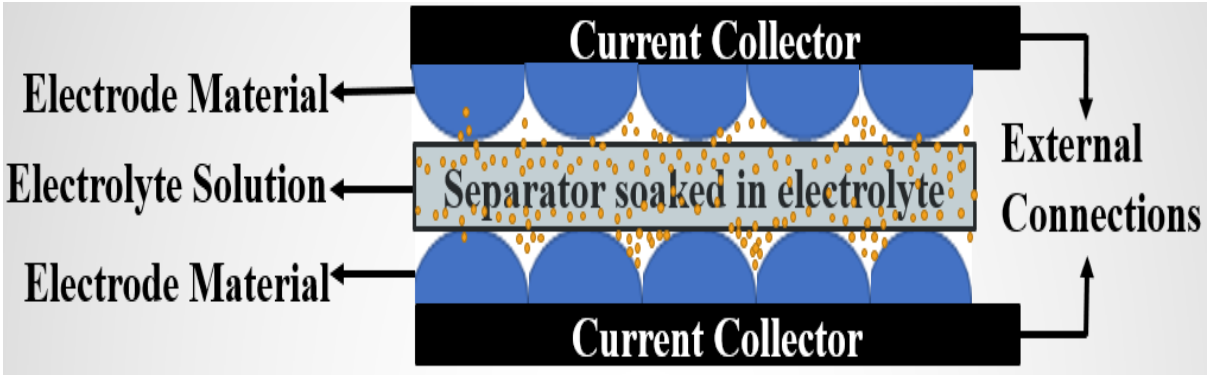

Figure 1.3: Schematic diagram of supercapacitor

by a factor of 10^3 than conventional capacitors. The values of the capacitance obtained by regular capacitors are rated in terms of Milli and Microfarads whereas the ultracapacitors provide capacitance in terms of tens, hundreds, or even thousands of farads. In the last few years, significant research and development have been carried forward in supercapacitor technology because of their outstanding potential to permit progress in energy storage. It has gained global attention because of its outstanding features of fast charging-discharging, high power density, long cycle life, a robust thermal operating range.

Further, the comparison of the batteries, capacitors, and supercapacitors in terms of energy density and power density [12] is shown in figure 1.4. The capacitor shows poor energy density because of the limited availability of surface area of the electrodes whereas, the battery shows poor power density because of the electrochemical charge storage mechanism. Whereas, the supercapacitor has greater energy density than capacitors because of the porous electrodes and very thin natural occurring layer at the interface between the electrode surface and the electrolyte solution. Moreover, the charge storage mechanism in supercapacitors occurs only at or near the surface of the electrode which thus provides greater power density than batteries.

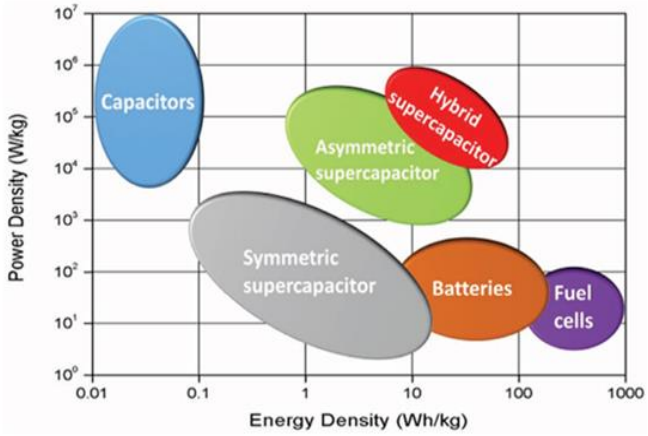

Figure 1.4: Classification based on energy density and power density [13]

1.2.TYPES OF SUPERCAPACITORS

The mechanism of supercapacitors is different from the conventional capacitors in the sense that they do not use the non-conducting dielectric to store charge but instead use an electrolyte which in turn gives either electrostatic double-layer capacitance mechanism [14] or electrochemical pseudocapacitance mechanism [15]. It can also be fabricated in a variety of arrangements based on its charge storage mechanism and can be termed symmetric, asymmetric, and battery type

supercapacitors [16]. The diagram illustrating these arrangements is shown in figure 1.5. The energy storage mechanism and the ion distribution from the electrolyte at the surface of electrode decides the principle of operation in supercapacitor. The taxonomy showing the division of supercapacitor is shown in figure 1.5.

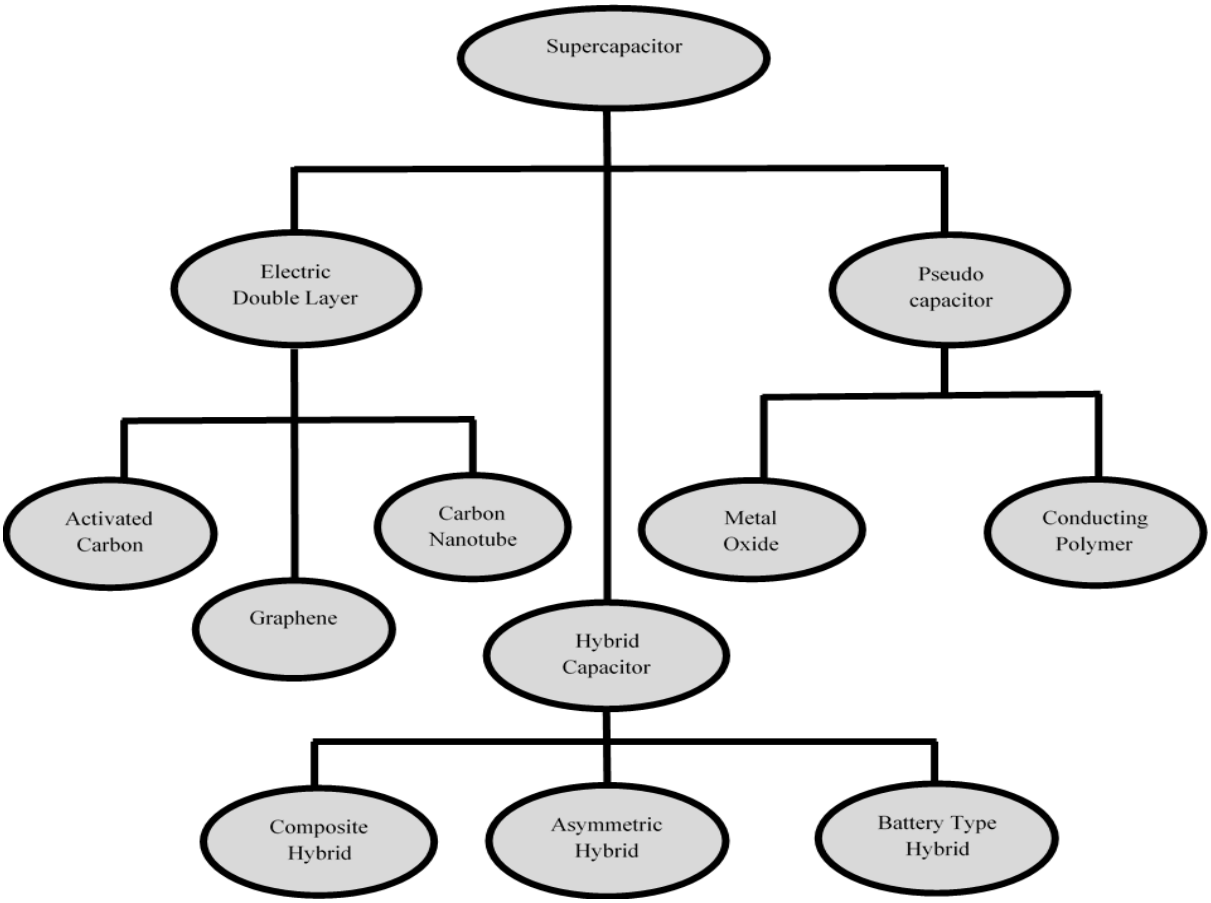

Figure 1.5: Taxonomy of supercapacitor

1.3. ENERGY STORAGE MECHANISM

Supercapacitors are divided into three different classes based on their charge storage mechanism as Electrochemical double-layer capacitors (EDLC), pseudocapacitors, and hybrid supercapacitors [16].

1.3.1. ELECTRIC DOUBLE-LAYER CAPACITORS (EDLCs)

Figure 1.6 shows the schematic illustrating the electric double layer behavior of the supercapacitor. It includes two electrodes that are separated with the help of separator mechanically but connected to each other ionically via an electrolyte. In an electrolyte solution, solvent such as water is present

which has both the positive and negative ions dissolved in it. At the surface of each electrode, there is an area where the electrolyte is in contact with the conducting surface of the electrode. This interface will lead to the formation of a double layer separation between the solid surface of the electrode and the liquid electrolyte.

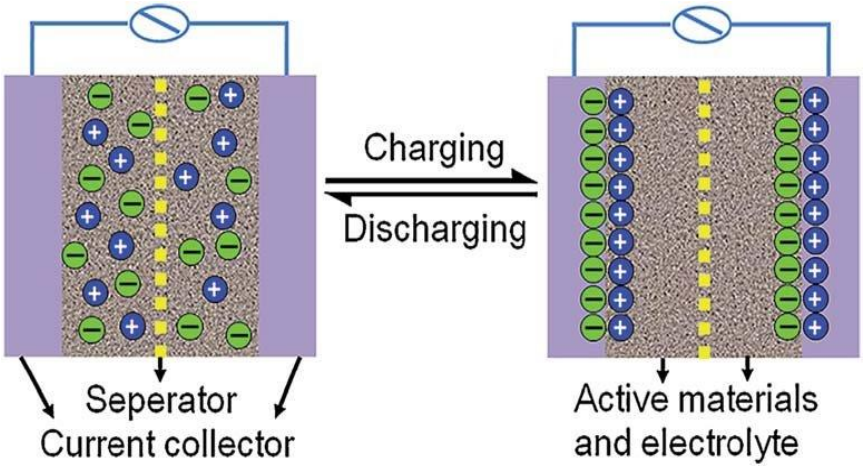

Figure 1.6: Charging and discharging mechanism in EDLC based supercapacitor [17]

This interface thus will lead to the formation of a special phenomenon which is known as a double layer effect. It can be seen that on applying an external voltage to the supercapacitor, both the electrodes generate an electric double layer. This double layer is made up of two layers of charges: one of them is an electronic layer that is present on the electrode surface while the other is the ionic layer off opposite polarity that emerges from the dissolved and solvated ions of the electrolyte [11]. The separation between these two layers is through a monolayer which is made of solvent molecules, *e.g.*, by the water molecules when water is considered as a solvent. This layer of solvent molecules is present in the inner Helmholtz plane (IHP) of the EDLC mechanism. The solvent molecules adhere to the electrode surface by the phenomena of physical adsorption to separate it from the counter polarised ions of the electrolyte ions. The solvent molecules can thus be seen as a molecular dielectric layer. During all this process, there is no transfer of charge or ions taking place between the electrode and electrolyte solution. So, the bond which helps in the adhesion is physical but not chemical. However, the molecules which are adsorbed on the electrode surface are polarized, but because of the no-charge transfer, no chemical reaction takes place. The static electric field due to the molecular layer in the IHP formed by the solvent molecules decided the strength of applied voltage. Moreover, it is seen from the conventional capacitors that the capacitance will be greatest if it shows high permittivity, large surface areas, and a smaller dielectric distance. So, it can be worth saying that double-layer capacitor shows a higher value of

capacitance than conventional capacitors because of the extremely large electrode surface area, extremely thin dielectric distance. In electrochemical capacitors, the electrode size governs the amount of charge to be stored per unit voltage. Also, the energy storage in double layers goes hand in hand with the charge stored which in turn shows its linear relationship with the number of adsorbed ions. As no chemical reaction takes place between electrode and electrolyte, the charging and discharging cycles in electric double-layer capacitors are unlimited. However, the commercial electric double layer supercapacitor lifetime is only limited by the evaporation effects of electrolyte solution. The behavior of electric double-layer capacitors is shown by the materials which have a large surface area such as carbon aerogels, graphene, carbon nanotubes, *etc*. [18], [19]

1.3.2. PSEUDOCAPACITOR

Despite EDLC, there is one more charge storage mechanism called pseudocapacitors. The mechanism of pseudocapacitance originates when the specifically adsorbed ions go out of the electrolyte and enter the double layer [20]. When an external voltage is applied to the pseudocapacitors, faradaic reactions that are fast and reversible (redox reactions) take place between the interface of electrode and electrolyte along with the electric double layer effect [21]. But pseudo-capacitor suffers from low power density and poor stability during various cycles because of chemical reactions occurring at the interface. The charge transfer between the electrode and electrolyte occurs because of the de-solvated and adsorbed ions with the participation of one electron per charge. No chemical reaction and no chemical bond is forming between the adsorbed ions and the atoms of electrode material as only charge transfer takes place as shown in figure 1.7 [22]. The materials showing pseudo capacitance are various metal

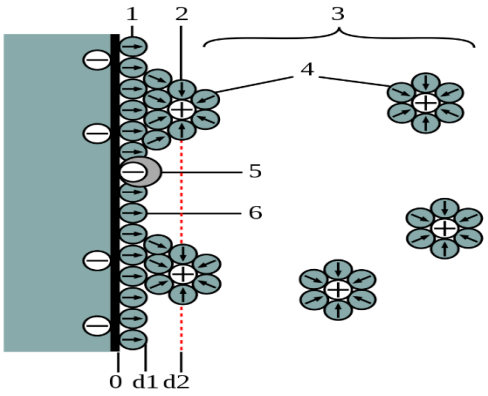

Figure 1.7: Pseudocapacitors-based supercapacitor

oxides and electrically conducting polymers such as ruthenium oxide (RuO_2) [23], manganese oxide (MnO_2) [24], polyaniline (PANI) [25], polypyrrole (PPy) [26] and vanadium nitride (VN) [27]. The process of faradaic pseudocapacitance occurs together with double-layer capacitance. However, the pseudocapacitance shows greater capacitance than electric double-layer capacitors even for the same surface area depending on the nature and structure of the electrode as the reactions in pseudocapacitors take place with de-solvated ions which are much smaller in radii than the solvated ions. The capacitance value shown by pseudo-capacitors is 10-10^3 times more than the electric double-layer capacitance [28]. The ability of electrode material to show pseudocapacitance either by redox reactions, electrosorption, or intercalation strongly depends on the chemical affinity of the electrode material to the adsorbed ions as well as on the structure and dimensions of pores of the electrode material. The mechanism of pseudocapacitance involves a redox pair where O and R signify the oxidized and reduced states of the redox species in the electrolyte solution.

1.3.3. HYBRID SUPERCAPACITOR

Hybrid supercapacitors consist of two electrodes that show different characteristics. The detailed discussion is given in the following subsection. It can be operated at a high operating voltage and delivers greater capacitance and energy density than a symmetric supercapacitor.

1.3.3.1. COMPOSITE

The composite hybrid supercapacitor comprises two electrodes. The material of one electrode has the properties of both EDLC and pseudocapacitive. It combines carbon-based materials with either metal oxides or conducting polymer in a single electrode which means a single electrode stores charge electrostatically and electrochemically.

1.3.3.2. SYMMETRIC

The symmetric hybrid supercapacitor device comprises two electrodes both of which are made with the same materials. Both the electrodes either show the EDLC behavior or the pseudocapacitive behavior.

1.3.3.3. ASYMMETRIC

The asymmetric hybrid supercapacitor comprises two electrodes both of which are of different

materials. One electrode is of EDLC type and the other electrode is of pseudocapacitive type. Since the pseudocapacitors operate at a greater voltage than EDLC, so the energy density of the whole device will increase. This is because the energy density is directly proportional to the applied voltage.

1.3.3.4. BATTERY TYPE

A battery-type supercapacitor combines two electrodes. One of the electrodes shows either EDLC or pseudocapacitive behavior whereas the other electrode will be of battery type. As the battery has the advantage of greater energy density and the supercapacitor has the benefit of greater power density. So, both the advantages of high-power density and high-energy density are combined in a single device.

1.4. ELECTRICAL PARAMETERS FOR SUPERCAPACITOR

1.4.1. CAPACITANCE

In commercial capacitors, rated capacitance C_R is the measurement of their capacitance value. It is the value for which that capacitor is designed. Thus, the measured value of capacitor has to lie within the limits provided. Typically, the capacitance values lie in the range of farads (F) which is larger than the value of electrolytic capacitors by the order of three. The value of capacitance can be calculated using equation 1.1.

$$C_s = \int_{v_1}^{v_2} Idv / Av\Delta V \quad \text{.....(1.1)}$$

where $\int Idv$ is the area under the curve, ΔV is the potential window, A is the area of the working electrode, *v* is the scan rate.

Moreover, the charge discharge curves in capacitor can also help in calculting the capacitance value. The voltage is applied in the forward as well as reverse direction for charging and discharging the capacitor at a constant value of discharge current $I_{discharge}$ value. Afterward, the time t_1 and t_2, corresponding to the values of voltage drop is measured. The formula for calculating the capacitance value from the charge-discharge curve is given in equation 1.2.

$$C_s = I_{discharge} * (t_2 - t_1) / (V_2 - V_1) \quad \text{.....(1.2)}$$

1.4.2. OPERATING VOLTAGE

Supercapacitors are low voltage devices. For operating the device safely, it is required that voltage

must remain within specified limits. The maximum DC voltage that runs the supercapacitor device safely is termed as the rated voltage U_R. The rated voltage also includes a safety margin value along with the voltage at which electrolyte decomposes. If the applied voltage exceeds the rated voltage, the solvent molecules are not be able to maintain the separation between the electrical charges and decompose into hydrogen gas or cause a short circuit. The electrolyte used, also plays an important role in deciding the operating voltage. While using aqueous electrolytes, the rated voltage has to be applied in the range of 2.1 to 2.3 V whereas when the organic solvents are used, the voltage range to be applied has to be between 2.5 to 2.7 V. However, if ionic electrolytes are used the operating voltage can exceed up to 3.5 V. If the supercapacitor operated voltage is kept less than the rated voltage, the charging-discharging cycles may get extended. However, in the applications where high voltages are required, the electrochemical cells have to be connected in series.

1.4.3. SPECIFIC ENERGY AND SPECIFIC POWER

In capacitors, the specific energy is defined as the amount of energy that can be stored per unit mass. It is measured gravimetrically in watt-hours per kilogram. Although the specific energy density in supercapacitors is less than batteries but their specific power density is greater as compared to batteries. The specific power can be defined as the ability of a device to deliver the stored energy quickly to the load. The formula for calculating energy and power density is provided in Equations 1.3 and 1.4.

$$E = \frac{C_s * \Delta V * \Delta V}{2} \quad \text{.....(1.3)}$$

$$P = \frac{E}{\Delta t} \quad \text{.....(1.4)}$$

Where E is energy density, C_s is specific capacitance, ΔV is discharging voltage, P is power density, Δt is the discharging time.

1.5. APPLICATIONS

The supercapacitors are used in those applications where rapid charge/discharge cycles, longer lifetime is required rather than in those applications which requires energy storage for long-term. The applications where the supercapacitors are used includes automobiles, trains, buses, elevators, flash lights, cameras etc. Its general applications range from milli amperes of currents or milli

watts of power for up to a few minutes to several amperes of current or several hundred of kilowatts power for much shorter period.

Energy Harvesting: In energy harvesting systems, supercapacitors act as a temporary energy storage device. While energy harvesting, the renewable sources are used to collect the energy from mechanical movements, light or electromagnetic fields which is then converted and stored in an energy storage device [29]. For example, the energy is collected from the radio frequency fields which can be stored in printed supercapacitor. The energy harvested thus, drives the integrated circuit for over 10 hours.

Smart cities: In previous times, usually batteries are used for energy storage because of their high energy density. However, they can harm the environment because of their disposal problem as they are made up of lithium ions. Thus, clean energy storage technologies overpower the batteries. Though supercapacitors have less energy density as compared to batteries, but a bank of supercapacitors can be used where low consumption is required. For e.g., the devices used in urban or rural area which are mainly concentrated for energy sector collect data and then correct it according to the changes in the particular area require fast supply of energy. In that case, supercapacitors are used. Moreover, in smart cities the smart transportation vehicles are used [30]. *e.g.,* in buses, supercapacitors store the braking energy and delivers it to start the vehicle [31]. The supercapacitor usage in buses provides other benefits as well such as the consumption of fuel has also been reduced to 10 or 15% as compared to conventional diesel vehicles. Moreover, the application of supercapacitor in buses was tested in 2002 in Luzen Switzerland on electric bus fleet known as TOHYCO-Rider. In that vehicle, after every transportation cycle, the recharging of supercapacitors is carried with a high-speed contactless power charger within 3 to 4 minutes. Afterward, in 2005 a new type of electric bus known as capabus has been tested in Shangai where the recharging is done partially using large onboard supercapacitors when an electric umbrella is above the bus at a bus stop whereas it gets fully charged when it reached the terminal. It has also been estimated that supercapacitor buses are cheaper as compared to the lithium-ion battery buses and the fuel saving in supercapacitor bus is also around $200,000.

Grid power buffers: There are a variety of non-linear loads such as electric vehicles, hybrid electric vehicles, air conditioners which produce harmonics and fluctuations in the current [32]. These current variations may cause unwanted voltage power fluctuations on the grid which not only degrades the grid efficiency but also produces voltage drop and frequency variations in

the entire system. Thus, to tackle this issue, supercapacitors as a buffer can be installed at the interface between grid and load [32].

Railways: The supercapacitors can be used in railways by capturing the braking energy during a full stop and later on delivers the peak current to start the diesel engine for accelerating the train.

Cranes: It can also be used in cranes while moving and stacking the containers because a large amount of energy is required in lifting the boxes. Using the supercapacitors, it can be possible to recapture some of the energy while unloading the boxes which results in improved efficiency.

Gondolas: The supercapacitor application can also be explored in aerial lifts where gondolas connect the city with the mountains. In gondolas, sometimes the operating time is 24 hours a day because of the requirement of electricity for door opening, lights. However, the time available to recharge batteries. In gondolas is only at the stations while the loading and unloading of guests which is very short span of time to recharge the batteries. So, supercapacitors can be used there as they offer fast charging, higher number of charging-discharging cycles and longer life time than batteries.

Screwdriver: The supercapacitor can also be used to operate a cordless electric screwdriver by getting fully charged in 90 seconds. Also, it retains 85% of its charge even it is left idle for three months.

Integrated solar: In parks, gardens, streets or public places the function of charging stations can be performed by supercapacitor systems. These are used for quickly charging the portable electronic devices [33]. Solar supercapacitors can also be installed at the roof of cars for charging various electronic such as indicators, sensors or multimedia devices, etc [34].

1.6. MOTIVATION OF THE WORK

Nowadays, energy storage is really important as life has taken a very fast pace. Energy storage is required in mobiles, laptops, computers, watches. Energy storage is defined as storing the energy at present which helps in meeting future needs. Since, the energy is available in various forms which cannot be easily used by an individual, so different energy storing devices are available that convert the energy from difficult form to more conveniently usable forms. The common examples of energy storage devices available are batteries and capacitors. The batteries have the limitation that it delivers energy at a very slow rate which restrict their use in those applications where fast delivery of energy is required. Whereas, in capacitor power delivery is quick but its capacity to store energy is very limited. The supercapacitor is the device having both qualities.

In a supercapacitor device, the component which plays an important role in the charge storage mechanism is the electrode material. In literature, a variety of electrode materials are available such as carbon derivatives, metal oxides, and conducting polymers. However, the issue in activated carbon is that its pore size distributions is uneven which leads to poor capacitance results. Moreover, studies on graphene have shown that its layers start getting agglomerated very easily. Further, the pseudocapacitive material such as ruthenium oxide (RuO_2) and manganese oxide (MnO_2) exhibit high cost and poor conductivity. Hence, it opens new avenues for other metal oxides to be used as electrode materials. While doing the investigations, a variety of new members of two-dimensional (2D) materials are discovered such as metal-organic frameworks (MoF), polyoxometalates (POM), MXene, and black phosphorus (BP). From all of these materials, it has been realized that MXene shows the potential application of using it as an electrode material with an excellent device performance as it is possible to systematically control the separation between their layers. This aspect of MXene is highly under investigation and requires detailed research to be carried out in this area. The MXene can be prepared using several etchants such as hydrofluoric acid (HF), lithium fluoride + hydrochloric acid (LiF+HCl), ammonium hydrazine (NH_4HF_2). However, the preparation of MXene is very confusing in the literature that how much time will be needed for the successful preparation of MXene as some papers have shown the preparation time of 3 days and some have successfully achieved it in 3 hrs only. Thus, there is a major gap in the study of optimization of the process parameters to obtain the MXene with the best properties. As MXene is a negatively charged compound so, its interaction with neutral electrolyte cations is enhanced by improving the binding strength between adsorbates and various functional groups of MXene. The best way to tune the surface activity is by doping the heteroatom into the electrode material. However, the dopants that have been tried are very few and thus, new dopants can show their potential applications in supercapacitors. Moreover, in the literature people are trying to synthesize vanadium carbide MXene as it is one of the lightest materials as well as its behavior, is highly pseudocapacitive in nature. There is vast literature available for vanadium carbides or vanadium nitrides however, vanadium doping in titanium carbide is not explored much.

Recently, due to high conductivity and redox activities showed by metal sulfides, they are gaining considerable attention and emerged as a new member in the family of electrode materials due to their high electronic conductivity, low cost, and easier availability. However, it has been shown that the growth of copper sulfides is carried on copper foam, nickel foam, and stainless steel as

the metal substrates provide better conductivity. However, metals are opaque which restricts their usage in the devices where transparency is required. Moreover, most of the research shows only the synthesis of copper sulfide with different morphologies without showing their application in the supercapacitor field. Afterward, the synthesis processes that have been used took either high temperature or longer time. Therefore, to reduce these drawbacks, the easier synthesis route of Cu_2S has to be the hot research topic that can be researched or worked on. However, none of the studies has been carried out using copper sulfide as electrode material in a transparent flexible supercapacitor.

1.7. ORGANISATION OF THESIS

The thesis deals with the synthesis of different electrode materials by varying various process parameters. The characterizations of the prepared samples such as scanning electron microscopy and X-ray diffractometer are performed to understand their structural properties. Then the fabrication of the electrode materials over rigid as well as flexible substrates are carried out followed by their electrochemical measurements to evaluate the kinetics behind their charge storage mechanism. Further, to enhance the performance of the electrode material, doping has been incorporated by varying the doping ratios. At last, the structural, as well as electrochemical measurements, are performed to understand the effect of doping on the performance of supercapacitors. The energy and power densities of all the samples are then calculated to get the information about stored and delivered energy.

Chapter 1 deals with the introduction of various energy storage devices such as batteries, a capacitor with the evolution of supercapacitor devices. The working and types of supercapacitor devices have also been discussed. Afterward, the problems associated with the previous literature, the motivation of doing the present research work, and the contribution of the work done are also presented.

Chapter 2 includes the literature survey of different energy storage devices. Afterwards, a detailed discussion on the different electrode materials, electrolyte, substrates that were used in the field of supercapacitor is presented. Moreover, the methods that were used in the synthesis of electrode materials are also discussed along the problems associated with the previously used materials are also mentioned. This chapter also includes the research gaps for doing present research work and objectives. Later on, the contribution of the present work is also summarized in this chapter.

Chapter 3 includes the synthesis mechanism of different electrode materials such as MXene, copper sulfide by varying various process parameters that can affect the electrode properties. Afterward, the characterizations such as XRD, SEM of the prepared material, and resistance of the film are carried out to observe the effect of varying process parameters on structural properties. Later on, the fabrication of the electrode material on the glass substrate is carried to observe the effect on electrical properties by varying the process parameters.

Chapter 4 deals with the fabrication of symmetric supercapacitor device using MXene and copper sulfide as an electrode material on rigid as well as flexible substrates. The rigid substrate is taken as glass and flexible substrates are taken as polyethylene terephthalate and polypropylene. Later on, the electrochemical investigation such as cyclic voltammetry (CV), galvanostatic charge-discharge (GCD), electrochemical impedance spectroscopy (EIS), and capacitance retention are performed using three-electrode cell configurations to understand the kinetics behind the electrode materials on the electrochemical performance of the working electrode.

Chapter 5 deals with the vanadium doping in the prepared titanium carbide MXene to further enhance the device performance. Initially, the synthesis of the vanadium doped MXene is carried by varying different amounts of the vanadium precursor to see the effect of doping concentration on the structural and electrochemical performance. The effect of doping on the structural characteristics of the electrode material has been evaluated using SEM, XRD. To further confirm the successful incorporation of the doping into the electrode material, SEM-EDS has been performed. Later on, the fabrication of symmetrical supercapacitor device using different ratios of doping has been carried on the glass substrate and graphite sheet to observe the kinetics behind the doping on the electrochemical performance of the electrode material.

Chapter 6: Finally, this chapter outlines the main conclusions drawn from this thesis and recommendations for future work that could be taken up to further extend the results of this work.

CHAPTER 2

LITERATURE SURVEY

This chapter deals with the work done so far in the various devices which are used to store energy. The energy is provided by various natural resources such as the sun, wind, water, *etc*. All these resources are highly abundant in nature. However, the energy provided by these resources is very difficult to use directly. Thus, it has to be stored somewhere so that it can be used whenever required *e.g.* if the sun is producing energy for the operation of household appliances which are operated at night, then the energy provided by the sun has to be stored in some energy storage devices so that it could be easily accessible. Moreover, the current consumption of available fuels for producing the energy affects the energy availability to the new generation [35]. Currently, various energy storage devices are available such as batteries [36], capacitors [37], and supercapacitors [38] to overcome the above problems. In the case of batteries, power density is a major issue as the storage mechanism occurs in the bulk of electrode materials. However, the capacitors have the limitation of limited surface area and thus restrict the energy density to a few KWh/Kg. To overcome these problems, researchers mainly focus on increasing the surface area without increasing the net area of the device. In this context, the supercapacitor devices have literature high prospect in future. It is found that the supercapacitor performance is mainly affected by electrode materials, substrates, and electrode fabrication method. This chapter starts with the extensive and detailed review on different energy storage devices which is given in section 2.1. Later, the literature review has been extended for supercapacitor devices which include the different electrode materials, various electrode fabrication methods, electrolyte solutions and different substrate materials, *etc*.

2.1. DIFFERENT ENERGY STORAGE DEVICES

The invention of electricity has led to the discovery of various energy storage devices for meeting energy needs. In the past few years, the energy storage industry has come up to innovate various energy storage devices that deal with the changing energy requirements. The commonly evolved different energy storage devices include batteries, capacitors, and supercapacitors.

The battery is the energy storage device that store energy chemically and later on, convert it into electricity. It consists of various individual cells operated on small power and voltage that aggregated to operate large power loads. The most common examples are lithium-ion cells and

lead-acid cells for electric grid applications. **Manwell et al.** [39] reported the use of lead-acid batteries in energy storage systems because they are cheap and easy to use. However, it delivers limited specific energy (35 Wh/kg) and thus, can not be used for electric vehicles. Moreover, due to its poor cycle life, it is required to be replaced very frequently. Also, these batteries require high currents to charge which affects their cycle life. Thus, all these drawbacks decline the use of lead-acid batteries in the future systems. Though, the lithium-ion cells [40] offer greater energy density and a large number of charging-discharging cycles but, it has a high cost, several safety issues, and delivers energy for only a few hours. Thus, extensive research has to be carried in these energy storage technologies to reduce cost, improve the safety of the system, better performance, and increased cycle efficiency. Currently, there are different types of lithium-ion cells such as lithium iron phosphate/graphite ($LiFePO_4$/C) [41], lithium manganese oxide/ graphite (LMO/C) [42], nickel manganese cobalt oxide/graphite (NCM/C) [42], *etc*. However, **X. Han** [43] in their study reported that the problem with $LiFePO_4$/C based battery is that it offers low energy density and low power density whereas LMO/C shows higher power density and higher energy density but poor cyclic stability. Further, NCM/C has serious safety issues towards health. Later on, **A. Kobayashi** [44] showed the development of nickel-metal hydride (Ni-MH) batteries for energy storage application because they are non-toxic, maintenance-free, environment-friendly, deliver a cycle life of 1500, and energy density of 70Wh/Kg. However, the cost to design these batteries is very high. Thereafter, **Xiaohui Shen *et al*.** [45] developed silicon-based anode in lithium-ion batteries which enhances the specific capacity to 4200mAh/g, and has low cost. However, as its operating voltage is lying outside the stabilized potential window of the electrolyte solution, it provides low coulombic efficiency during the first cycle because of the formation of a solid electrolyte interface (SEI) layer. Furthermore, while the lithiation process, there was an expansion of 300%-400% of silicon which results in contact loss with the current collector. Thus, lithium-ion batteries are very complicated with various degradations such as cycle life and power delivery because of multiple and complex redox reactions. All these redox reactions are highly influenced by various factors such as the design of the battery, material, and mechanism of charge storage.

Thereafter, the other commonly used device is a capacitor which stores the energy in the order of microfarads (µF). The structural layout of capacitors is similar to that of batteries, however, in capacitors both the electrodes are of the same material such as aluminum, tantalum, *etc*. The invention of the capacitor technology started in 1745 with the discovery of the Leiden jar [46]. In the early days, capacitors are mainly used in either electronic or electrical products however,

nowadays its applications are ranging from industrial to automobiles to aircraft, space, medicine, and much more. **M. Jayalakshmi et al.** [47] have shown that the output of the silicon-based capacitor is limited because of their low surface-to-volume ratio. However, **V. Lehmann et al.** [48] have presented that if silicon is used as a substrate material, the surface area has been enhanced by using the electrochemical etching method. Further, other classes of capacitors are invented such as tantalum (Ta), aluminum (Al), and ceramic electrolytic capacitors. **A. Nishino et al.** [49] in their study uses tantalum capacitors which are also known as solid electrolytic capacitors with MnO_2 as a solid electrolyte. However, these capacitors provide very low capacitance in the range of 0.1 to 10 μF at such a high voltage window of 25 to 50 V. Afterwards **S. Niwa and Y. Taketani** [50] showed the improvement in the performance of electrolytic capacitors by modifying the electrode or electrolyte using electrolytic etching of aluminum substrate before anodization. Further, **Meiqi Liu et al.** [51] discovered potassium-ion hybrid capacitors. They are considered to be the potential candidate for replacing lithium or sodium ion capacitors because potassium is abundant in nature and cost-effective as well. However, potassium-ion hybrid capacitors still show various drawbacks such as low energy density, poor cycle stability because of their larger ionic radii.

Thereafter, the discovery of supercapacitor has been started in the 1970s and 1980s for energy storage using the principle of the polarization of electrolytes. The performance of supercapacitors lies between batteries and traditional capacitors [52]. These devices are considered as one of the most efficient device for energy storage because of various advantages such as high-power density, cycle stability, rapid charge-discharge cycles, cost-effective, no wear and tear, and environment friendly. These devices provide fast energy delivery than batteries. In literature, the energy storage in supercapacitor occurs either by electric double layer mechanism [19] or pseudo mechanism [20]. The description of the double layer has been provided by the researchers in the nineteenth century when it has been first designed and used in the projects of von Helmholtz on colloidal suspensions [55], [56]. However, **H.I. Becker** [57] of General Electric first showed the practical application of charge storage by double layer in 1957. In their patent, they have utilized porous carbon electrodes with greater surface area in an electrolyte solution [58]. However, after 1966, **R.A. Rightmire of the Standard Oil Company of Ohio (SOHIO) and SOHIO co-worker D.L. Boos** [59] confessed that no redox reactions had occurred and the charge storage mechanism occurs in the electrical double layer which is formed at the interface between electrode and electrolyte. Then, the first commercially available double layer supercapacitor with two porous carbon

electrodes separated by a separator soaked in an electrolyte solution was originated by **SOHIO** [59]. Moreover, SOHIO had also used the non-aqueous electrolyte solution to prepare the supercapacitor device. After that the different types of supercapacitors are invented and used by the industries on large scale. Later on in 1980 and 1987, NEC/Tokin, Panasonic and Mitsubishi Products had started to industrialize supercapacitor [60]. Afterward, Econd and ELIT launched electrochemical capacitors for high power start-up in 1990. These remarkable progresses encourage the companies such as NEC, Panasonic, Maxwell and EPCOS in the discovery of supercapacitors. The supercapacitor technology has gained huge attention from the world since the day they have been introduced in the market. Thus, the supercapacitors are found to be used in consumer electronics products, industry, medical fields, defence, transportation *etc* [18].

The next section surveys the detailed literature on supercapacitors as the main work of this thesis is on supercapacitor devices.

2.2. LITERATURE REVIEW ON SUPERCAPACITOR

It is found from the literature that the performance of supercapacitor devices is affected by mainly electrode materials, the synthesis process of electrode materials, various electrolytes, and different substrates used. The electrode materials used mainly in literature are carbonaceous, metal oxides or conducting polymers, metal sulfides, and two-dimensional (2-D) materials. Thus, the detailed literature survey on different electrode materials that were used for the study of supercapacitors is reviewed in section 2.2.1. Further, the thorough discussion on various methods for the fabrication of electrode material with different process parameters is elaborated in section 2.2.2. Moreover, section 2.2.3. includes the study of different substrate materials used for the deposition of different electrode materials.

2.2.1. ELECTRODE MATERIALS FOR SUPERCAPACITOR APPLICATIONS

The charge storage mechanism in a supercapacitor depends on the type of electrode material used. In literature, different family of electrode materials are used such as activated carbon [61], carbon nanotubes [62], carbon aerogels [63], graphene [64][65], ruthenium dioxide [66], magnesium oxide [67], polypropylene (PPy), polyaniline (PANI) and poly-ethyl dioxythiophene [68] copper hydroxides, nickel-cobalt oxides, nickel oxide, copper hydroxide, lead sulfides [69], zinc sulfides [70], cadmium sulfides [71], copper sulfides [72], bismuth sulfides [73], and nickel sulfides [74]

etc. Thus, a detailed review of the performance of supercapacitors in terms of capacitance, energy density, power density, cycle retention using various electrode materials is illustrated below:

2.2.1.1. CARBON-RELATED MATERIALS.

The most widely used material for supercapacitor electrodes is carbon and its derivatives. They are found to be the sixth most abundant material in the earth's crust which makes them highly cost-effective. Also, these materials offer other advantages such as high conductance, low corrosion resistance, and cost-effectiveness, *etc*. [75][76]. Thus, all these benefits make carbon materials to be the topmost material as supercapacitor electrodes. These can be formed in a large variety of structures, such as onions, composites, nanotubes, thin films, and powders, *etc* [77]. Moreover, carbon materials such as graphene, carbon nanotubes, amorphous carbon remain stable under a wide potential window in different electrolytes which suggests their use in different electrochemical devices [78][79].

Toshiro Otowa et al. [80] had successfully used activated carbon as an electrode material due to its various advantages such as greater specific surface area of up to 3000m^2/g, availability, simple method of production. The natural precursors such as (wood, coal and coconut shell) as well as chemical precursors can be used for its production. However, it delivers limited capacitance results because of uneven pore size distributions [81] created during its activation.

David pech et al. [18] synthesized 0D carbon onion-based electrodes using electrophoretic deposition technique. The deposition of a several micrometer thick layer of nanostructured carbon onions (500 m^2/g) with a diameter of 6-7 nm is carried on the gold current collectors. In this study, carbon onion-based microdevice delivers the specific capacitance of 0.9F/cm^2 at a scan rate of 100 V/s. Moreover, the results of the prepared onion-like carbon were compared with the results of activated carbon (1700-1800 m^2/g) and it has been seen that the activated carbon capacitance decreases more quickly than the carbon onions due to the limitation of the poor ion transport in the inner pores of the activated carbon. However, the process of producing onion-like carbon requires a very high temperature of 1800 ºC which increases the cost. Further, the interdigital schematic of gold current collectors is patterned using an etching process which is highly temperature-sensitive and is very difficult to control.

Zhe Weng et al. [82] presented their research on the fabrication of graphene-cellulose paper (GCP) membranes by vacuum-assisted filtration method. In this paper, the flexible GCP electrode in H_2SO_4–PVA gel electrolyte delivers a capacitance of 81 mF/cm^2 and capacitance retention of

99% over 5000 cycles. However, it has been observed that there is a limitation of limited capacitance possessed by the graphene structure because the layers of graphene are easily agglomerated which does not allow to access its complete surface area by the electrolyte ions.

Dingshan Yu et al. [83] implemented their work in the fabrication of Graphene/Carbon Nanotube Hybrid Films. The hybrid films of graphene/ carbon nanotube are the interconnection of carbon structures with well-defined nanopores thus, providing a nearly rectangular behaviour of cyclic voltammogram with a specific gravimetric capacitance of 120 F/g at a scan rate of 1 V/s. Although the problem of agglomeration in graphene has been fixed by modifying its surface with poly(ethyleneimine) however, plenty of time *i.e.*, 48 hours has been taken for the preparation of poly(ethyleneimine) modified graphene nanosheets.

2.2.1.2. PSEUDO-BASED MATERIALS.

It has been seen that the capacitance offered by carbon-based materials is less than 300 F/g. Thus, the alternative electrode materials from the pseudocapacitive family have to be reviewed to understand their behavior on supercapacitor performance. These are redox-active materials exhibiting fast reversible and irreversible redox reactions at their surface thus providing an electrochemical behavior with greater volumetric capacitance than carbonaceous materials [84].

Conway et.al. [68] designed a supercapacitor device with ruthenium oxide (RuO_2) as electrode material because of its several advantages such as high conductivity, fast reversible redox reactions, good cycle stability, *etc*. In this paper, the RuO_2 thin film delivers almost constant capacitance under a potential window of 1.4 V in an aqueous acid electrolyte solution. However, the high cost and toxicity restrict its uses in the commercialization of RuO_2 based supercapacitor applications which thus opens new doors for other metal oxide materials.

Magnesium oxide (MnO_2) can be a good alternative to ruthenium oxide because of its cost-effectiveness, low toxicity. So, **Xingyou Lang et al.** [85] fabricated MnO_2 nanoparticles on the gold current collectors using the electroless plating method. However, MnO_2 shows poor conductivity of 10^{-5}-10^{-6} S/cm which limits their charge/discharge rate for high-power applications but it has been predicted to deliver higher capacitance. Hence, it must be deposited on the conducting material to enhance its conductivity thus allowing fast diffusion of ions between the electrolyte and the MnO_2. In this paper, the value of capacitance delivered was 1,145 F/g at a scan rate of 50mV/s with power and energy density of 57 Wh/kg and 16 kW/kg, respectively. Moreover, the capacitance retention of 85% was achieved up to 1,000 cycles. However, a long processing

time of 8 hours has been employed for the preparation of nanoporous gold sheets. Moreover, the waste products formed during the process of electroplating are very difficult to dispose off in the environment because they are hazardous for health.

Additionally, **Jun Du et al.** [86] presented a ultrathin porous $NiCo_2O_4$ nanosheet arrays based supercapacitor device on flexible carbon fabric (CF) substrate. The number of electroactive sites for the penetration of electrolyte ions are increased due to the porous feature of $NiCo_2O_4$ nanosheets. In this study, $NiCo_2O_4$ nanosheet arrays on CF results in the specific capacitance of 743 F/g at 80 mV/s. However, for obtaining ultrathin porous $NiCo_2O_4$ nanosheet arrays on carbon fiber, the calcination process has been carried at a high temperature of 300 ºC for 2 hours.

Later on, **Jizhang Chen et al.** [87] used a facile and scalable one-step anodization method for preparing three-dimensional $Cu(OH)_2$ nanoporous nanorods on a copper foil substrate in 1 M NaOH aqueous solution. The results of this paper have achieved the specific capacitance of 213 mF/cm^2, capacitance retention of 92% after 5000 cycles, the energy density of 3.68 mWh/cm^3, and power density of 5314 mW/cm^3. Although the transitional metal hydroxides show greater spacing, however, their cycle stability and capacitance performance are poor as compared to transitional metal oxides.

Further, Polyaniline (PANI) is considered one of the most widely used conducting polymers because of its high stability, better electroactivity, greater conductivity, and easier processability. **Kwang Sun Ryu et al.** [88] showed the fabrication of symmetric redox supercapacitor using conducting polyaniline electrodes dipped in Et_4NBF_4 electrolyte solution. In this paper, the working electrode delivers a specific capacitance of 107 F/g initially and 84 F/g after 9000 cycles. However, it can be seen that the processing time taken to prepare polyaniline is 72 hours. Moreover, the polymeric chain in the conducting polymer undergoes continuous contraction and expansion while charging and discharging thus, it restricts the cyclic stability and life span of the electrode.

Thus, the transitional metal oxides and conducting polymers have limited electronic conductivity, poor cycle stability, and poor robustness that affects their use in practical applications. To overcome these drawbacks, metal sulfides are discovered [89]–[92] because they show good electrical conductivity, high specific capacity, and greater redox activity because of the replacement of oxygen atoms by sulfur atoms. **Tingkai Zhao *et al.*** [93] have shown the synthesis and performance of copper sulfide microspheres for supercapacitor applications on nickel foam substrate. The experimental results of this paper have shown that electrochemical capacitance of

444.2 F/g was obtained at a current density of 1 A/g and capacitance retention of 87% over 6000 cycles with an energy density of 25.4 Wh/kg and power density of 4.1 kW/kg. However, this paper has prepared an asymmetric supercapacitor with reduced graphene oxide as a negative electrode which has the problem of agglomeration due to which its surface area is not completely accessible to the electrolyte ions.

Shi *et al.* [94] synthesized Cu_2S for an "all-in-one" mesh-typed integrated energy unit as an electrode material for photoelectric conversion and energy storage applications on stainless steel substrate using electron beam evaporation and sulfurization method. The device fabricated delivers the specific capacitance of 487.8 F/g. However, the process to prepare the all-in-one mesh electrode is very complex as it uses two techniques that require a temperature of 300 ºC. Thus, there is a need for researching techniques requiring less processing temperature and time.

2.2.1.3. TWO-DIMENSIONAL MATERIALS

Afterward, one more important class of material known as transitional metal carbides (2D) are discovered as electrode materials because they offer high electrical conductivity, resistance to corrosion, mechanical stability, remarkable catalytic activity. After the successful exfoliation of 2D graphene from their 3D graphite, researchers are discovering new 2D electrode materials from their various layered precursors for energy storage applications because of their better physical and chemical properties as compared to their properties in bulk [95]. In this context, the investigation leads to the discovery of different MAX phases which leads to the formation of transitional metal carbides, nitrides, and carbonitrides [96]–[98] known as MXene.

In 2011 **Naguib et al.** [99] showed the potential application of using MXene as electrode material for supercapacitor application with their excellent device performance. The first-ever multi-layered MXene discovered was $Ti_3C_2T_x$ and found to be a successful candidate in energy storage devices. This study showed the preparation of MXene from 10 g of MAX powder which was immersed in 100 mL of a 50% concentrated HF solution at room temperature for 2 hrs. However, the study does not include the process parameters variation and its effect on the device performance.

Mashtalir *et al.* [100] filtered delaminated MXene sheets of thickness of 20–50 nm for the preparation of additive and binder-free MXene based paper electrodes. It can be seen that the capacitive results of 340 F/cm^3 were obtained with KOH electrolyte solution and these results are better than those obtained by **Naguib *et al.*** [101] for Ti_2C. This is because of the large surface area

(98 m^2/g), hydrophilic nature, and good conductivity of MXene based paper electrodes. Thus, to obtain the greater value of capacitance, the key parameter is to increase the surface area. However, the capacitance results in multilayer MXene is less because of the low surface area which is approximately 23 m^2/g [102]. Hence, it motivates the researchers to find new methods for the preparation of mono or few-layer MXene sheets of few nm thickness to fabricate various flexible energy storage devices [100], [101], [103]

Further, to obtain the few-layered MXene, intercalation using dimethyl sulfoxide is carried out by **Naguib M *et al*.** [100]**.** To exploit the unique properties of two-dimensional solids, delamination and intercalation play an important role. This paper has presented that when intercalation of MXene is carried using DMSO, a stable colloidal solution has been formed which on filtering turned into MXene 'paper' that delivers excellent capacity with fast charging rates.

Further, **Yunfeng Guan *et al*.** [104] showed the synthesis of vanadium carbide using hydrofluoric acid-free etchant (NaF/HCl) as a supercapacitor electrode. In this study, the vanadium carbide MXene has been synthesized in 120 hours and delivers volumetric capacitance of 164 F/g at 2 mV/s with capacitance retention of 90% after 10,000 cycles in 1 M Na_2SO_4 electrolyte solution. However, it has been seen that NaF/HCl etchant can only be used for the effective preparation of highly pure V_2C MXene and this etchant always took greater time for the successful preparation of MXene as compared to HF etchant.

Shuangshuang Zhao *et al*. [105] prepared flexible niobium carbide MXene having large interlayer spacing for supercapacitor applications using tetramethylammonium hydroxide electrolyte (TMAOH). In this study, the electrochemical performance of niobium carbide has been compared in different electrolytes such as 1M H_2SO_4, 1M KOH, and 1M $MgSO_4$, respectively. This paper has shown that the niobium carbide MXene delivers specific capacitance of 1075, 687, and 506 F/cm at a scan at of 5 mV/s in H_2SO_4, KOH, and $MgSO_4$ electrolytes. However, it has been seen if etching has to be performed with TMAOH electrolyte, pre-treatment has to be carried first with HF solution. Thus, TMAOH alone doesnot have the capability to produce MXene from the MAX precursor.

Ghidiu *et al*. [106] synthesized clay-like MXene ($Ti_3C_2T_x$) using LiF and HCl solution at 40 °C for 45 hrs. This finding has shown that because of the hydrophilic property of MXene, it can take a clay-like shape and on drying, it can be turned into a highly conductive solid or rolled into films having dimensions of tens of micrometers thick. Further, with the addition of acidic electrolyte, $Ti_3C_2T_x$ films resulted in a volumetric capacitance of 900F/cm^3 (or 245F/g). Later on, **Qiu Jiang**

et al. [107] prepared all pseudocapacitive MXene-RuO_2 based asymmetric supercapacitor on carbon fabric. This paper has shown that the composite of the electrode material has achieved an energy density of 37 μWh/cm^2 with a power density of 40 mW cm^2 and capacitance retention of 86% after 20000 charge-discharge cycles. However, it can be seen that the LiF and HCl etchant method requires a longer period to prepare MXene. Moreover, ruthenium oxide material is highly expensive and the fabrication of ruthenium oxide electrode requires a high temperature of 180 °C for 24 hrs.

Afterward, **Ravuri Syamsai and Andrews Nirmala Grace** [108] have shown the synthesis and performance of vanadium carbide MXene as supercapacitor electrodes on carbon paper. It has been reported in this paper that for the synthesis of vanadium carbide MXene (V_4C_3) from MAX precursor, 1 g of MAX phase in 40% of the hydrofluoric acid solution is etched for 3 days. in this study, the MXene based electrodes deliver the specific capacitance of 330 F/g at a scan rate of 5 mV/s in 1 M sulphuric acid with a cycle retention rate of 90% after 3000 cycles. However, it has been seen that the long processing time of 3 days and high temperature of 1500 °C is used for the preparation of MXene which hinders this method to be used for flexible supercapacitors.

Qi Xun Xia *et al.* [109] annealed MXene nickel oxide electrode and achieved greater volumetric energy density of the fabricated asymmetric supercapacitor. In this paper, the electrode material has been synthesized using the hydrothermal method in a 50% hydrofluoric acid solution. The nanocomposite electrode material TiO_2/C-$Ti_3C_2T_x$ MXene over nickel foam delivered a remarkable specific capacity of 92 mAh/cm^3 at a current density of 1 A/g. Moreover, it has been claimed in this paper that increased capacitive performance is because of the newly formed high-surface-area multilayers of the nanocomposite on the nickel foam. However, it has been observed that the maximum reported acidic content of hydrofluoric acid (50%) had been taken to etch the MAX precursor for a long time i.e., 24 hrs.

Mahjabeen Fatima *et al*. [110] discovered niobium-doped two-dimensional MXene electrodes with enhanced energy storage capacity and stability. The ionic size of niobium is comparable to the ionic size of titanium which makes it a suitable candidate for doping in Ti_3C_2 MXene material. In this paper, X-ray diffraction (XRD) characterization showed an enhancement in the c-lattice parameter from 19.2 A° to 23.4 A° after the doping of niobium which suggests the increase in interlayer spacing between various MX layers. Moreover, the niobium-doped MXene electrode delivers linear triangular behavior and specific capacitance of 442.7 F/g till 10,000 cycles which suggests the faster accumulation and separation of ions at the electrode surface.

Liangzhu Zhang *et al.* [111] have successfully prepared molybdenum dioxide-doped MXene as a pseudocapacitive electrode for high-performance flexible asymmetric supercapacitor using vacuum filtration and laser technology. The device has operated at a 1.2 wide voltage window and delivers the specific areal capacitance of 19 mF/cm2 at 2 mV/s with an energy density of 9.7 mWh/cm3 and power density of 0.198 W/cm^3. However, the preparation of MXene has been carried using LiF and HCl etchant which is a tedious task as it requires a lot of time.

2.2.2. SYNTHESIS METHODS OF ELECTRODE MATERIAL

In this section, different synthesis methods to prepare thin-film electrodes on various substrates are reviewed and presented below:

Xiaoqian Cheng *et al.* [112] implemented carbon nanotubes-graphene composites on a paper substrate by the rod-rolling method. The sheet resistances shown in this paper were 440.2 and 90.5 ohms/sq. of the SWCNT and composite thin films at room temperature with a specific capacitance of 95F/g for composites and 28F/g for SWCNT. However, the initial cost or the investment in the rod rolling method is very high. Moreover, the arc discharge system used to prepare SWCNT is very tedious and complex.

Later on, **Hui Xia *et al.*** [113] published their work on the fabrication of MnO_2 nanotube and nanowire arrays on the platinum substrate by electrochemical deposition using the porous alumina template method. Electrochemical characterization demonstrates that MnO_2 nanotube and nanowire array delivers the specific capacitance of 320 and 101F/g with about 81% of the capacitance retention even after 2000 cycles. Since it has been discussed previously that the conductivity of MnO_2 is poor. Thus, to increase the conductivity, composites of MnO_2 and carbon are fabricated. **Zhibin Lei *et al.*** [114] refluxed graphitic hollow carbon spheres (GHCS) in a $KMnO_4$ aqueous solution for vertically growing the 0D MnO_2 nanofibers on the external surface of (GHCS). An energy density of 22.1 Wh/kg and a power density of 7.0 kW/kg is recorded with coulombic efficiency of 90% after 1000 cycles. Further, **Zhibin Lei *et al.*** [115] used chemical vapor deposition method for the preparation of hollow carbon spheres (HCS) with specific surface areas of 2239 m^2/g employing colloidal silica spheres as the template and ferrocene as the carbon precursor. It has been observed a layer of polyaniline (PANI) was yielded on the external surface of the HCS by using chemical oxidative polymerization. Results showed that the HCS before and after PANI coating delivers specific capacitances of 268 and 525 F/g respectively in H_2SO_4 electrolyte solution.

However, the issue with the template-assisted method is that the template needs to be removed after the synthesis of electrode material which is a complex process. Moreover, the temperature involved in the preparation of graphitic hollow carbon spheres is very high *i.e.*, 550 ºC for 60 minutes and 850 ºC for 90 minutes which makes the process very costlier.

Liang Kou *et al.* [116] have published their research using wet-spun assembly for the preparation of graphene/carbon nanotube core-sheath (GO@CMC) yarn-based supercapacitor. The supercapacitor device showed an areal capacitance of 269 mF/cm^2 and energy density of 5.91 mWh/cm^2 with almost no decay of capacitance after 2000 times of charge-discharge cycles. However, the disadvantage of the wet spun method is that its production rate is very low.

Kai Chi *et al.* [117] fabricated graphene−polyaniline nanocomposite electrode material by inkjet printing on graphene paper. It has been mentioned in this work that the working electrode exhibits an energy density of 24.02 Wh/kg with a power density of 400.33 W/kg for an operating voltage of 0.8V along with the excellent mechanical flexibility. However, the ink synthesis procedure and nozzle jamming in the inkjet printing technique is uncontrollable which provides low resolution.

Babak Anasori *et al.* [118] **have** prepared flexible, transparent, and conductive titanium carbide MXene films showing high volumetric capacitance using the spin casting method followed by vacuum annealing of the film at 200 °C. The fabricated electrodes showed the volumetric capacitance of 676 F/cm^3 with an energy density of 0.05 $\mu Wh/cm^2$. In this work, although the spin casting technique is easy, however, the time employed for the electrode material preparation is long.

Dr. Na Wng et al. [119] fabricated a double-sided micro supercapacitor by cutting the interdigital patterns using an ultraviolent laser (UV) over 20 μm thick nickel foil having both sides coated with MXene films. It can be seen from this study that both sides of the Ni foil were used for energy storage thus providing a specific areal capacitance of 52 mF/cm^2. However, during the fabrication of electrode material over different substrates, it is very difficult to optimize the speed, wavelength, and resolution of the laser cutting method.

Lianghao Yu et al. [120] have fabricated the electrochemical supercapacitor based on N-Doped MXene electrodes using the inkjet printing method. In this paper, the melamine-formaldehyde template is used for the preparation of the MXene nanoflakes which were then annealed at 550 °C for 2 hrs in an argon atmosphere. Finally, the study revealed that the 3D-printed nitrogen-doped MXene based supercapacitor delivers an areal capacitance of 8.2 F/cm^2 with an areal energy density of 0.42 mWh/cm^2.

Cheol-Hwan Mun et al. [121] prepared micro flower-like binder-free composite electrodes of nickel sulfide and lead sulfide for high supercapacitor applications onto nickel foam using chemical bath deposition technique. The paper has shown that the composite micro flower structure possesses faradic active sites which helps in fast redox reactions. Moreover, the composite electrode delivers the specific capacity of 125.89 mAh/g at a current density of 2 A/g in 3 M KOH electrolyte solution which is 2.67 and 1.62 times higher than the bare PbS and NiS electrodes with capacitance retention of 88.97% even after 3000 cycles. However, lead sulfide has the drawback that it is highly toxic in nature and hazardous to health. Moreover, the limitation of the chemical bath deposition technique is that the solution gets wasted after every deposition.

Panpan Xu et al. [122] successfully prepared cadmium sulphide-based electrodes on nickel foam for supercapacitor applications using the one-step hydrothermal technique. This paper showed that the specific capacitance of 909 F/g is obtained at a current density of 2 mA/cm^2. Moreover, capacitance retention of 88% was obtained at a current density of 50 mA/cm^2 which suggests the quick delivery and separation of ions, thus contributing significantly to the fast reversible redox reactions. Moreover, a high energy density of 28 Wh/kg was delivered with a power density of 160 W/kg.

Agata Moyseowicz [123] synthesized bismuth sulfide-based nanorods at different temperatures as an electrode material for supercapacitor applications using the chemical precipitation method. It has been shown in this paper that at a synthesis temperature of 75 °C, bismuth sulfide material provides the best capacitance value as compared to 0 °C and 25 °C. However, during the chemical precipitation technique, a large quantity of silt is produced and if it is precipitated as a useful by-product, then it acts as dangerous waste and removal of which leads to high processing costs.

The comparison of various synthesis techniques along with supercapacitor performance is shown in table 2.1

Table 2.1: Comparison of various techniques used by researchers to fabricate supercapacitor device.

S. No	Author	Substrate	Technique	Capacitance	Energy density	Power density
1.	Xiaoqian Cheng et al. [112]	CNT@ Graphene composite	Rod-rolling method	95F/g	-	-
2.	Hui Xia et al.	MnO_2 nanotube	Template method	320 F/g	-	-

		MnO_2 nanowire	Template method	101F/g		
3.	Zhibin Lei *et al.* [114]	MnO_2@GHCS	Template method	104 F/g	22.1Wh/kg	7.0 KW/Kg
4.	Zhibin Lei *et al.* [115]	PANI@HCS	Template method	525 F/g	17.2Wh/kg	-
5.	Liang Kou *et al.* [116]	GO@CMC	Wet-spun assembly	269 mF/cm^2	5.91mWh/cm^2	-
6.	Kai Chi *et al.* [117]	Graphene@ PANI nanofiber	Inkjet printing	190.6 mF/cm^2	24.02 Wh/kg	400.33 W/Kg
8.	Babak Anasori *et al.* [118]	$Ti_3C_2T_X$	Spin casting	676 F/cm^3	0.05μWh/cm^2	2.4 μW/cm^2
9.	Dr. Na Wang *et al.* [119]	$Ti_3C_2T_X$	UV laser	52 mF/cm^2	2.62μWh/cm^2	1.26 mW/cm^2
11.	Lianghao Yu *et al.* [120]	N-doped MXene	Inkjet printing	8.2 F/cm^2	0.42mWh/cm^2	-
12.	Cheol Hwan Mun *et al.* [121]	NiS@PbS	CBD	125.89 mAh/g	-	-
13.	Panpan Xu *et al.* [122]	Cadmium Sulphide	Hydrothermal technique	909 F/g	28Wh/kg	160 W/kg
14.	Agata Moyseowicz [123]	Bismuth Sulfide	Chemical precipitation met	457 F/g	2Wh/kg	2.9 KW/ kg

2.2.3. ELECTROLYTE

In the literature, a large variety of the electrolytes have been used to enhance the performance of supercapacitors in terms of power density, energy density, capacitance retention, cycle stability. The various factors related to electrolyte solution such as conductivity of ions, mobility, ionic radii, solvation shell, *etc.* affect the performance of supercapacitor. The electrolyte and electrode interface has been greatly affected by the electrochemical processes occurring between the active material and the electrolyte solution. In literature, a variety of electrolyte solutions are used such as aqueous, organic, ionic, gel polymer, *etc*. This section provides the survey on various electrolyte materials which are used by the researchers.

Jianbo Zhu et al. [124] presented the effect of different electrolytic cations on polypyrrole/RGO based asymmetric supercapacitors. In this study, the effect of HCl, LiCl, NaCl, and KCl respectively was investigated. The results have shown that the difference in capacitance results was obtained only by changing the cationic species in the electrolyte solution. The capacitance results obtained were 280.3, 255.4, 210.4, and 197.9 F/g for HCl, KCl, NaCl, and LiCl electrolytes because of varied cationic mobility, cationic radii, and conductivity. Since the ionic mobility and conductivity of H^+ ion is greater which helps in providing fast charge delivery. Moreover, the small ionic radius of the H^+ ion provides greater ionic adsorption and desorption at the electrolyte/electrode interface. Thus, the electrolyte cations show a significant effect on the electrochemical performance of the supercapacitor device.

Later on, **Hao Wu et al.** [125] investigated the effect of electrolytic anions on the electrochemical performance of calcium carbide-derived carbon supercapacitors. The study of KOH, K_2SO_4, KCl, and KNO_3 electrolytes were investigated and found that the faster ioic mobility and greater conductivity of OH^- ion provides greater current density as compared to Cl^-, NO_3^- and SO_4^{2-} ions which lead to its enhanced capacitive behavior. Moreover, the radii of the radii of other anions were greater than OH^- ion which led to decrease in the entry of ions into the electrode pores. After 2000 cycles, KOH, KCl, KNO_3, and K_2SO_4 delivers 68, 52, 31, and 25F/g of capacitance for the calcium carbide-derived carbon electrodes.

Yangyang Wen *et al.* [126] have synthesized nitrogen-doped two-dimensional MXene (N-$Ti_3C_2T_x$) by post-etch annealing MXene in the presence of ammonia. This paper deals with two different electrolyte solutions which are sulphuric acid and magnesium sulphate. In this study, the capacitance obtained with 1 M H_2SO_4 (192 F/g) is lower as compared to the capacitance obtained with 1 M $MgSO_4$ (82 F/g) at 200ºC. The author suggests that the conductivity of $MgSO_4$ is lower than that of H_2SO_4 which leads to the lower value of capacitance.

John K. McDonough *et al.* [127] compared the performance of carbon-based supercapacitor in tetrabutylammonium tetrafluoroborate and tetraethylammonium tetrafluoroborate electrolyte solutions. The study shows that tetrabutylammonium tetrafluoroborate (TBA-BF_4) delivers greater capacitance of 3.5µF/cm^3 as compared to tetraethylammonium tetrafluoroborate (TEA-BF_4) of 3 µF/cm^3. This is because the better separation of ions has been provided by the greater alkyl chains of TBA^+ cation from their counter-ions at the charged carbon surface thus, providing better charge screening. However, the limitation of using organic electrolytes is that they possess greater

resistivity because of their large size molecules which require greater pore sizes in the electrode material.

Victor L. Pushparaj *et al.* [128] implemented their work on nanoporous cellulose paper embedded with aligned carbon nanotube electrodes using the chemical vapor deposition technique. The ionic nature of room temperature ionic liquid (RTIL) permits it to be used as an electrolyte in supercapacitors. It has been shown that the CNT cellulose@RTIL nanocomposite showed a higher operating voltage (2.3 V) as compared to the operating voltage with KOH electrolyte (0.9 V). Moreover, the specific capacitance calculated for KOH and RTIL electrolytes was 36 F/g and 22 F/g respectively. However, it has been observed that although the operating voltage of RTIL is greater, it delivers low specific capacitance as compared to KOH solution because the dielectric constant and ionic mobility of the former is lower.

Qiao Chen *et al.* [129]investigated the effect of six different PVA polymer gel-based electrolytes in KOH, H_2SO_4, H_3PO_4, NaOH, NaCl, and KCl on graphene-based supercapacitors. In this study, it has been seen that PVA–H_3PO_4 delivers highest capacitance as compared to other PVA-based electrolytes because, in H_3PO_4–PVA, H^+ ion has smaller ionic radii among other ions (Na^+, K^+, OH^-, and Cl^-). Thus, H^+ ion can diffuse quickly into graphene layers and prevents the problem of agglomeration. Moreover, H_3PO_4 generates a large number of free ions than NaCl or NaOH at the same molar concentration. However, the gel polymer electrolyte suffers from the drawback of narrow operating temperature because of the presence of water. Moreover, it also provides poor mechanical strength.

Thus, there are still several challenges which are required to be addressed for designing better electrolyte solutions that enhance the supercapacitive performance of the device.

2.2.4. SUBSTRATES

The fast development of smart electronic devices for wearable and healthcare applications focuses on designing improved flexible energy storage devices. To tackle the issues related to durability and flexibility, the combination of supercapacitors with flexible substrates brings a revolution in human lives because they are lightweight, cost-effective, safe to use, comfortable, *etc*. The performance of the supercapacitor device depends not only on the working electrode material but also on the substrate which acts as a current collector. For obtaining the high-performance flexible supercapacitor device, the electrode material should have low cost, high stability, greater mechanical strength, high melting point, *etc*. The working of flexible supercapacitors is affected under various folding and bending conditions. In this context, this section surveys various flexible

substrates which are used to fabricate high-performance supercapacitor devices. The detailed discussion is presented below:

In the literature, a variety of electrode materials are fabricated on glass substrate because there are no constraints of the temperature at which it can be heated. However, in designing a flexible supercapacitor one must be aware of the materials that can withstand only low temperature as the flexible substrates cannot be operated at high temperature. Thus, the selection of proper electrode material has to be done.

Previously, the supercapacitors were made on three-dimensional metallic current collectors because of their high conductivity, mechanical strength. However, the greater thickness and increased areal mass density contribute toward the greater proportion of inactive component thus limiting the energy density of the device. Thus, the fragile and rigid nature of these metallic current collectors emphasises on the requirement of flexible substrates to design a flexible energy storage device.

In the early days, like rigid substrates, the fabrication of flexible supercapacitors also starts with carbon-based materials. However, these materials show different variations in their structure and performance which governs the possibility of their combination with each other to form new materials. Thus, carbon materials represent nearly unlimited research space.

Rajib Paul and Ajit K.Roy [130] prepared a flexible supercapacitor using brush-like nanostructures of boron nitride doped carbon nanotube electrodes (BNCNT) which remains stable till 40-50 °C which makes it a suitable candidate for flexible supercapacitors. In this study, boron and nitrogen-doped carbon nanotubes are first synthesized on carbon cloth substrate (CC) using CVD and then the device fabrication is carried using the above electrode on copper foil to form a flexible asymmetric supercapacitor. It delivers the specific capacitance of $106.8\ mF/cm^2$ with capacitance retention of 86.4% after 5000 cycles. Although in this study, the capacitance results are better, however, there are two main limitations of this study which are: first, the two different types of flexible substrates are used separately for electrode preparation and device preparation. Second, the process of growing CNT over CC substrate is complicated as it requires high temperature which ultimately increases the cost.

Yong Li et al. [131] presented the application of fibrous CNT-aerogel electrodes for flexible and stable supercapacitor using electrochemical activation and freeze-drying method and holding its one end to copper or silver pasting for contacts. In this study, the fabricated flexible supercapacitor works normally in the temperature range of 0-80 °C which makes it a suitable candidate. It delivers

an electrochemical capacitance of 6.9 mF/cm^2 at a current of 0.1 mA with capacitance retention of 94.7% after 10,000 cycles. However, the device delivers low specific areal capacitance which may be because of the low operating temperature of the device which may produce low-quality electrode films. Moreover, the synthesis of CNT aerogel involves the freeze-drying (<1Pa pressure) of CNT hydrogel in the sample is kept under vacuum.

Further, **Weijia Zhou et al.** [132] synthesized free-standing porous core-shell carbon fiber electrodes for flexible supercapacitor using acid oxidation method at 120 °C. The device fabricated using PVA/H_2SO_4 gel electrolyte delivers specific areal capacitance of 20.4 F/g at a current density of 1 A/g with a power density of 122 W/kg and an energy density of 3.3 Wh/kg. Thus, self-standing carbon-based material acts both as current collectors and working electrodes which results in reducing the overall weight of the device. However, it put a burden on electrode material to provide strong mechanical support. Although, the operating temperature of carbon fiber is high it delivers poor specific capacitance thus it is mainly used only as a current collector. However, its performance could be improved by treating it with strong oxidants such as H_2SO_4 and $KMnO_4$.

The next most widely used flexible substrate is stainless steel because of its mechanical strength, durability, corrosion resistance, stability, *etc.*, for depositing various active materials. **Gund et al.** [133] and **Chou et al.** [134]fabricated MnO_2 nanorod forests and $Co(OH)_2$ nanoflake films directly on the stainless steel substrate. Moreover, the other metallic substrates such as aluminum, titanium, copper, nickel have also been used for designing supercapacitors because of greater specific surface area, open-cell hierarchical structure, and excellent cycling stability. **Xinrui He et al.** [135] and **Bulakhe et al.** [136] **show the growth of** 3D hollow tubular Cu2S nanorods on copper substrate and nickel foam for high electrochemical performance. Both the functions of the current collector and the copper source are performed by the Cu substrate which thus reduces the contact resistance. However, the metallic-based flexible electrodes are opaque and less stretchable which hinders their usage where transparency is required such as in touch screen displays. Thus, transparent substrates are used.

Shunqiong Jiang et al. [137] fabricated a flexible micro supercapacitor by transferring mask-printed graphene nanoscrolls on transparent PET substrate. In this study, the greater aspect ratio of graphene nanoscrolls provides greater mechanical strength and stability to the flexible device. Moreover, the device has delivered the capacitance of 4.4 mF/cm^2 at a current density of 1 mA/cm^2. However, the limitation with the synthesis process of graphene nanosheets is that they require vacuum. Also, the capacitance results obtained in this paper are very less which might be

because of the complications that occur while transferring graphene nanoscrolls on PET substrate as it may affect the efficiency of electrode material. Thus, if the process involves direct fabrication of electrode material on a flexible substrate, it helps in enhancing the device's performance.

Later on, **Niu et al.** [138] prepared single-walled carbon nanotubes electrodes (SWCNT) on flexible transparent polydimethylsiloxane substrate which delivers the capacitance of 48 F/g. In this study, the PDMS substrate is prepared by baking silicone-elastomer base at 90 °C followed by peeling which makes the process complex. It is also mentioned in this study that the prestretching of PDMS substrate has been performed before depositing the SWCNT which produces some wrinkles. Moreover, the capacitance results obtained are very poor which may be due to the cracks formed while prestretching.

Further, **Haibo Hu and Tao Hua** [139] have shown the patterning of MXene on a paper substrate for supercapacitors applications using laser printing, vacuum-assisted deposition, and physical sputtering technique. This study has shown that the fabricated supercapacitor delivers a specific areal capacitance of 27.29 mF/cm^2. Since, the paper substrate is non conducting, the gold film is deposited over the paper substrate to make it conducting using the magnetron sputtering method which is a highly expensive technique.

Hence, after the detailed literature on the supercapacitor devices based on the different electrode material, synthesis method, electrolyte, and substrate, the research gaps found are discussed in next section.

2.2. RESEARCH GAPS

After going through the literature, it is found that for the efficient working of supercapacitor devices, proper selection of process parameters for the synthesis of electrode material is very important as it influences their electrical and structural properties. Thus, there is a huge lack in selecting the threshold value of process parameters to successfully synthesize the electrode material. Moreover, in literature, one more way is discovered to enhance the device performance which is by doping various heteroatoms into the electrode material. However, very few heteroatoms are tried for incorporation into the electrode material which thus opens various new avenues for finding several other elements from the same group in the periodic table because of their similar physical and chemical properties. Further, it can be seen that deposition of electrode materials is carried widely on the metal-based substrates and very few studies have been performed

with transparent flexible substrates. Thus, as per the discussion, the research gaps are summarized as:

- The process parameters highly affect the structural and electrical properties of the electrode material. However, the thorough study of synthesis parameters has not been reported in the literature.
- Very few studies have been carried on depositing electrode materials over flexible transparent substrates as compared to the metallic substrates.
- Limited doping of heteroatoms has been tried into the electrode material for enhancing the device's performance.

2.3. OBJECTIVES

Based on the research gaps, the objectives to work upon are decided as:

- To synthesize and characterize different electrode materials for supercapacitor applications.
- To fabricate and characterize the flexible supercapacitor devices.
- To explore the effect of doping in electrode material on the performance of supercapacitor.

2.4. CONTRIBUTION OF THESIS

- Synthesis and characterization of different electrode materials such as MXene and copper sulfide have been carried out for the application of supercapacitor devices.
- Successful fabrication of supercapacitor devices on graphite, PP, PET, and glass substrates with the maximum capacitance of 1.1F/cm^2 is obtained for vanadium doped MXene on graphite sheet substrate.
- Vanadium doping has been successfully incorporated into the MXene to enhance its charge storage.
- Vanadium doped MXene based supercapacitor exhibits remarkable capacitance retention of 92.7% after 3500 cycles.

CHAPTER 3

SYNTHESIS AND CHARACTERIZATION OF DIFFERENT ELECTRODE MATERIALS

In this chapter, the procedure involved in the synthesis of electrode materials such as MXene and copper sulfide is presented. The electrodes in supercapacitors are a thin coating of the material deposited over a conductive, metallic current collector. The external supply voltage is provided to the electrodes through the current collectors. The properties that a supercapacitor electrode must possess are high conductivity, greater temperature, and better chemical stability, corrosion-resistant, and greater specific surface area per unit mass and volume. Also, it must be environment-friendly and cost-effective. Since the amount of charge storage per unit voltage in double-layer capacitors and pseudocapacitors strongly depends on the surface area of electrodes. While synthesizing an electrode material, there are a variety of process parameters present which significantly alter the properties of the materials prepared. Thus, the study of these process parameters has to be thoroughly observed. In literature, various members from the family of MXene are prepared using various etchants however, they are either time taking or require a higher processing temperature. Thus, in this work, the hydrofluoric acid is taken for the preparation of titanium carbide MXene as it involves less processing time. Moreover, the concentration, quantity, and etching time with HF have been varied to observe their effect on the structural and electrical properties of the MXene formed. Afterward, for the preparation of copper sulfide as another electrode material, the concentration of copper sulphate and sodium thiosulphate is varied using the hydrothermal method. The hydrothermal method is chosen because of the requirement of less processing time and temperature. After the synthesis of MXene and copper sulfide powder, structural and electrical characterizations such as SEM, XRD, and resistance measurements are performed to evaluate the change in the behavior of the electrode material on varying different process parameters.

3.1.SYNTHESIS OF MXene ($TI_3C_2T_X$) POWDER

There are a variety of methods available for the preparation of MXene in the literature but one should have to be aware of the properties required to obtain the best-optimized material. The synthesis of the MXene ($Ti_3C_2T_x$) starts with the titanium aluminum carbide (Ti_3AlC_2) precursor which is commonly named as “MAX” precursor. The MAX precursor is layered hexagonal

structures of carbides and nitrides having the formula $M_{n+1}AX_n$ where n is having the value from 1 to 4, M can be an early transition metal, A belongs to the elements from 13 and 14 group in the periodic table and X can be either carbon and/or nitrogen. The flow chart given in figure 3.1 shows the synthesis of MXene layers.

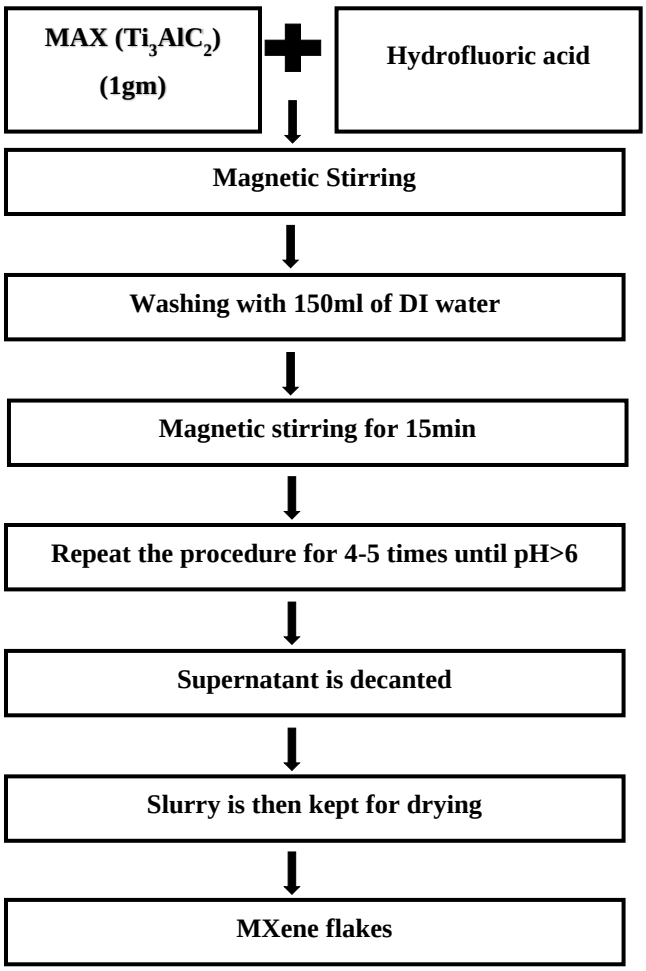

Figure 3.1: Flow chart for the steps followed for synthesizing MXene

Initially, 1g of MAX powder is added gradually to the hydrofluoric acid (HF) solution to avoid the exothermic reaction. The suspension of MAX and HF is then stirred magnetically. The magnetic stirrer is used to stir the suspension as shown in figure 3.2. In the MAX precursor, aluminum is responsible for the bonding of different MX sheets. However, the bonding of M and A is weaker as compared to the bonding between M and X which ensures the successful and selective etching of aluminum using hydrofluoric acid [140]. The chemical exfoliation is the only route to selectively remove the aluminum because the bond between M and A is covalent rather than Van

der Waals. Thus, etching is not governed through mechanical exfoliation or simply shaking. Further, the suspension is washed 5 times with simultaneous addition of deionized water (150ml) followed by magnetic stirring and decanting in the various

Figure 3.2: Illustration of magnetic stirrer equipment

repeated cycles of 15min to remove the residual acid and by-products until a safe pH value (≥6) is reached as shown in figure 3.3. The color of the supernatant is changed from transparent to dark green indicating the change in pH value from acidic to basic [141]. The hydrous slurry thus collected is dried in air for 1 day to obtain multi-layered MXene powder. The properties of MXene can be altered by varying

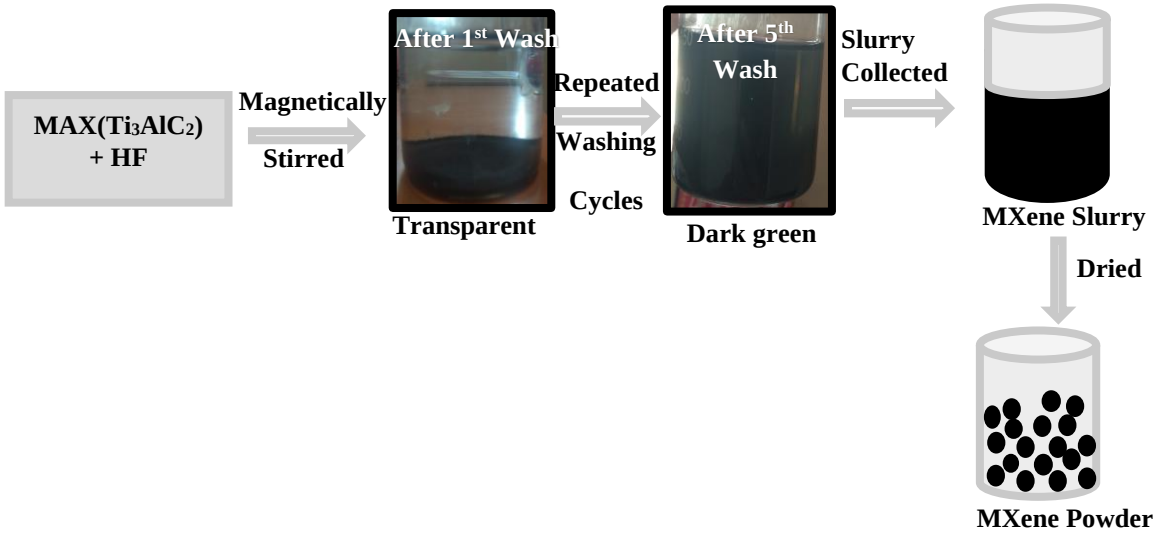

Figure 3.3: Mechanism involved in MXene synthesis.

various parameters as per the flow chart shown in figure 3.1. The parameters that can be varied to understand the effect on structural and electrical parameters of MXene include MAX precursor quantity, HF concentration, HF quantity, and HF etching time. However, in this study MAX precursor is taken as constant and the other process parameters defined are varied to obtain the MXene powder. So, all these parameters are varied to understand the effect on MXene structural and electrical properties are discussed in further sections.

3.1.1. PREPARATION OF THE MXene FILMS

The performance of the supercapacitor device has been examined by depositing the thin film of MXene over rigid as well as flexible substrates. The resistance measurement has also been performed by preparing the electrical contacts over the thin film on the glass substrate using silver paste. The I-V characteristics of the film are plotted and analyzed using Keithley 4200A-SCS. The resistance measurements are performed on different MXene films in the voltage range of -5V to +5V. Scanning Electron Microscopy (SEI 15KV SS35) is used to analyze and characterize the morphology of the different samples prepared. The XPERT-PRO diffractometer system with Cu Kα radiation is used to characterize the crystalline structure. The Electrochemical Impedance Spectroscopy (EIS) is performed using the Metrohm auto lab workstation.

3.1.2. EFFECT OF HF CONCENTRATION

Hydrofluoric acid is highly toxic, so precautions must be taken to handle it and one must be aware of the risk involved and should follow the safety measures. The synthesis and properties of the MXene are highly affected by the HF concentration. The different process parameters related to HF concentration keeping other parameters constant are shown in Table 3.1 for obtaining different properties of the MXene.

Table 3.1: Synthesis of MXene at different experimental parameters.

Samples	HF Concentration	Etching Time	HF Quantity
1.	20%	7hrs	20ml
2.	30%	7hrs	20ml
3.	35%	7hrs	20ml
4.	40%	7hrs	20ml

In literature, it has been observed that people have taken 10% to 50% HF for removing the aluminum layer from the MAX precursor. However, avoiding the higher concentration of HF is also a prime concern in the literature. In this section, different concentrations of HF are taken to understand their outcomes on the MXene electrical and structural properties. In this study, the maximum concentration of HF is taken as 40% because the more the HF concentration, the more will be the toxicity.

3.1.2.1.MORPHOLOGICAL ANALYSIS

SEM images of titanium carbide (MXene) at different HF concentrations are shown in figure 3.4 (a-e), however, their corresponding other experimental parameters are kept constant and given in Table 3. Figure 3.4 (a) illustrates the MAX structure in which all layers are tightly

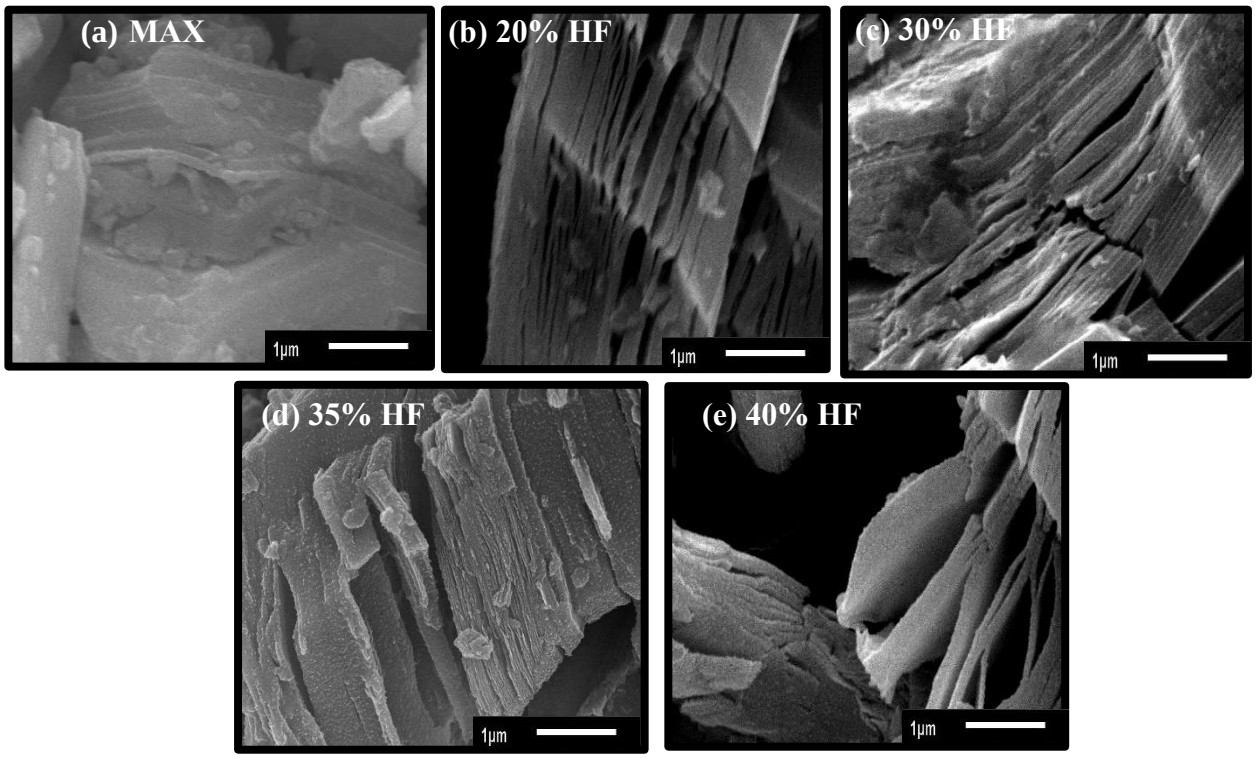

Figure 3.4: SEM corresponding to (a) MAX, (b) 40%, (c) 30% HF, (d) 20% HF. All the measurements are at 1µm of magnification and with (7hrs and 20ml of HF).

packed and shows negligible spacing whereas figure 3.4 (b-d) shows the MXene structure corresponding to 20%, 30%, and 35%. It can be observed from figure 3.4 (b-d) that exfoliation initiated only at some locations in the MAX phase leaving the majority of the layers unaffected which still resulted in a compact structure and yet not forming an accordion-like structure. Further, as the HF concentration has been increased to 40%, maximum spacing has been observed as shown in figure 3.4 (e) because a greater concentration of fluorine is present to etch the aluminum forming AlF_3 by-product. This implies that etching with 20%, 30%, and 35% HF is not sufficient to remove the aluminum from the MAX phase.

To confirm the successful etching or removal of aluminum from the MAX phase, XRD measurements are performed. The XRD patterns for 20%, 30%, 35%, and 40% of HF concentrations and MAX precursors are compared and shown in figure 3.5. The appearance of (104) peak corresponding to 39º represents the presence of aluminum whereas the appearance of a peak at 27º represents that its elimination starts from the MAX phase. It is clear from the XRD graphs that the intensity of the peak at 39º depends on the HF concentration. It can be seen that when the HF concentration has been increased from 20% to35%, the intensity of (104)

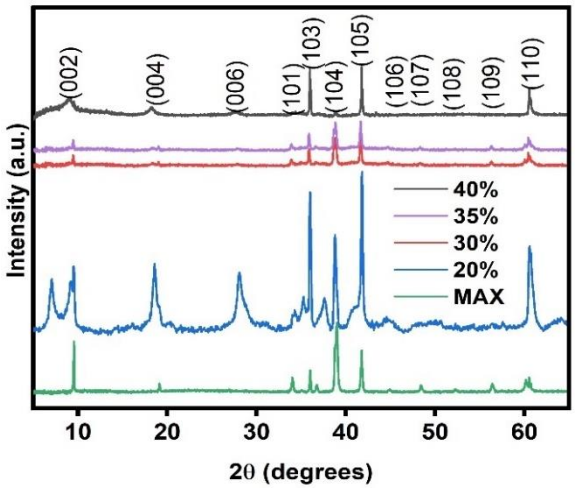

Figure 3.5: XRD for different concentrations of HF with (7hrs and 20ml of HF).

peak reduces whereas when the concentration of HF is 40%, the (104) peak disappeared. This indicates the complete removal of Al in MXene layers formed at 40 % HF. The peak height thus influences the properties of MXene formed. The appearance of (110) peak at 60º in all XRD patterns of figure 3.5 confirms the layered structure of the MXene as observed in the SEM images of figure 3.4 (a-e). The appearance of several by-products and defects formed during the reactions

involved in MXene formation is confirmed by the appearance of (108) and (109) peaks in 20%, 30%, and 35% of HF.

The effect of the aluminum removal on the c-lattice parameter or d-spacing can be governed through the (002) peak as illustrated in Table 3.2. The shifting of the (002) peak in Table 3.2 at a lower angle indicates the increase in d-spacing between MXene sheets. In MAX precursor it can be observed that the (002) peak is present at 9.5º however, in 20% HF, it can be observed that the

Table 3.2: Angles corresponding to (002) peak

S.NO	Samples	(002) Peak position	d-spacing (nm)
1.	As received MAX precursor	9.5º	0.926
2.	Treatment with 20% HF	9.4º	1.292
3.	Treatment with 30% HF	9.0º	1.022
4.	Treatment with 35% HF	8.9º	1.002
5.	Treatment with 40% HF	6.9º	0.980

(002) peak position remains at the same angle as in MAX structure which suggests that no increase in spacing occurs between the different MX sheets. Whereas in 30% and 35% HF, the (002) peak is observed at 9.0º and 8.9º which confirms that the d-spacing between the MX sheets starts increasing. Moreover, with 40% HF, the (002) peak get shifted towards a 6.9º angle confirms the increase in d-spacing. Moreover, two different peaks corresponding to (001) and (002) appeared in 20% HF indicates that a varied amount of exfoliation occurs at different locations.

3.1.2.2.EFFECT OF HF CONCENTRATION ON THE RESISTANCE OF FILM

The variation of resistance with the HF concentration is shown in figure 3.6. It can be seen that with an increase in the concentration of hydrofluoric acid, the resistance increases.

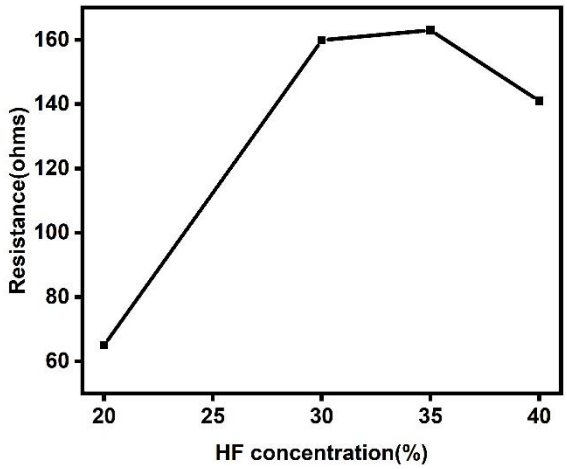

Figure 3.6: Relation between resistance and HF concentration.

It can be seen from the SEM image in figure 3.4 that on increasing the HF concentration, the MAX structure is transforming successfully into MXene forming accordion-like structure. This leads to more and more removal of aluminum which thus increases the resistance. Whereas in 20% HF, the MXene accordion-like structure is not formed and it still appears similar to MAX structure thus, its resistance is minimum.

Thus, while preparing the MXene, the most important criterion is the formation of an accordion-like structure [142]. In the SEM images, it can be seen that the accordion-like structure has been successfully formed in the 40% HF with 7hours of etching time and 20ml of HF quantity. Moreover, during the synthesis of electrode material, its resistance must be less. It can be observed from the resistance measurement graph that the resistance value with 40% HF is less than 30% HF but higher than 20% HF. However, no accordion-like structure is achieved in 20% HF and its morphology is similar to that of MAX precursor which shows that the conversion of MAX to MXene has not successfully occurred although its resistance is less. Thus, the 40% HF is selected for further studies. But the resistance results with 20% HF have created a dilemma and thus the 20% HF is also taken for further studies by increasing the HF quantity that whether increasing the quantity helps in achieving the accordion-like structure along with the decreased resistance. Hence, results with 20% HF are thus carried forward in section 3.1.4.

3.1.3. VARYING THE ETCHING TIME

The HF etching time is one of the major process parameters that will affect the process of MXene synthesis and MXene properties. Different etching times will lead to different flake sizes, the color of MXene slurry, morphology, *etc.* Experimental parameters for the different samples synthesized

corresponding to different etching times while keeping other parameters constant is summarized in Table 3.3.

Table 3.3: Synthesis of MXene at different experimental parameters.

Samples	Etching Time	HF Concentration	HF Quantity
1.	3:30hrs	40%	20ml
2.	5hrs	40%	20ml
3.	7hrs	40%	20ml
4.	9hrs	40%	20ml

3.1.3.1.MORPHOLOGICAL ANALYSIS

As per the previous study on HF concentration, 40% of the HF is kept fixed because of the successful synthesis of the accordion-like MXene structure. In this study, the etching time has been varied from 3:30 hrs to 9 hrs to see the effect on structural and electrical properties of MXene and the results are compared with MAX precursor. Figure 3.7 depicts their corresponding SEM images.

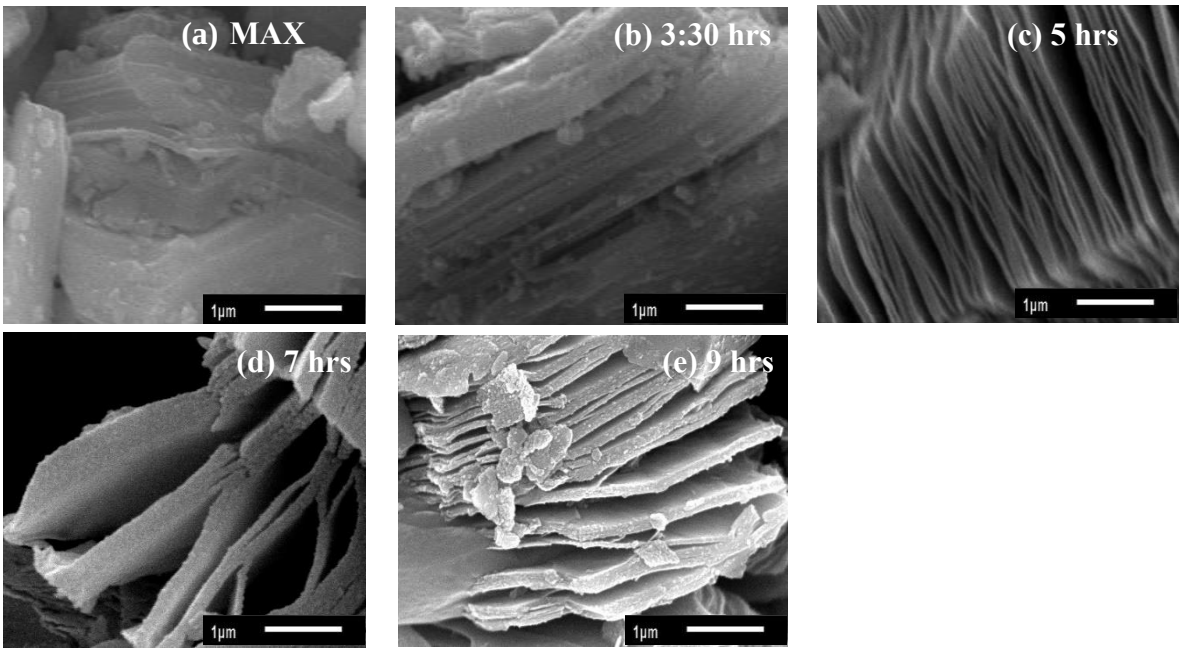

Figure 3.7: SEM for different etching times (a)MAX, (b) 3:30 hours, (c) 5hours, (d) 7 hours and (e) 9 hours. All the measurements are at 1µm of magnification and with (40% and 20ml of HF)

Figure 3.7 (a) shows the MAX precursor layered morphology. It can be observed in the MAX structure is tightly packed with no spacing i.e., different M and X layers are tightly bonded with aluminum thus, exhibiting a 3D structure. Figures 3.7 (b-e) show the layered MXene structure on treating MAX with hydrofluoric acid at various etching times. It can be seen in figure 3.7 (b) that etching with 3:30 hours are not sufficient as the spacing of the layers is not enhanced and still exhibits a packed structure. However, it can be observed from figure 3.7 (c-e) that increasing the etching time the spacing between the MX layer keeps on increasing leading to the formation of requiring accordion-like MXene structure. However, it can be seen in figure 3.7 (d) that spacing has been enhanced by increasing the etching time as compared to the spacing obtained in figure 3.7 (c).

Moreover, in figure 3.7 (e), it has been observed that as the etching time has been further increased to 9 hours a similar kind of structure with almost similar spacing is obtained as shown in figure 3.7 (d). Hence, it can be summarized that the etching time of 7 hours or more will lead to saturation in exfoliation and spacing between the different MX sheets.

To further confirm the removal of aluminum from MAX, XRD is performed at different etching times and compared in figure 3.8. The peaks corresponding to (002), (104) are the two main peaks that provide complete information about the formation of MXene. The effect of varying etching time on these two peaks are explained below. The height of (104) peak at 39º accounts for the presence of aluminum content in the MXene [143]. It clearly shows that the highest intensity of the (104) peak appears in MAX precursor whereas the peak height remains almost constant in 3:30 hrs etching, decreases in 5hrs etching, and disappears finally on etching with HF at 7hrs and 9hrs.

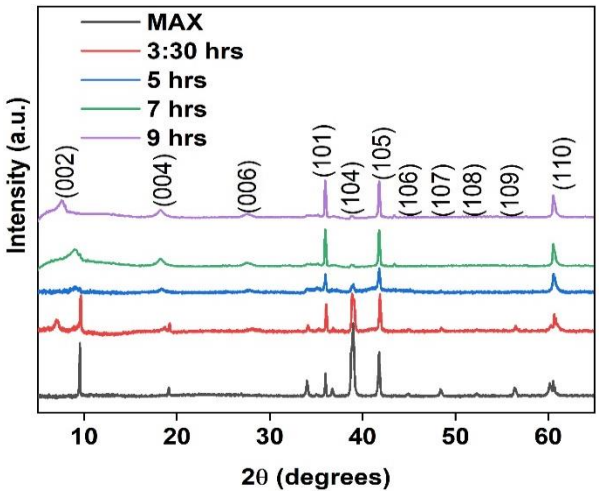

Figure 3.8: XRD patterns depicting MXene formation at different etching times with (40% and 20ml of HF).

Also, the peak at (002) provides information related to the spacing between different MXene sheets[143]. It is observed that the (002) peak is very sharp and narrow in the MAX precursor which means the spacing between different MXene layers is negligible and aluminum presence is maximum. Whereas, on increasing the etching time from 3:30 hr to 9 hr the (002) peak starts to broaden and also shifts from a higher angle to the lower angle as can be seen from figure 3.8. This shifting towards a lower angle shows that the d-spacing of MXene layers has been increased. Hence, such MXene layers with high spacing are the best 2-D electrode material for supercapacitor application as more spacing will increase the intercalation of different ions and thus enhances the energy storage. The d-spacing of different MX sheets at different etching times is illustrated through Table 3.4. Moreover, the XRD peaks at (106), (108), and (109) corresponds to the presence of defects or the by-products which are formed during the reaction of hydrofluoric acid with the MAX precursor.

Table 3.4: Angles and d-spacing corresponding to (002) peak

S.NO	Etching time	(002) Peak position	d-spacing (nm)
1.	MAX	9.5º	0.926
2.	3:30hrs	9.0º	0.980
3.	5hrs	7.1º	1.242
4.	7hrs	6.9º	1.292
5.	9hrs	6.6º	1.310

The appearance of these peaks in 3:30 hrs etching is due to the insufficient time the HF acid receives to etch the aluminium and removal of the by-products formed during the reaction. On increasing the etching time further to 7hrs and 9hrs, these peaks completely disappear which confirms the successful removal of all the by-products formed during the reaction.

3.1.3.2.EFFECT OF ETCHING TIME ON THE RESISTANCE OF MXene

The resistance of an electrode material affects the properties of the energy storage device significantly.

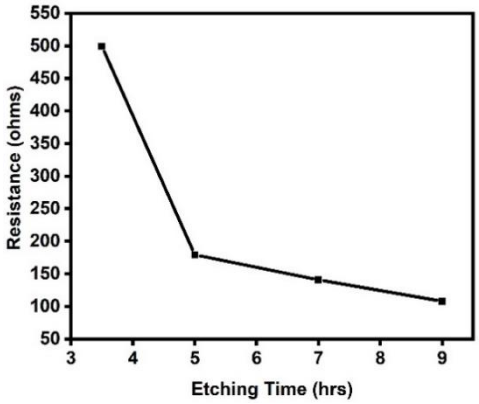

Figure 3.9: Variation of resistance at different etching times and with (40% and 20ml of HF).

The different MXene powder synthesized by varying the etching times is transformed into thin films on the glass substrate and further compared for the resistance measurement. It can be seen from figure 3.9 that as the etching time increases, resistance decreases. This is because when the concentration remains the same, the 9hrs solution gets the maximum time to remove the byproducts. Thus, the value of resistance decreases to a minimum of 108 ohms in 9hrs as compared to 499.5 ohms in 3:30hrs.

Thus, the results of varying the etching time have shown that increasing the time after 7 hours produces similar results as with 9 hours. The accordion-like structure, interlayer spacing and the resistance results obtained with 9 hours are comparable to the results obtained with 7 hours of etching time. Moreover, the etching times less than 7 hours have not successfully produced the accordion-like structure with increased resistance. Thus, in this work, 7 hours of etching time is selected for further studies.

3.1.4. EFFECT OF HF QUANTITY ON MXene PROPERTIES

One more important factor affecting the MXene synthesis is the HF quantity for etching aluminum from the MAX phase. The HF quantity is increased to investigate its effect on MXene synthesis. In this study, two different experiments have been designed which are as follows:

A) Effect of HF quantity with 20% HF concentration: as it can be seen from figure 3.4 (b) when HF concentration was taken 20%, the exfoliation of MAX layer gets initiated only at some locations. The idea of this experiment was to keep the HF concentration as low as possible.

Table 3.5: Synthesis of MXene at different experimental parameters.

S.No	HF quantity	HF concentration	Etching time
1.	20 ml	20%	7hrs
2.	40 ml	20%	7 hrs

Thus, the HF quantity has been varied to 40 ml by keeping HF concentration at 20% to see its effect on the structural properties of MXene layers. Summary of different experimental parameters is given in table 3.5.

The effect of varying the HF quantity on the XRD pattern with 20% HF is depicted in figure 3.10. It can be seen that the intensity of (104) peak remains high in both the graphs shown in figure 3.10. Moreover, in both cases, two different (002) peaks are observed which suggests the non-uniform etching of Al. Hence, it can be clearly said that on increasing the HF quantity, aluminum removal remains the same even when the quantity of HF is increased. However, as expected, (109) peak appears in 40 ml HF which corresponds to the occurrence of defects since the greater HF quantity

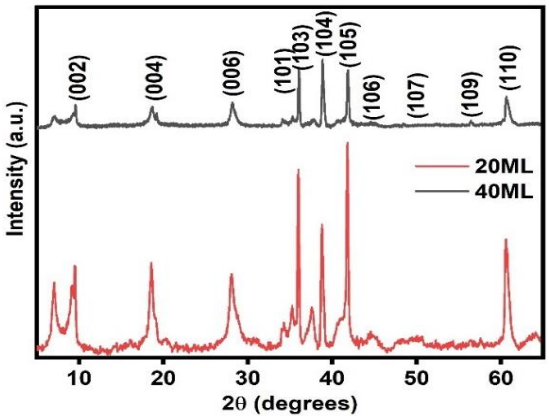

Figure 3.10: XRD pattern for different quantities of HF at 20% HF.

leads to the increase in fluorine content. Also, in Table 3.6 it can be seen that on increasing the HF quantity with 20% HF, the resistance in 40ml HF is comparable to that obtained in 20ml HF which depicts that the quantity does not affect in enhancing the electrical and structural performance of MXene.

Table 3.6: Resistance values for different values of HF quantity at 20% HF concentration.

S.No	HF quantity	Resistance
1.	20 ml	65 ohms
2.	40 ml	59 ohms

Thus, it can be seen that 20% HF is not sufficient to etch aluminum at all which suggests that a greater concentration of HF is the necessary condition for the successful formation of MXene.

B) Effect of HF quantity with 40 % HF concentration: In this experiment, the HF quantity has been varied from 20 to 40 ml by keeping the 40 % HF concentration. Summary of different experimental parameters is given in Table 3.7.

Table 3.7: Synthesis of MXene at different experimental parameters.

Samples	HF Quantity	HF Concentration	Etching Time
1.	40ml	40%	7hrs
2.	20ml	40%	7hrs
3.	30ml	40%	7hrs

SEM images of titanium carbide (MXene) at an increased quantity of HF are shown in figure 3.11. It is observed that with 20ml, 30ml, and 40ml HF quantity, the accordion-like structure is formed successfully. However, the small particles start accumulating on the surface of MXene as we

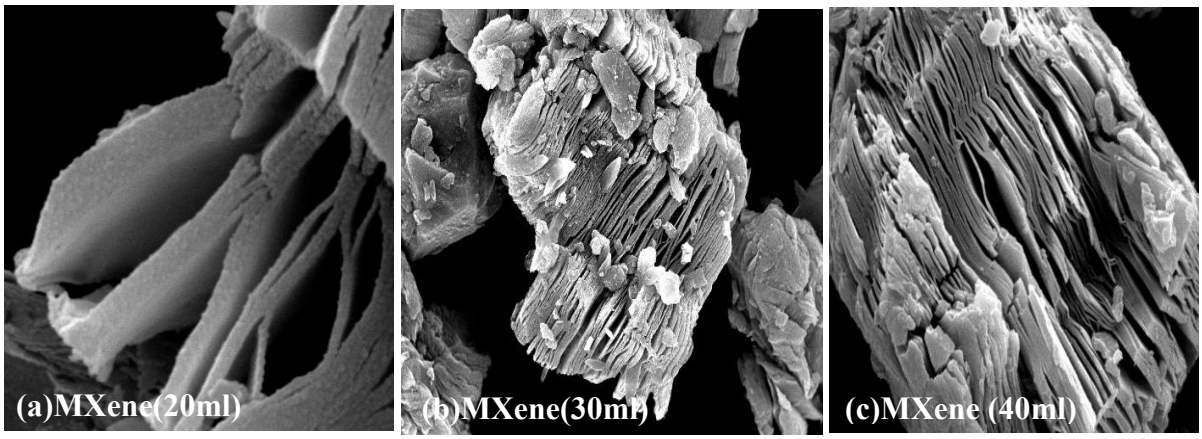

Figure 3.11: SEM corresponding to 20ml, 30ml ,and 40ml of 40% HF. All the measurements are at 1µm of magnification and with (7hrs and 20ml of HF).

increase the HF quantity to 30ml and 40ml. These small particles may correspond to fluorine groups appearing on the side view of the MXene. This illustrates that the defects start forming on the surface of MXene due to the use of a higher quantity of fluorine which thus increases the growth of AlF_3.

To confirm the successful etching or removal of aluminum from the MAX phase, XRD measurements are performed. XRD patterns for the 20ml, 30ml, and 40ml of HF quantity are

shown in figure 3.12. The (104) peak at 39º corresponds to the aluminum presence and the peak at 27º represents that aluminum elimination starts from the MAX phase.

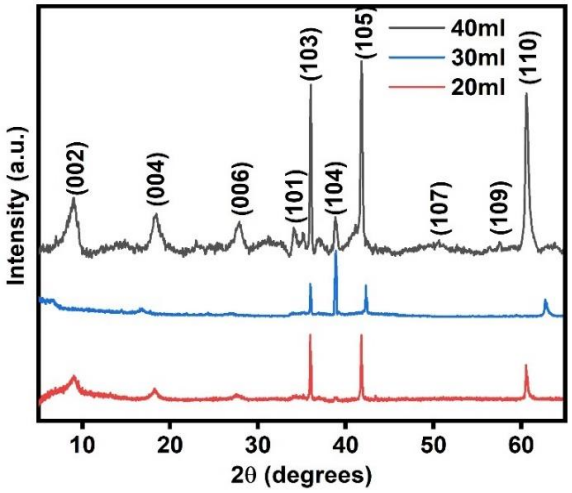

Figure 3.12: XRD pattern for different quantities of HF at 40% HF etched for 7 hours.

It can be seen from the XRD that the HF quantity strongly influences the MXene properties. It is observed that the (104) peak intensity starts increasing as the quantity has been increased from 20 ml to 40 ml. As observed from the SEM images of 30ml and 40ml HF in figure 3.11, the small particles accumulating on the surface of MXene may be of AlF_3. These particles may lead to the presence of (104) peak in the XRD pattern of 30ml and 40ml HF. However, the appearance of (110) peak in all the samples at 60º confirms that the MXene structure is layered as observed from its SEM images. Moreover, (109) peak start appearing because of the several by-products and defects with increased HF quantity.

Hence, it can be concluded that increasing the HF quantity will lead to an increase in the growth of AlF_3 because of the increase O/F ratio. This will lead to an increase in the number of defects.

3.1.4.1.EFFECT OF HF QUANTITY ON THE RESISTANCE

Moreover, the effect of HF quantity on the resistance is analyzed using Keithley 4200-SCS. It can be observed from figure 3.13 that on increasing the HF quantity, the resistance first decreases and then increases. The byproducts, defects, and aluminum content in the 20ml HF is minimum as confirmed by figure 3.12 which provides maximum resistance as shown in figure 3.13. However, in 30 ml and 40ml HF, although the resistance decreases because of the aluminum presence, the increased fluorine content starts appearing on the surface of MXene which start increasing the defects as can be seen from figure 3.11. Thus, it restricts the surface area available for the

electrolyte ions to penetrate the electrode material. Thus, the 30ml and 40ml HF quantities are rejected as it reduces the surface area although the resistance is less.

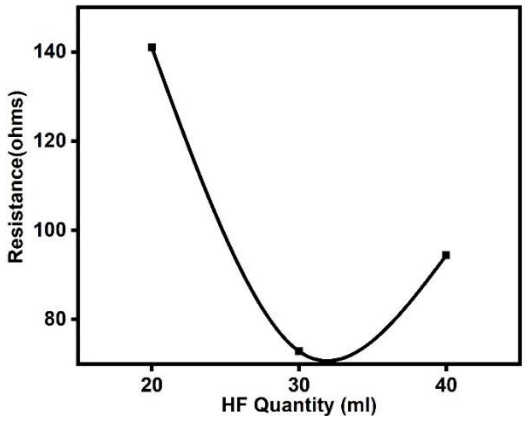

Figure 3.13: Effect of HF quantity on resistance of the film.

Thus, from all the experiments performed above, the MXene formation parameters are selected to be maximum etching time(7hrs), sufficient concentration (40%), and minimum quantity (20ml).

3.1.5. PREPARATION OF FEW-LAYERED MXene

Further, to obtain the few-layered MXene from a multi-layered structure, the prepared powder is mixed in an inorganic compound named dimethyl sulfoxide (DMSO).

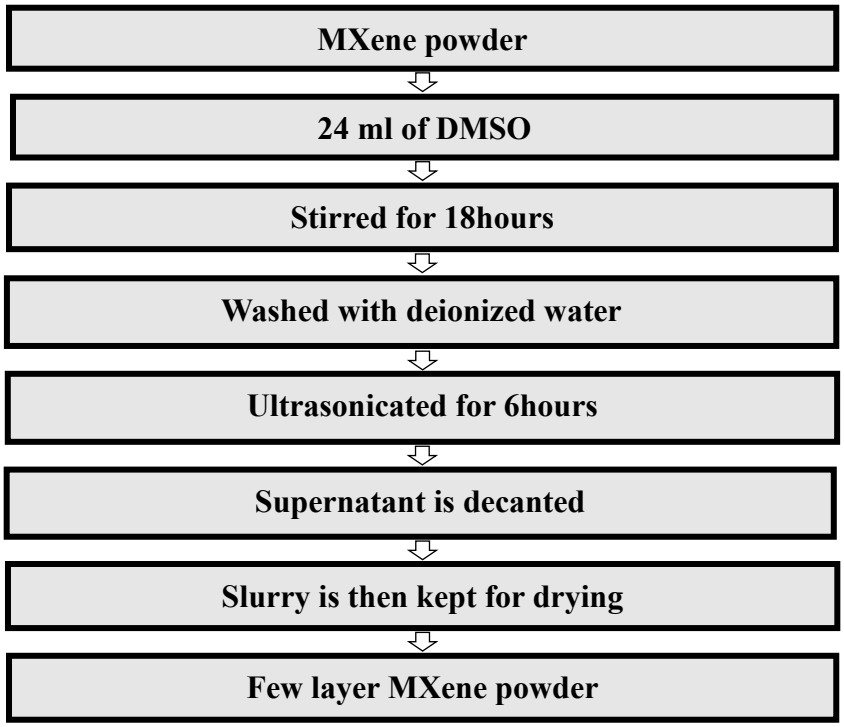

Figure 3.14: Flow chart showing the synthesis of few-layered MXene

The steps involving the formation of a few-layered MXene from the MAX precursor and are illustrated through the flow chart diagram as shown in figure 3.14. Initially, 24 mL of inorganic compound DMSO is added into 1g of multi-layered MXene powder. It is then stirred magnetically at room temperature for 18 hours. Further, to the above-stirred solution, deionized water is added in the weight ratio of 1:300 and ultrasonicated for 6 hours to obtain the small flakes of a few-layered MXene. Thereafter, the centrifugation at an rpm of 3500 of the few-layered colloidal solution of MXene ($Ti_3C_2T_x$) is carried for 1 hour using centrifugate as shown in figure 3.15. Finally, the precipitated DMSO intercalated MXene is collected and the supernatant is decanted. The slurry thus collected behind is then kept for drying at room temperature.

Figure 3.15: Diagram illustrating the centrifuge equipment.

3.1.5.1 STRUCTURAL MORPHOLOGY

Figure 3.16 illustrates the SEM images corresponding to MXene, DMSO treated MXene. It can be seen from figure 3.16 (a) that $Ti_3C_2T_X$ MXene layers show layered morphology and have a multilayer accordion-like structure which indicates the successful removal of aluminum layers.

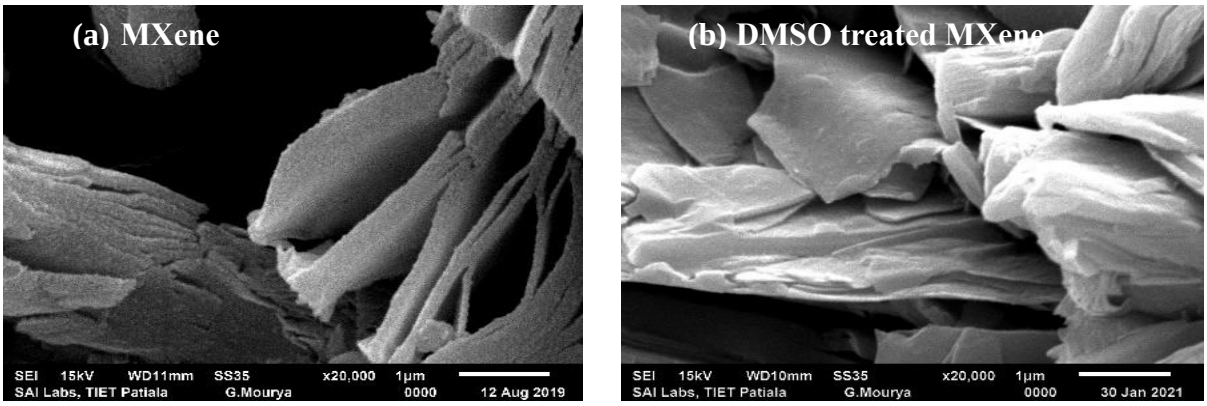

Figure 3.16: SEM images of (a) bare MXene, (b) DMSO treated MXene.

However, in figure 3.16 (b), the multilayer structure becomes few-layered nanosheets after sonication. The crumpled surface of few-layered MXene shows good flexibility with ultrathin thickness, demonstrating the successful preparation of high-quality few-layered MXene nanosheets.

3.2.SYNTHESIS OF COPPER SULFIDE (Cu_2S) POWDER

Copper sulfide (Cu_2S) has a bandgap of 1.2eV and is a p-type semiconductor material [144]. However, the use of copper sulfide in a supercapacitor is very limited which thus opens various

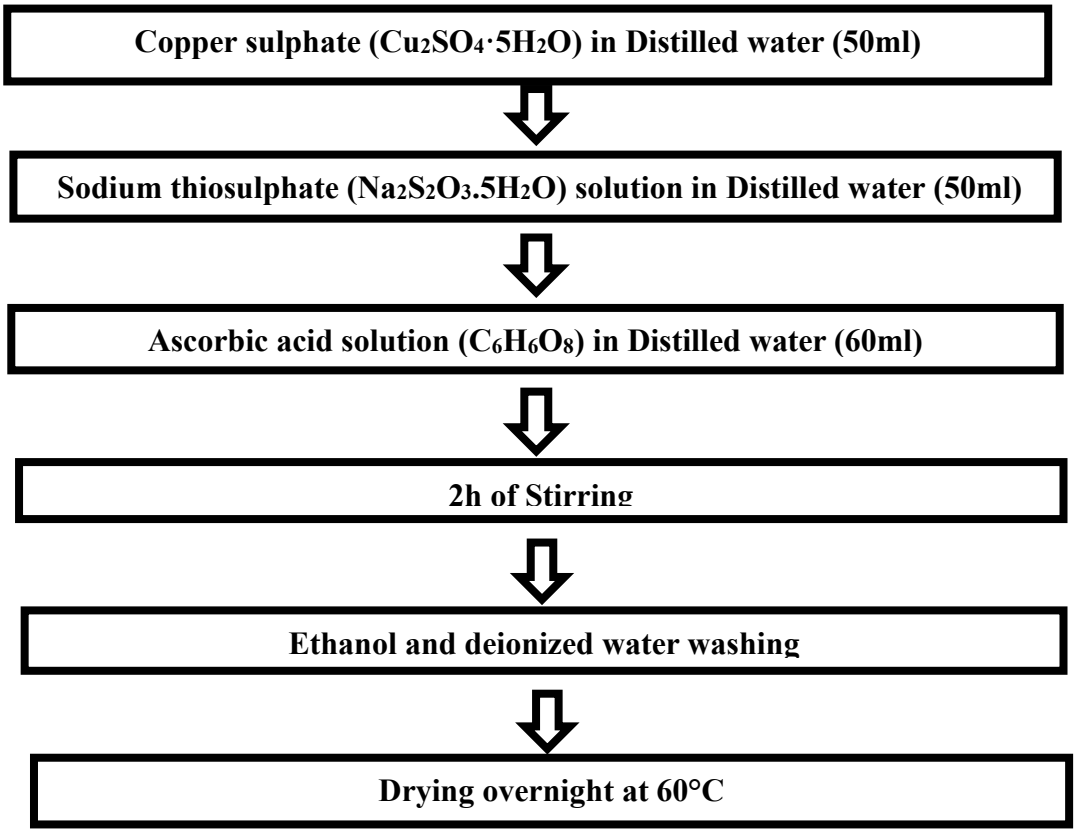

Figure 3.17: Flow chart illustrating the steps for synthesis of Cu_2S.

new interests and avenues for various researchers to meet the growing energy demands. In the present work, sodium thiosulphate is used as a reducing agent that reduces Cu^{2+} to Cu^{1+} and helps in preparing Cu_2S hollow rods taking shorter reaction times. All the reagents used for the preparation of copper sulfide hollow rods are used directly without any further processing technique. The process begins by stirring 10 mmol of copper sulphate pentahydrate ($CuSO_4 \cdot 5H_2O$) into 50 ml of distilled water as shown in figure 3.17. This results in a clear blue solution. Afterward, 7.5 mmol of sodium thiosulphate ($Na_2S_2O_3 \cdot 5H_2O$) is added into the copper sulphate solution. Next, 3.4 mmol of ascorbic acid is magnetically stirred in 60 mL distilled water which is then

added dropwise to the solution containing copper sulphate and sodium thiosulphate and magnetically stirred for 2h. During stirring, it is perceived that the solution changes its color from blue to green to yellow and then finally into red-brown as shown in figure 3.18. Later, the prepared sample is washed thoroughly with ethanol and deionized water till its pH becomes neutral. Then the slurry collected behind is kept for drying at 60°C overnight for obtaining copper sulfide powder.

The reactions occurring during the preparation of copper sulfide is shown in equation (1) [145]:

$$2CuSO_4 + Na_2S_2O_3 + C_6H_6O_8 + H_2O \rightarrow Cu_2S + Na_2SO_4 + 2H_2SO_4 + C_6H_6O_6 \quad \text{.....(1)}$$

Figure 3.18: Effect of precursors on the color of supernatant.

The concentration of sodium thiosulphate has a strong impact on the preparation of copper sulfide because it acts as a reducing agent which leads to the oxidation of copper from Cu^{2+} to Cu^{1+}. Thus, in this study, the impact of $Na_2S_2O_3 \cdot 5H_2O$ on the properties of copper sulfide has been studied. The ratio of copper sulphate and sodium thiosulphate has been varied from 1:0.5 to 1:1.5 with the step size of 0.5 and the samples termed as Cu_2S-1:0.5, Cu_2S-1:1, and Cu_2S-1:1.5 respectively.

3.2.1. MATERIAL CHARACTERIZATION

The composition and morphological analysis of all the copper sulfide samples (Cu_2S-1:0.5, Cu_2S 1:1, and Cu_2S-1:1.5) are examined through X-ray diffraction (XRD) and scanning electron microscopy (SEM).

3.2.2. STRUCTURAL MORPHOLOGY

The XRD is used to examine the purity and composition of the synthesized samples termed as and morphology Cu_2S-1:0.5, Cu_2S-1:1, Cu_2S-1:1.5 as shown in figure 3.19.

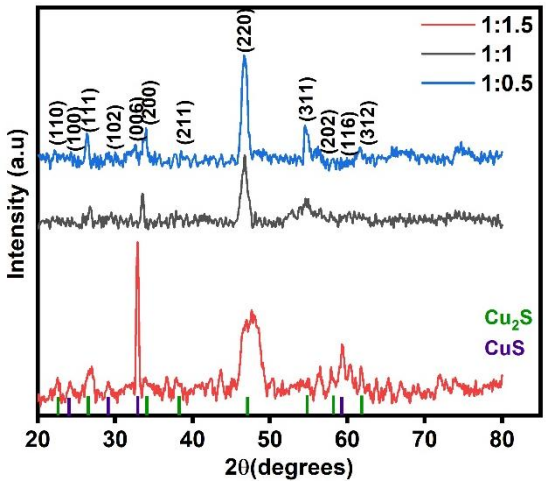

Figure 3.19: XRD pattern for different Cu_2S samples synthesized.

The corresponding XRD patterns of Cu_2S-1:0.5, Cu_2S-1:1, Cu_2S-1:1.5 are shown in figure 3.19. The dominant diffraction peaks in all the three samples are assigned to the Joint Committee on Powder Diffraction Standards (JCPDS) data of Cu_2S (JCPDS card No. 53-0522), which are located at 2θ = 22.581°, 27.766°, 32.111°, 39.645°, 46.103°, 54.672°, and 61° corresponding to the crystallographic planes d(110), d(111), d(200), d(211), d(220), d(311), and d(312) respectively. It thus, confirms the successful preparation of Cu_2S. Despite all the above-mentioned peaks for Cu_2S, there are peaks indexed at d(100), d(102), d(006), d(202), and d(116) in Cu_2S(1:1.5) which corresponds to the occurrence of CuS.

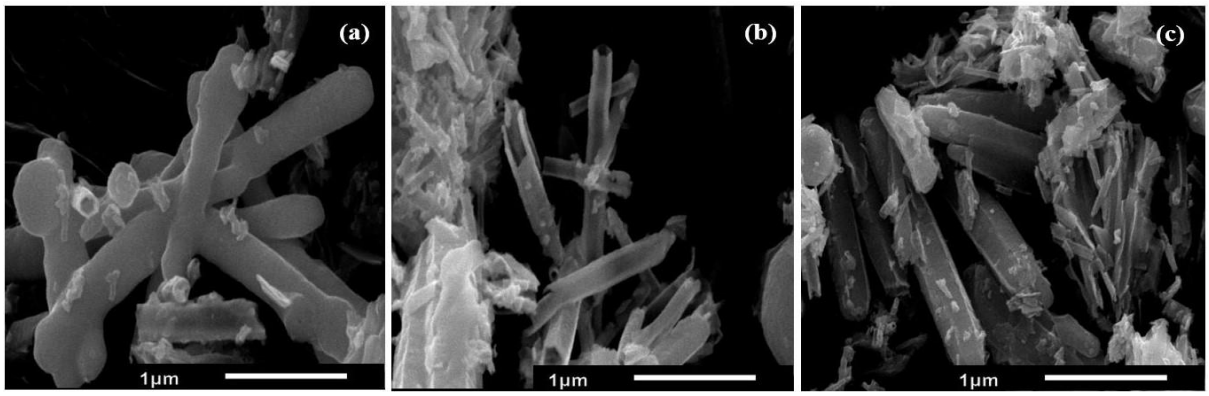

Figure 3.20: SEM images of (a) Deformed microspheres (1:0.5), (b)Hollow rods (1:1), and (c)Nanoparticle arrangement on the surface of the prepared sample (1:1.5).

Further, scanning electron microscopy is used to analyze the structural morphology of all the Cu_2S samples synthesized. The respective SEM images are shown in figure 3.20 (a-c). In figure 3.20 (a) for (1:0.5) Cu_2S sample, it can be observed that at some places the microsphere surface is formed and, in a few locations, the formation of Cu_2S solid rods has been initiated. However, in figure

3.20 (b) when the ratio of copper sulphate and sodium thiosulphate has been increased to 1:1, more sulphur concentration is available to react with copper. The large number of alveolate pores are presented on the surface of the nanorods which act as the driving forces mainly for hollow rods. The sulphur particles react faster on corners rather than sides converting the closed structure hollow. The growth of crystal domain in the wall structure leads to the opening of crystal boundaries in the polycrystalline structure which thus resulted in the porous surface. The development of the hollow structure of Cu_2S (1:1) is observed from the captured SEM images. The distinct cavities can be seen from the partially broken rods which will benefit the electrolyte ions to penetrate in the electrode material providing better capacitance performance. Afterward, on increasing the ratio further to Cu_2S-1:1.5 in figure 3.20 (c), a higher percentage of thiosulphate solution occurs in the reaction medium, which will lead to a stack of various nanoparticles on the surface of hollow rods and thus reducing its surface area. An excess of thiosulphate appears to perform the reduction completely which leads to the further oxidation of Cu_2S to CuS. Unlike the Cu_2S (1:0.5 and 1:1) sample, the instantaneous existence of excessive Na_2S leads to immediate non-equilibrated transformation into small CuS particles with random morphologies. Thus, it can be concluded from the SEM images that changing the ratio of copper sulphate to sodium thiosulphate seems to have a remarkable effect on the structural properties of Cu_2S. This is highly expected as sodium thiosulphate [$Na_2S_2O_3 \cdot 5H_2O$] dissolves in water to give thiosulfate ion ($S_2O_3^{2-}$) and acts as a useful reducing agent however, copper (II) sulphate [$CuSO_4 \cdot 5H_2O$] dissolves to give cupric ion (Cu^{2+}) and thus acts as an oxidizing agent. The result shows that the optimum addition of sodium thiosulphate allows for the formation of a hollow Cu_2S structure.

CHAPTER 4

FABRICATION AND CHARACTERIZATION OF SUPERCAPACITOR DEVICES

In this chapter, the fabrication of a supercapacitor device using MXene and copper sulfide (Cu_2S) as an electrode material is carried on flexible polypropylene substrate, polyethylene terephthalate as well as a rigid glass substrate. The fabrication of MXene and copper sulfide (Cu_2S) based supercapacitor on the polypropylene substrate is reported for the first time. The flexible PP and PET substrates are selected because of their excellent moisture barrier characteristics, flexibility, high melting point, good tensile strength, great mechanical properties such as toughness and stiffness.

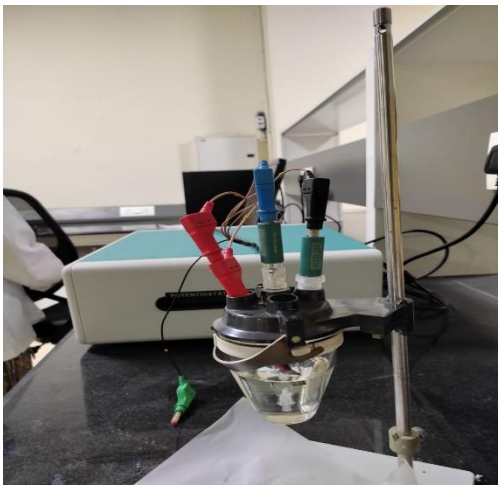

Figure 4.1: Electrochemical setup for three-electrode cell test system.

The behavior of the fabricated samples of MXene and copper sulfide (Cu_2S) are analyzed by performing the electrochemical experiments such as Cyclic voltammetry (CV), Galvanostatic charge-discharge (GCD), Electrochemical impedance spectroscopy (EIS), capacitance retention on the Metrohm auto lab workstation as shown in figure 4.1. The electrochemical measurement results of the MXene and copper sulfide on the polypropylene substrate are compared with their results on the glass as well as polyethylene terephthalate substrates.

4.1. CALCULATION OF VARIOUS PARAMETERS

The Metrohm auto lab workstation is used to calculate various parameters for evaluating the device performance which is calculated using the formulas as mentioned below:

4.1.1. CAPACITANCE FROM CYCLIC VOLTAMMETRY

The calculation of specific capacitance, C_s (F/cm^2) is carried from cyclic voltammetry curves according to equation (4.1)

$$C_s = \int_{v_1}^{v_2} Idv / Av\Delta V \text{.....(4.1)}$$

where $\int Idv$ is the area under the curve, ΔV is the potential window, A is the area of the working electrode, *v* is the scan rate.

4.1.2. CAPACITANCE RETENTION FROM GALVANOSTATIC CHARGE-DISCHARGE CURVES

The capacitance retentions have been measured from galvanostatic charge-discharge curves according to equation (4.2)

$$C_s = I\frac{\Delta t}{m\Delta V} \text{.....(4.2)}$$

Where I/m is the current density in A/g, Δt is the discharge time and ΔV is the discharge voltage.

4.1.3. ENERGY DENSITY AND POWER DENSITY FROM GALVANOSTATIC CHARGE-DISCHARGE CURVES

The device performance has been evaluated by calculating the energy density and power density of the supercapacitor. The formula for solving the energy density (Wh/Kg) and power density (W/Kg) is given in equation 4.3 and 4.4 as:

$$E = \frac{C_s * \Delta V * \Delta V}{2} \text{.....(4.3)}$$

$$P = \frac{E}{\Delta t} \text{.....(4.4)}$$

Where E is energy density, C_s is specific capacitance, ΔV is discharging voltage, P is power density, Δt is the discharging time.

The three electrode test system is used to investigate the samples in 6M KOH electrolyte at room temperature. The test system comprises the working electrode, reference, and counter electrode. The voltage is applied between the working and reference electrode whereas the measurement of current is taken across the working and counter electrode. The reference and counter electrodes comprise platinum and silver/silver chloride electrodes. The working electrodes are prepared by mixing active materials with polyvinylidene fluoride (PVDF) binder and conducting carbon black

in a weight ratio of 80: 10: 10 with a few drops of N-methyl-2-pyrrolidone (NMP) solvent to obtain a homogenous slurry. The slurry is then spin-coated to obtain a uniform film on glass, PET, and PP substrates having a geometric surface area of about 1cm^2 as shown in figure 4.2 (a-c). The film is then dried at 60°C for 24 hours The working electrode is composed of 2mg of active material after drying.

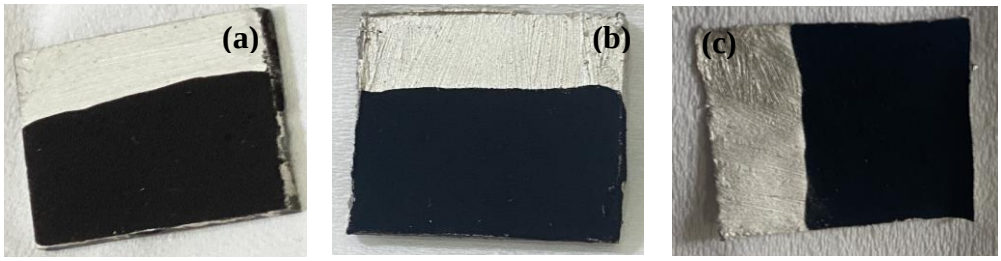

Figure 4.2: Fabrication of working electrode over (a) Glass, (b) PET, and (c) PP substrates.

4.2. MXene BASED SUPERCAPACITOR DEVICE

The MXene based supercapacitor device is fabricated using the optimized parameters such as etching time(7hrs), HF concentration (40%), and HF quantity (20ml) for MXene formation from the MAX precursor. The MXene layer is deposited on different substrates *i.e.* both rigid and flexible such as PET, PP, and glass. The electrochemical measurement of electrode materials such as MXene and copper sulfide (Cu_2S) deposited on the flexible PP substrate are then analyzed and compared with the MXene deposited over PET and glass substrate.

The fabricated images of the supercapacitor device on the glass as well as flexible PET and PP substrates are shown in figure 4.3 (a-c). In figure 4.3 (a) the symmetrical supercapacitor is formed by depositing MXene on two glass slides in between which a filter paper as a separator

Figure 4.3: Fabrication of symmetrical supercapacitor device on (a) Glass, (b) PP, and (c) PET substrates.

is present dipped in an electrolyte solution. Moreover, to hold the device, paper clips are attached. Similarly, in figure 4.3 (b) and figure 4.3 (c) symmetrical supercapacitor is made by depositing MXene over two PP sheets and PET sheets separately in between which a separator (filter paper) is present. Again to hold the device, paper clips are attached.

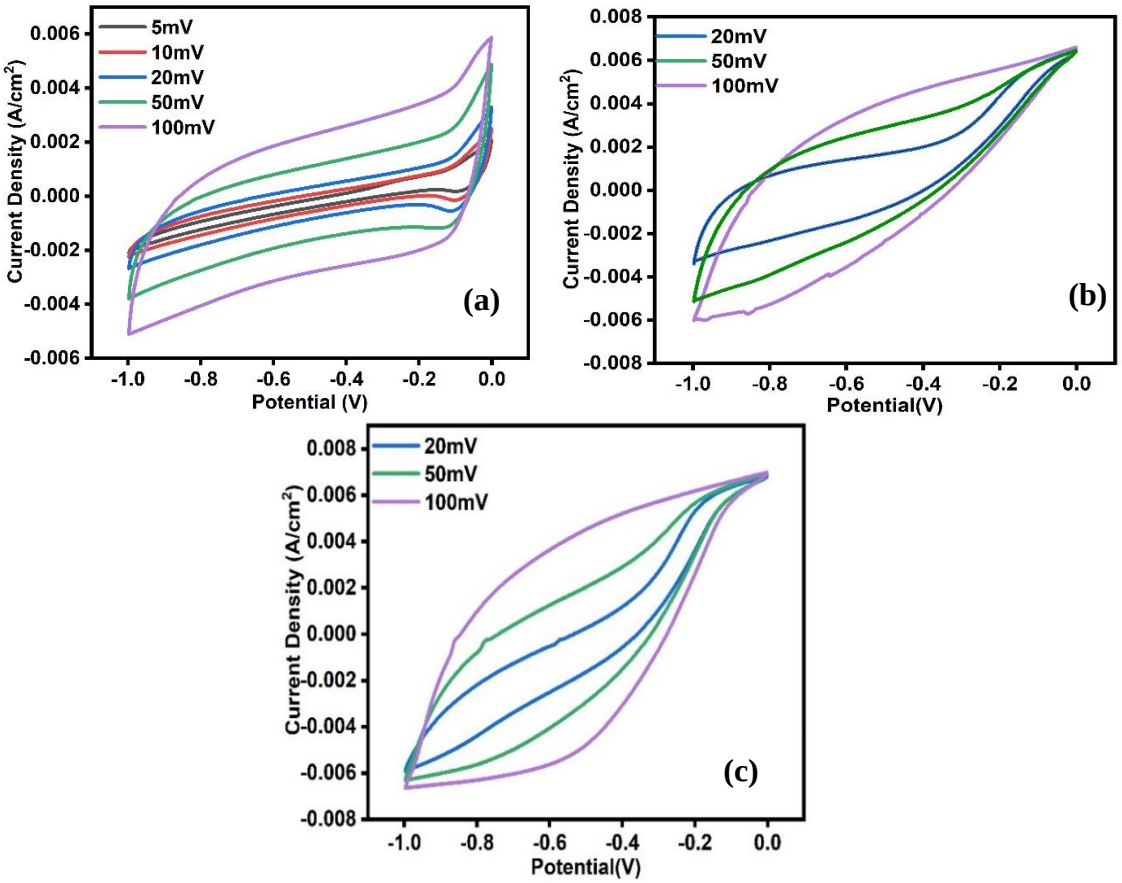

Figure 4.4: Electrochemical performance of MXene based supercapacitor deposited on different substrates (a) Polypropylene (b) Poly-ethylene terephthalate (c) Glass.

The cyclic voltammograms (CV) measurements at the MXene as working electrodes are carried by applying the voltage between -1V to 0V to the working electrode at the scan rates between 5 to 100mV/s on PP substrates and 20, 50, 100 mV for PET and glass substrates as shown in figure 4.4. Figure 4.4 (a) shows the CV of MXene deposited on the PP substrate whereas the CV of MXene for PET and glass substrate is plotted in figures 4.4 (b) and 4.4 (c). From the equation of power law, the relation of current and scan rates can be observed from equation 4.5 in which the value

$$I = aV^b \text{.....(4.5)}$$

of b tells the mechanism behind energy storage. If the value of b is close to 0.5, the process is diffusion-controlled whereas if the value of b is near to 1, the process is surface capacitive

controlled [26]. When log(I) is plotted against log (V) at a potential of -0.10656 corresponding to figure 4.4 (a), the value of b=1.345 indicated the pseudocapacitive behavior. Thus, the appearance of a couple of redox peaks in PET and PP becomes obvious that again signifies their pseudocapacitive behavior. However, the slight change in the rectangular shape is due to the current overloading with respect to the voltage. It can be seen in figure 4.4 that the electrochemical curves do not show any detectable change in the shape of the graph on increasing scan rate which shows that electron transport and the charge separation rate is very fast. On increasing the scan rate, the ions do not get much time to interact with the electrode material hence the current density increases with increasing the scan rate, and then the diffusion-controlled process begins. However, the nearly rectangular and symmetric shape of the cyclic voltammetry curves in figure 4.4 (c) is observed for the MXene deposited on the glass substrate indicating superior capacitive performance.

Further, the cyclic voltammetry performance of MXene deposited on PP, PET, and glass substrates are compared at a scan rate of 50mV/s and illustrated in figure 4.5. The MXene based electrodes on glass, PET, and PP show a maximum specific capacitance of 70mF/cm^2, 66.8 mF/cm^{2,} and 54.44 mF/cm^2 at a scan rate of 50mV/s.

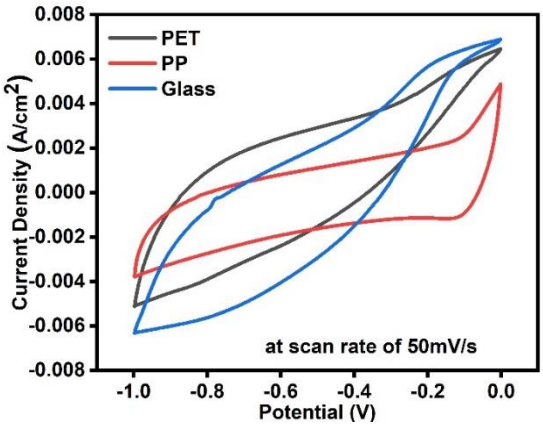

Figure 4.5: The comparison of cyclic voltammetry curves of MXene deposited on Glass, PET, and PP substrates at a scan rate of 50mV/s.

The galvanostatic measurements of MXene deposited over the glass, PP, and PET substrates are shown in figure 4.6. From the results, it can be seen that MXene shows nearly triangular behavior on all of the substrates which indicates that the charge storage and separation are occurring at a fast rate. Moreover, as calculated from the cyclic voltammetry graphs of figure 4.5 that the charge storage is maximum with the glass substrate, which is also confirmed from the galvanostatic

charge-discharge measurements because the maximum time to charge is taking place in the glass substrate and very little time is taken by the MXene on PP substrate because of low capacitance.

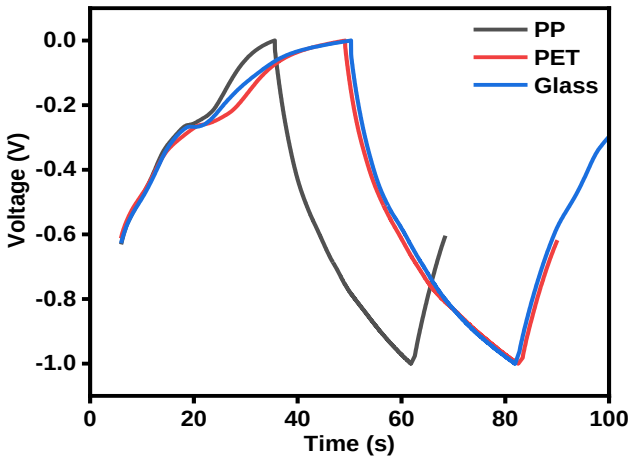

Figure 4.6: Galvanostatic charge-discharge measurement of MXene on Glass, PET, and PP substrates

Further, to understand the capacitive properties shown by MXene on different substrates, the charge transfer, and diffusion-controlled processes are described by performing electrochemical impedance spectroscopy (EIS)[146]. The EIS behavior of the supercapacitor device on glass, PET, and PP substrates is performed in the frequency range of 100 kHz to 0.01 Hz as can be seen from figure 4.7.

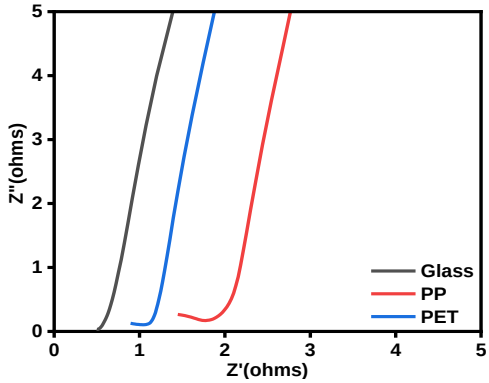

Figure 4.7: EIS behavior of MXene over Glass, PET, and PP substrate at 0.01 Hz to 0.4 Hz.

In the high-frequency i.e., the region with low impedance, the equivalent series resistance (R_s) is represented by the intercept of Nyquist plot on the real axis (Z') which is the sum of intrinsic resistance of the electrode, ionic resistance due to electrolyte, and the contact resistance between the interface of active material and electrode substrate[147]. It can be seen that the minimum series resistance is shown by the MXene over glass substrate which can also be validated from the maximum capacitance in CV and GCD charging time. This is due to that the film on the glass

substrate is crack-free as compared to the film on PP and PET substrate. The value of series resistance calculated for the MXene sample on glass, PET, and PP substrate is 0.5, 0.9, and 1.4 ohms. Further, in the medium frequency region, the arc radii of the semicircle indicate the resistance because of the charge transfer of ions which is also known as the Faraday resistance of the electrode. It has been seen clearly that at medium frequencies, the MXene on glass substrate shows the least arc radii as compared to the film on PET and PP substrate which indicates the charge transfer occurs maximum in glass with minimum resistance. Moreover, in the (high impedance) low-frequency region, the diffusion resistance is shown by the sloped portion of the Nyquist plots which results from the diffusion/transport of electrolyte ions in electrolyte and electrode material. It can also be due to the resistance between the current collector and the electrode material. The more the slope of the Nyquist plots is vertical, the behavior is more capacitive. This sloped portion in impedance is named as Warburg diffusion (Z_w). It can be seen that the glass substrate shows the low values of Z_w as compared to the value of Z_w in PET, PP which indicates the faster nature of the charge storage mechanism in the glass substrate.

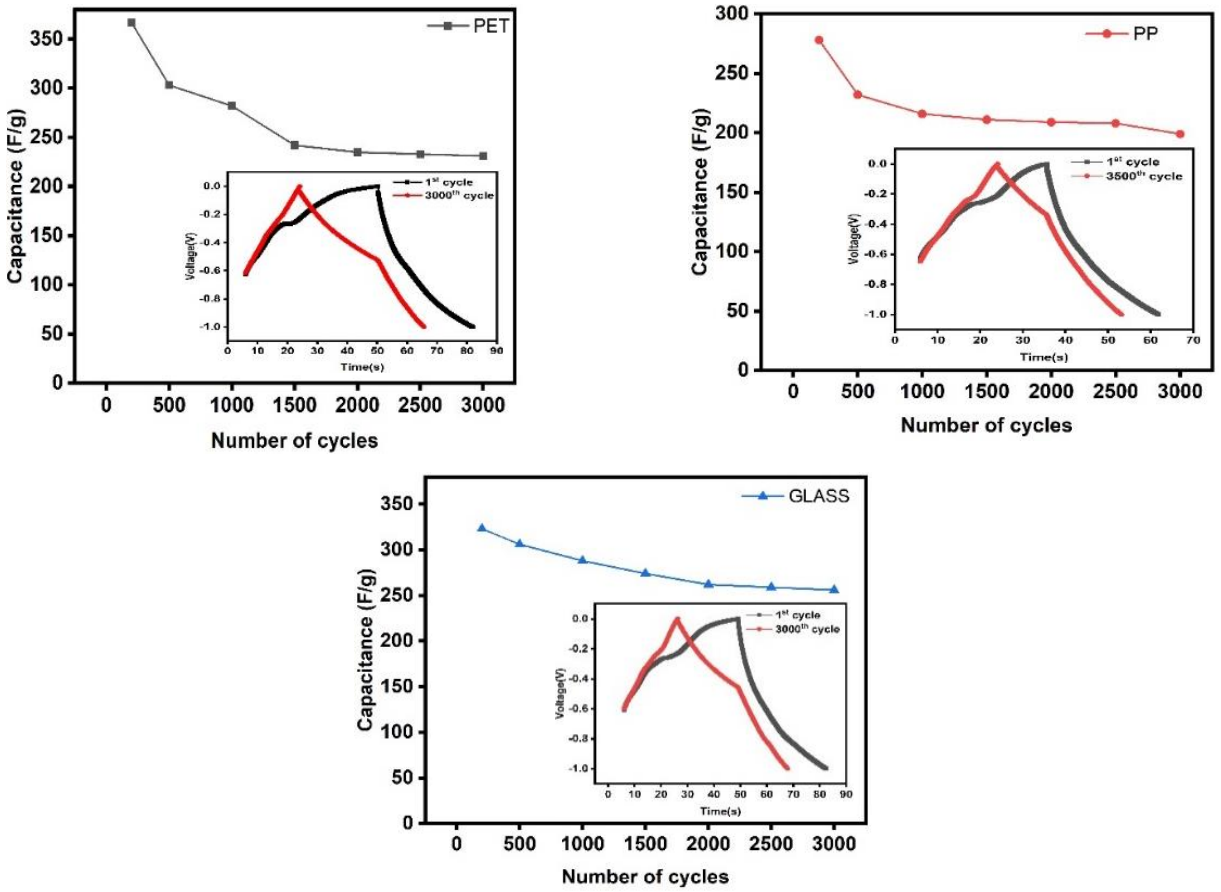

Figure 4.8: Capacitance values vs cycle number of MXene on PET, PP and Glass substrate. The inset image is the galvanostatic charge and discharge curve at 1st and 3000th cycle.

Afterward, the capacitance retention behavior of the MXene sample on Glass, PET, PP substrates is shown in figure 4.8. Here, it can be seen that all the samples exhibit excellent cycle stability with the capacitance retention of 86.7%, 78.7%, and 74.14% respectively on the Glass, PET, PP substrate after 3000 cycles.

Moreover, as per Equations 4.3 and 4.4 the device exhibits an energy density of 4.82Wh/Kg, 5.60Wh/Kg, and 6.37Wh/Kg, and power density of 624.14W/Kg, 624.17W/Kg and 624.80W/Kg on PP, PET, and glass substrates.

4.3. COPPER SULFIDE BASED SUPERCAPACITOR DEVICE (Cu_2S)

The electrochemical characterization such as cyclic voltammetry (CV), galvanostatic charge-discharge (GCD), and EIS are performed to investigate the supercapacitive performance of the prepared samples using Metrohm auto lab electrochemical workstation. For the cyclic voltammetry measurement, the Cu_2S based supercapacitor devices are coated on polypropylene (PP), polyethylene terephthalate (PET), and glass substrates which act as a working electrode.

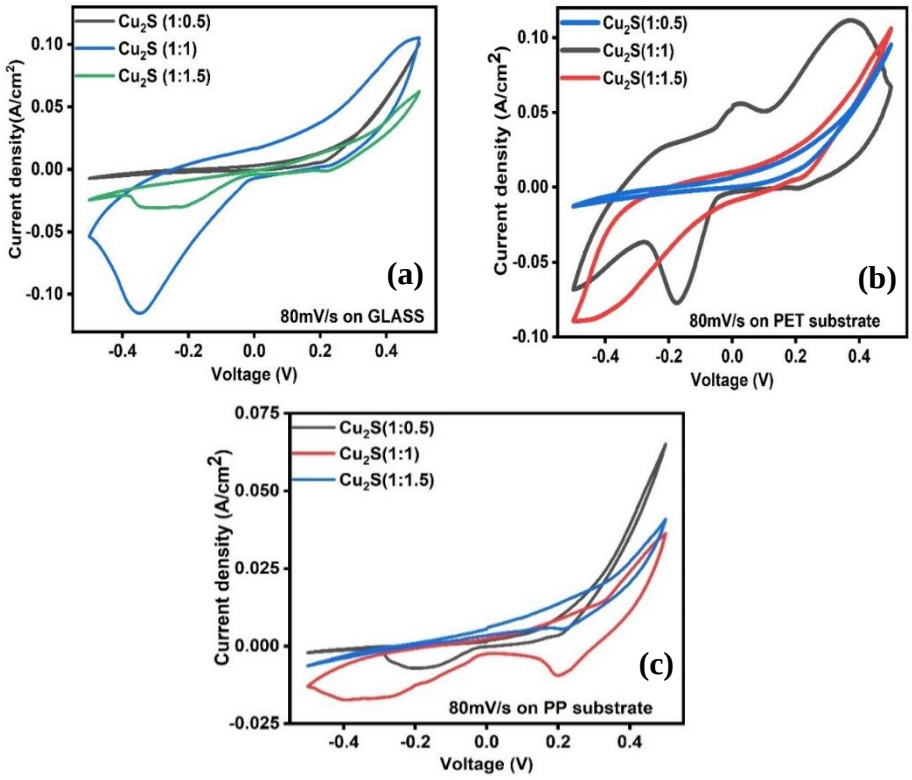

Figure 4.9: Comparison of CV curves of Cu_2S-1:0.5, Cu_2S-1:1, Cu_2S-1:1.5 samples coated on (a) Glass (b) PET, (c) PP substrates at a scan rate of 80 mV/s respectively.

The voltage from -0.5V to 0.5V is applied to the working electrode, to obtain the electrochemical measurement at various scan rates. The supercapacitor devices are fabricated using synthesized

Cu_2S by varying the ratio of copper sulphate and sodium thiosulfate which are termed as Cu_2S-1:0.5, Cu_2S-1:1, and Cu_2S-1:1.5 on glass, PET, and PP substrates. It is observed from figure 4.9 (a) that when the ratio of (Cu_2S) is varied on the glass substrate at a scan rate of 80mV/s, the value of capacitance obtained is maximum for Cu_2S-1:1 as compared to Cu_2S-1:1.5 and Cu_2S-1:0.5. The corresponding values of capacitance are 587, 128.5, 30 mF/cm^2 is obtained using equation 4.1 for the samples Cu_2S-1:1, Cu_2S-1:1.5, and Cu_2S-1:0.5 on the glass substrate respectively. The higher capacitance observed for Cu_2S-1:1 is because of the hollow rod structure which allows the electrolyte ions to penetrate, thus proving greater capacitance. A similar trend for capacitance value has been observed that when the samples with different ratios are taken on PET and PP substrate as can be seen from figure 4.9 (b) and (c).

The capacitance value obtained for the samples Cu_2S-1:1, Cu_2S-1:1.5 and Cu_2S-1:0.5 are 430, 341.1, 66.25 mF/cm^2 respectively for the PET substrate. However, on the PP substrate the value of capacitance is observed as 131, 42.3, 41mF/cm^2 for the samples Cu_2S-1:1, Cu_2S-1:1.5, and Cu_2S-1:0.5, respectively. It can also be observed from the CV curves that all three samples show redox peaks which confirm that the behavior of the supercapacitor is pseudocapacitive.

Thus, the Cu_2S-1:1 sample is selected for further studies because while performing cyclic voltammetry measurements, it can be seen in figure 4.9 that Cu_2S-1:1 delivers maximum capacitance as compared to Cu_2S-1:0.5 and Cu_2S-1:1.5 on any of the substrates.

As the Cu_2S-1:1 sample shows better performance as compared to other samples, so the GCD, EIS, and capacitance retention measurements are performed only with the Cu_2S-1:1 sample. Further, to recognize the capacitive properties of the Cu_2S-1:1 sample, the charge transfer, and mass transport processes are discussed by performing electrochemical impedance spectroscopy (EIS) as shown in figure 4.10 [146].

For the calculation of electrolyte resistance and electrode resistance, adsorption, faradaic reactions termed as the equivalent series resistance (R_s) and charge- transfer resistance (R_{ct}), the EIS spectra is fitted into an equivalent circuit. The EIS behavior of the supercapacitor device on glass, PET, and PP substrates in the frequency range of 1 kHz to 0.01 Hz as can be seen from figure 4.10. In the high-frequency region (low impedance), the equivalent series resistance (R_s) is the intercept of the Nyquist plot on the real axis (Z') which arises because of the ionic resistance caused by the electrolyte, intrinsic resistance of the electrode and contact resistance between the interface of active material and electrode substrate [147]. The value of series resistance for Cu_2S-1:1 sample on glass, PET, and PP are 2.20, 1.85, 2.50 ohms. This is because the film on the glass substrate is

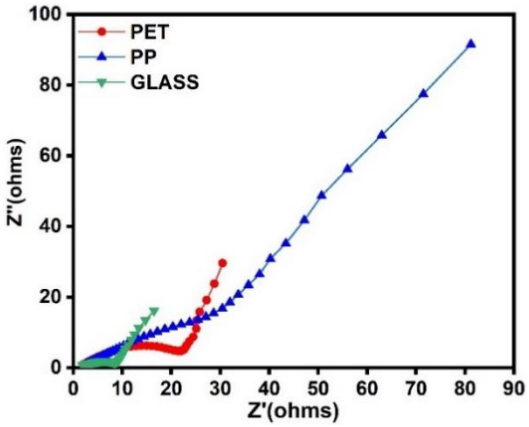

Figure 4.10: Comparison of the EIS behavior of Cu_2S-1:1 on PET, PP, and glass substrate.

crack-free as compared to the film on flexible substrates such as PET and PP. Also, in the medium frequency region, the diameter of the semicircle is an indication of the resistance due to the charge transfer of ions which is also known as the Faraday resistance of the electrode. It has been seen clearly that at medium frequencies, the Cu_2S-1:1 on glass substrate shows the least arc radii as compared to PET and PP. This is an indication of low charge transfer resistance in glass as compared to PET and PP. In the (high impedance) low-frequency region, the diffusion resistance is represented from the sloped portion of the Nyquist plots which results from the diffusion/transport of electrolyte ions in electrolyte and electrode material. With a decrease in frequency *i.e.,* the increased impedance region, change in impedance line occurs from a semicircle to 45˚ to nearly vertical, which implies the movement of electrolyte ions within electrode interphases. This change in impedance is named as Warburg diffusion (Z_w). At low frequencies, the diffusion-controlled region is represented from the tail of the EIS plot. It can be seen that the glass substrate shows the low values of Z_w as compared to the value of Z_w in PET and PP which indicates the faster nature of the charge storage mechanism in the glass substrate. Moreover, the nearly vertical increase in the impedance line indicates the pseudocapacitive charging of the electrodes which attributes to more accessibility of ions in the electrode material.

Figure 4.11 shows the galvanostatic charge-discharge behavior of Cu_2S-1:1 on a glass, PP, and PET substrate at a current density of 0.01A/g. The triangular shape of the graph in figure 4.11 illustrates that charge-discharge occurs very fast. It delivers the capacitance of 18.9, 464.94, 443.81 F/g on PP, glass, PET substrates. Moreover, on the glass substrate, the device takes the maximum time to charge. However, on PP substrate, the time taken is very little which is because the film on PP substrate is very fragile and flexible and the film is not that stable as compared to the film on

glass and PET substrate.

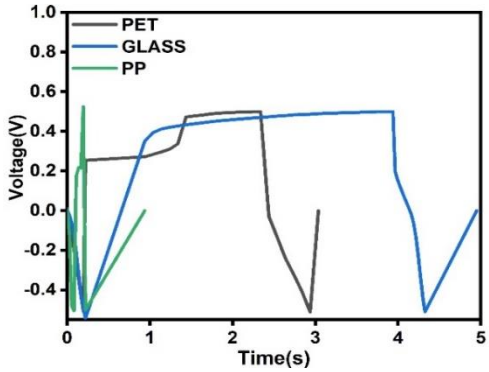

Figure 4.11: Galvanostatic charge-discharge behavior of Cu_2S-1:1 on glass, PET, and PP substrates at 0.1 A/g.

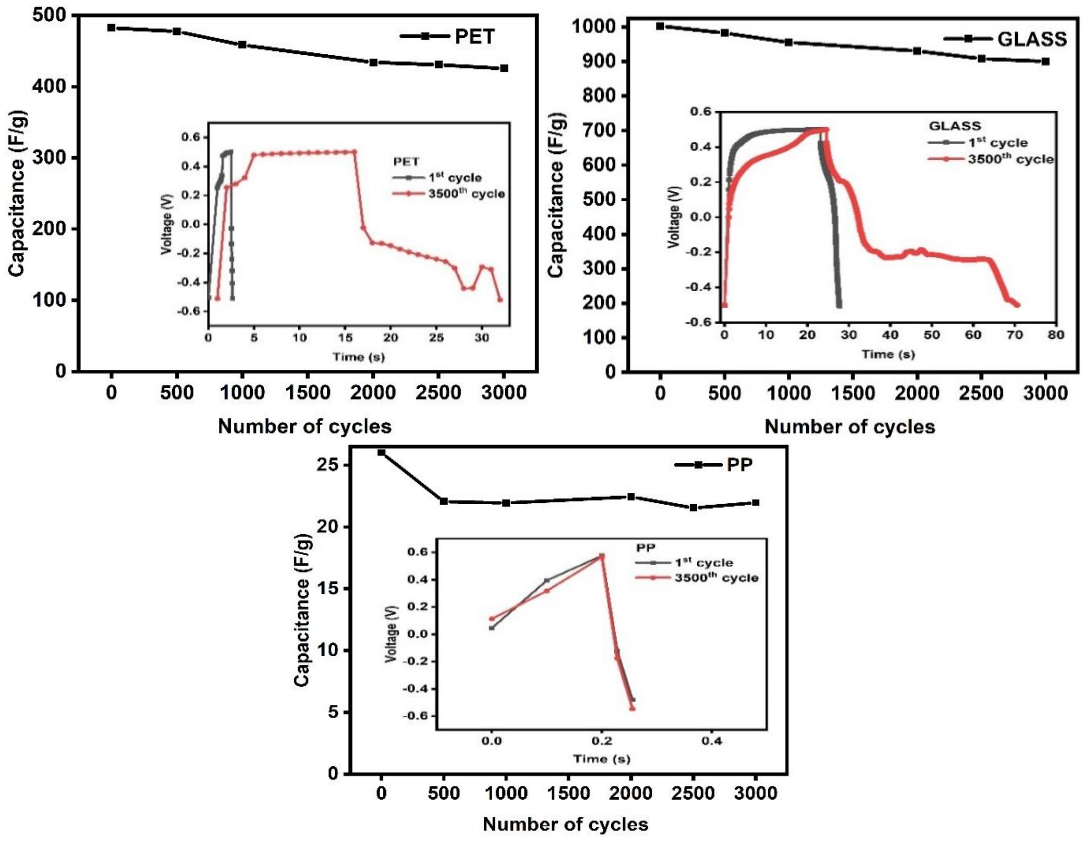

Figure 4.12: The capacitance values vs cycle number of Cu_2S-1:1 on glass, PET, and PP substrates at 0.01 A/g. The inset image is the galvanostatic charge and discharge curve at 1st and 3500th cycle.

Figure 4.12 shows the capacitance retention of the Cu_2S-1:1 sample on Glass, PET, and PP substrates. The synthesized (Cu_2S) 1:1 sample exhibits excellent stability with capacitance retention values of 85.7%, 91.1%, 86.18% respectively on the PP, Glass, and PET substrates after 3500 cycles.

Further, the device performance of Cu_2S-1:1 in terms of energy density and power density is calculated from equation 3 and equation 4. The calculation shows that the device exhibits an energy density of 0.656Wh/Kg, 7.43Wh/Kg, and 16.14Wh/Kg and power density of 84.9KW/Kg, 47.7KW/Kg, and 138.3KW/Kg on PP, PET, and glass substrates. Thus, it shows that Cu_2S can act as a promising candidate as an electrode material for supercapacitor applications on transparent flexible substrates as mostly all of the fabrication with copper sulfide has performed on metal substrates.

CHAPTER 5

EFFECT OF VANADIUM DOPING IN MXene ON SUPERCAPACITOR PERFORMANCE

Recently, a new family of 2D materials named transition-metal carbides and nitrides (MXene) is emerging as energy storage materials because of its various properties such as conductivity, hydrophilicity, *etc*[148]. Till now, the most widely studied 2D transitional metal carbide is the titanium carbide MXene with the formula $Ti_3C_2T_x$ where T represents metal surface species terminated by various functional groups (T_x) such as oxygen, hydroxyl, fluoride, *etc*.[149], [150].

The MXene is a negatively charged compound and the interaction of neutral electrolyte cations with the MXene is determined from the binding strength of adsorbates and MXene functional groups which thus contribute to the pseudocapacitive property[151]. So, in neutral electrolytes, the performance of MXene is enhanced by improving the binding strength between adsorbates such as lithium, sodium, and potassium ions of the electrolyte and various functional groups of MXene[152], [153]. The best way to tune the surface activity is by doping the heteroatom into the electrode material[154]. From the available options of dopants in the literature, niobium is used for doping in the titanium carbide MXene because it belongs to the group which is just next to titanium in the periodic table, and its atomic size is also very near to the titanium which confirms that doping can be possible in Ti_3C_2 MXene [110]. Thus, it opens the possibility of doping various other elements into titanium which belongs to the same group of niobium in the periodic table. Moreover, alkali metal ions have better interaction with the vanadium atom[152]. So, there can be the possibility of considering vanadium as the best choice for doping into the titanium carbide MXene. Further in the literature, the vanadium carbide and vanadium nitride-based MXene are studied however, very limited study has been carried on doping vanadium in titanium carbide MXene. [104], [108], [155]

In the present work, vanadium doping is carried out in the best-optimized $Ti_3C_2T_x$ MXene which further enhances the capacitive performance of $Ti_3C_2T_x$. The influence of vanadium doping on the structural and morphologic properties of MXene (V-MXene) are investigated through X-ray diffractometer (XRD) and scanning electron microscopy (SEM). The electrochemical properties are investigated in detail through cyclic voltammetry (CV), galvanostatic charge-discharge (GCD), and electrochemical impedance spectroscopy data (EIS).

5.1. PREPARATION OF VANADIUM-DOPED MXene POWDER (V-MXene)

To obtain the vanadium-doped MXene powder, different amounts of ammonium vanadate are added into 0.1g of DMSO treated MXene powder. The V-doped MXene was synthesized by the one-step hydrothermal method[156]. In this method, the first step is to obtain a homogenous solution of MXene and ammonium vanadate (NH_4VO_3). The homogeneous solution is then transferred into a Teflon-lined autoclave and heated at 120 °C for 24 hours.

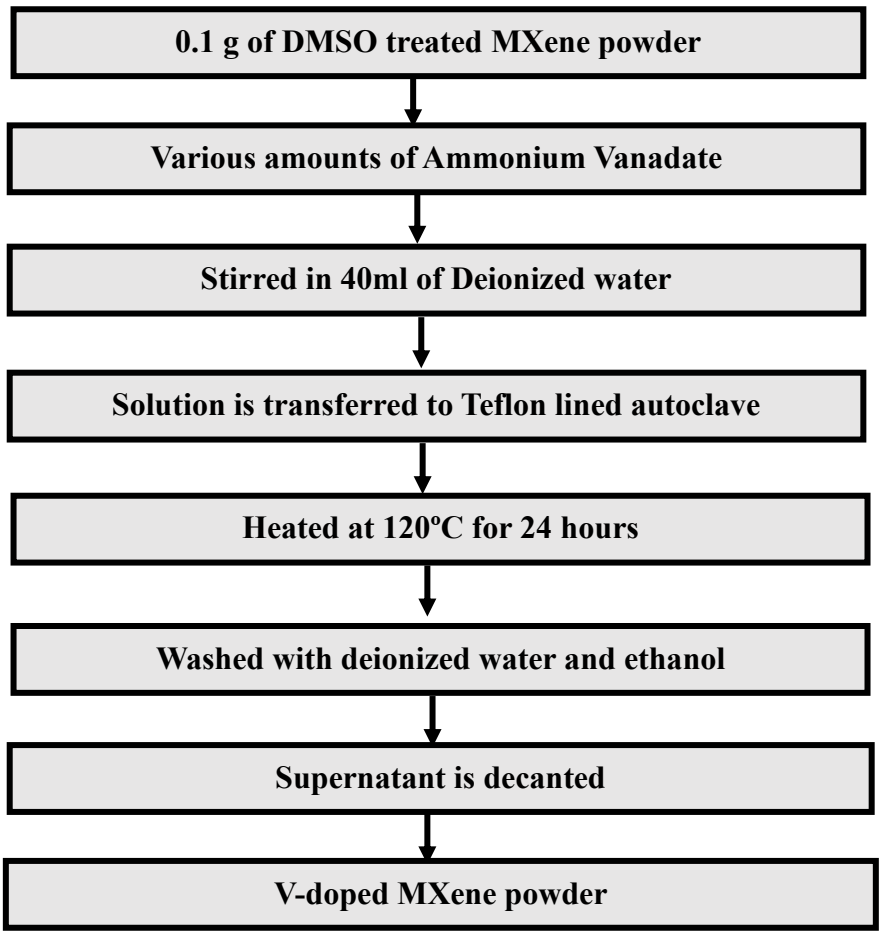

Figure 5.1: Flow chart showing the mechanism of Vanadium doping into the MXene.

Afterward, the precipitates from the Teflon-lined autoclave are rinsed in ethanol and deionized water for several times to obtain a neutral pH solution. Afterward, high-speed centrifugation and vacuum drying are carried to obtain V-MXene powder. The steps involved in the formation of vanadium doped MXene are shown in figure 5.1.

5.2. PREPARATION OF V-DOPED MXene FILM

To prepare the working electrode, a slurry is made with a mixture of active material, carbon

black, and polyvinyl difluoride (PVDF) binder in the ratio of 80:10:10 in N-methyl pyrrolidone (NMP, 99%) solvent which is to be used to analyze the electrochemical properties. The slurry thus formed is spin-coated over the flexible graphite sheet and glass substrate of dimensions (1×1 cm^2) using a spin coater with a mass loading of 0.5 mg/cm^2 of the active material as shown in figure 5.2. The film is then dried at 70°C for 1 day. The reference and counter electrodes are taken as Platinum foil and Ag/AgCl electrodes respectively.

Figure 5.2: Fabrication of electrode material on graphite sheet.

5.2.1. STRUCTURAL MORPHOLOGY

The comparison of structural change in undoped and vanadium doped MXene is analyzed in figure 5.3 (a). It can be observed from XRD patterns that no additional peak is observed in any of the samples which indicates that the layered structure of MXene is preserved. However, 0.025 V-MXene and 0.05 V-MXene shows the shifting of (002) peak towards lower angle which indicates the increase in d-spacing. These results are highly expected as the 0.025 V-MXene and 0.05 V-MXene are already treated with dimethyl sulfoxide (DMSO).

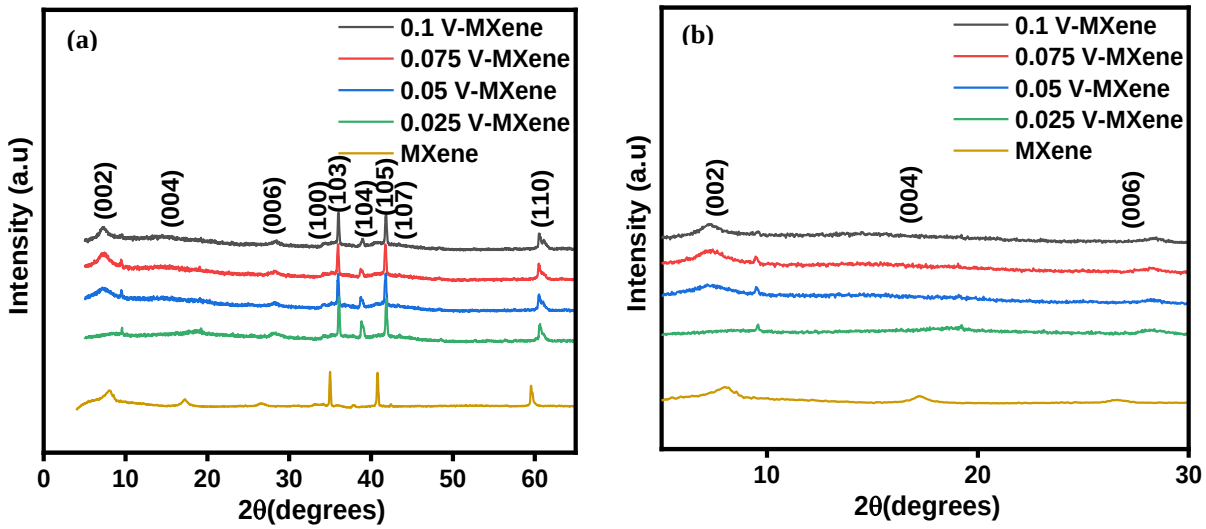

Figure 5.3: XRD patterns of (a) different vanadium doped MXene treated samples and (b) Magnified image of figure 5.4 (a) from angle 5 to 30 degrees.

However, on further increasing the V-doping to 0.075 and 0.1, the (002) peak shifts slightly towards the greater angle indicating a slight contraction in d-spacing[157]. This may be due to the excessive vanadium doping has now covered the entire surface of DMSO- treated MXene thus decreasing the space between different MX layers. The presence of (004) in MXene is an indication of a stacked-layered structure as can be seen from figure 5.3 (b). Also, the presence of a 60° peak confirms the layered structure in all the MXene treated samples.

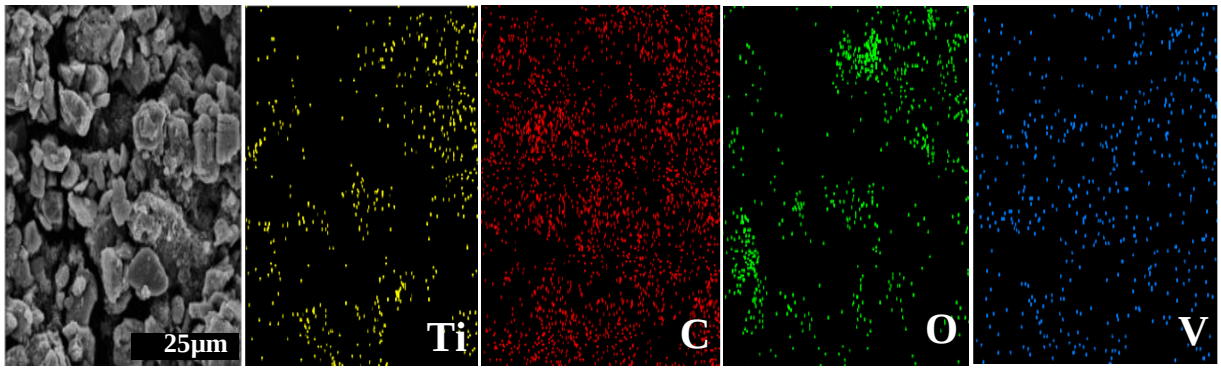

Figure 5.4: EDS mapping of 0.025 V-MXene.

Moreover, the successful vanadium incorporation is validated with element mapping from EDS. Figure 5.4 shows the uniform distribution of titanium, carbon, oxygen, and vanadium over the entire nanosheet.

To examine the vanadium doping level in as-prepared V-MXene, energy-dispersive X-ray spectroscopy (EDS) is engaged and the results are summarized in Table 5.1. Based on the emerging vanadium proportion in EDS spectra at various levels of doping, the vanadium to titanium atomic ratios calculated are 0.035, 0.125, 0.156, and 0.209.

Table 5.1: List of V/Ti atomic ratios in different vanadium doped MXene.

S.No	**V**	**Ti**	**C**	**O**	Atomic ratio of V/Ti (at./at. %)
DMSO	------	18.08	42.68	39.24	----------
0.025 V-MXene	0.75	20.87	43.31	35.07	0.035
0.050 V-MXene	3.53	28.05	46.49	21.93	0.125
0.075 V-MXene	4.10	26.24	31.87	40.79	0.156
0.10 V-MXene	5.77	27.57	24.88	41.78	0.209

Figure 5.5 illustrates the SEM images corresponding to MXene, DMSO-treated MXene, and MXene treated with different amounts of ammonium vanadate. It can be seen from figure 5.5 (a) that Ti_3C_2 MXene layers show layered morphology and have a multilayer accordion-like structure which indicates the successful removal of aluminum layers. However, in figure 5.5 (b), the multi-layered structure becomes few-layered nanosheets after sonication.

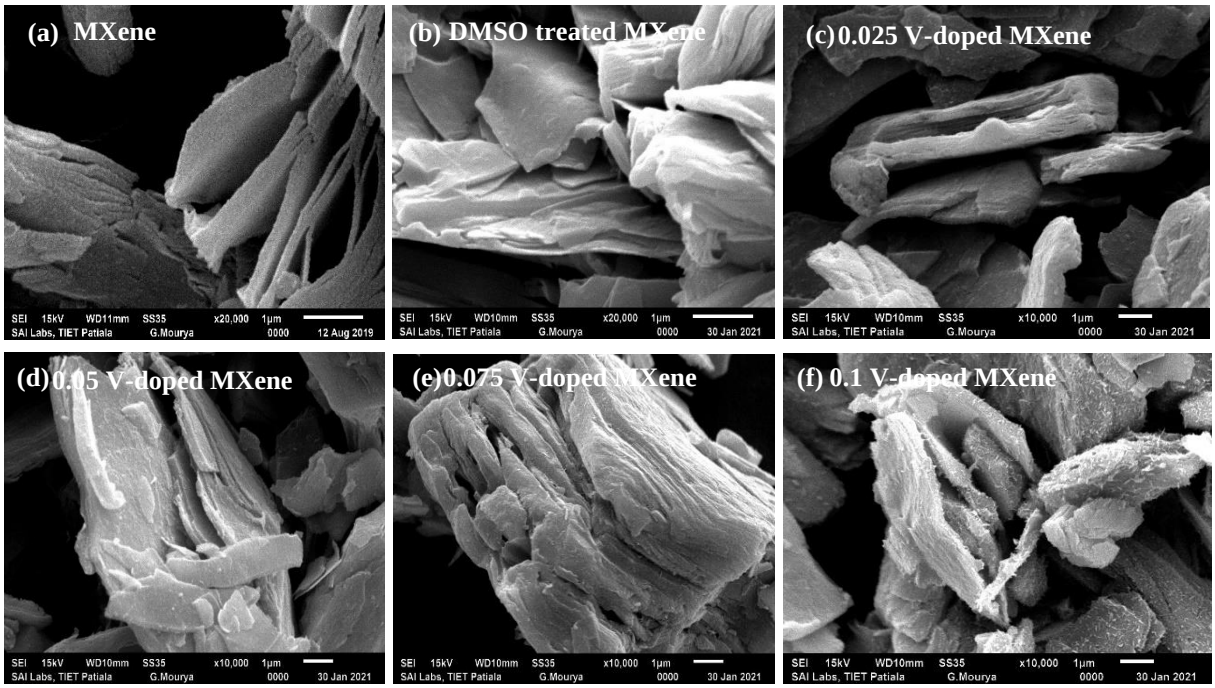

Figure 5.5: SEM images of (a) bare MXene, (b) DMSO treated MXene (c) MXene with 0.025 V- doping, (d) MXene with 0.05 V-doping, (e) MXene with 0.075 V-doping and (f) MXene with 0.1 V-doping.

The crumpled surface of the few-layered MXene shows good flexibility with ultrathin thickness, demonstrating the successful preparation of high-quality few-layered MXene nanosheets. Furthermore, the effect of vanadium doping has been seen by varying the ratio of vanadium to MXene as 0.025:0.1, 0.05:0.1, 0.075:0.1, and 0.1:0.1. It can be seen from figure 5.5 (c) that when the amount of vanadium is 0.025 g, the effect of vanadium particles is less on the surface of MXene layers which may be due to the presence of less amount of ammonium vanadate to be doped into the MXene. However, when the vanadium amount is increased to 0.05g to 0.075g and further to 0.1g as can be seen from figure 5.5 (d-f), a thread-like structure starts appearing on the surface of MXene. On increasing the doping, the surface of MXene becomes rough which indicates the influence of higher V-doping on the surface of MXene. Also, in all the cases the structure of MXene is still preserved and shows the layered morphology.

5.3. ELECTROCHEMICAL MEASUREMENTS

The electrochemical behavior of the prepared samples is analyzed by conducting the electrochemical experiments on Metrohm auto lab workstation which includes cyclic voltammetry (CV), galvanostatic charge-discharge (GCD), and electrochemical impedance spectroscopy (EIS). The three-electrode cell test system is used at room temperature to investigate the samples in a 6M potassium hydroxide (KOH) electrolyte solution. The voltage supply is provided between the working electrode and the reference electrode. However, the measurement of current is carried across the counter and working electrodes. The reference and counter electrodes are platinum (Pt) and silver/silver chloride (Ag/AgCl) respectively. The fabrication of the supercapacitor device is carried from the prepared undoped DMSO and vanadium doped DMSO treated MXene over graphite sheet and glass substrate.

In the present work, the synthesis of vanadium doped MXene film is carried on a flexible graphite sheet for the first time and the results are then compared with the film on the glass substrate. The flexible graphite sheet as a substrate is selected because of its low cost, high conductivity, good thermal properties, and higher processing temperature. The cyclic voltammograms (CV) measurements are performed on rigid as well as flexible substrate by applying the voltage range of -0.5V to 0.5V to the working electrode with the scan rates of 10 to 100mV/s.

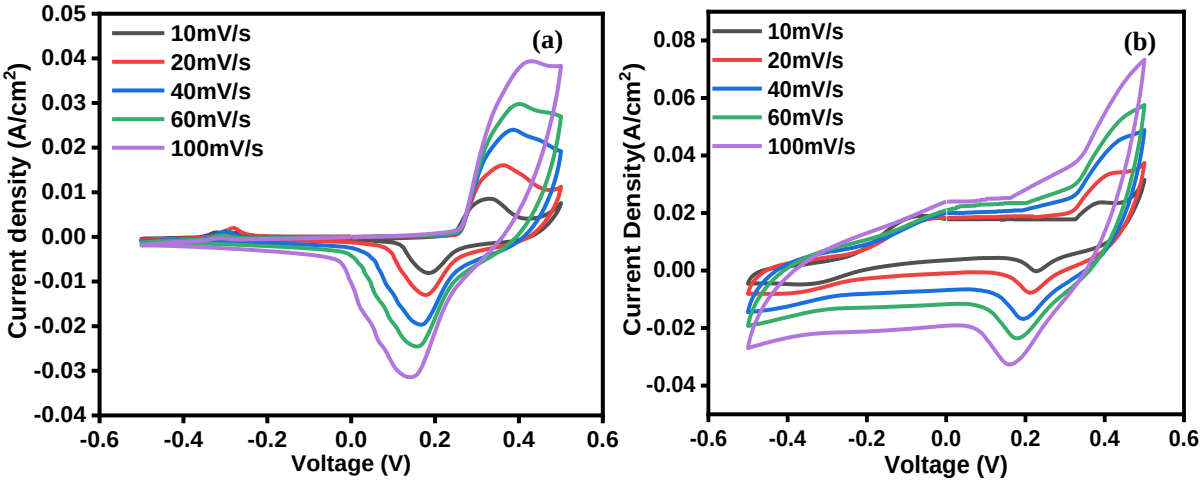

Figure 5.6: (a) Cyclic voltammetry of 0.025 V MXene deposited over (a) glass substrate, (b) graphite sheet

The cyclic voltammetry (CV) behavior of 0.025 vanadium doped DMSO treated MXene deposited on the glass substrate and graphite sheet is plotted in figure 5.6 (a) and 5.6 (b) respectively. To better understand the performance of MXene on flexible as well as rigid substrates, kinetics is studied in detail by varying the scan rate from 10 to 100mV/s. The

appearance of a couple of redox peaks in the glass substrate and graphite sheet is expected as MXene shows the pseudocapacitive behavior [158]. It can be seen that the cyclic voltammetry curves do not show any detectable change in the shape of the graph on increasing scan rate which shows that electron transport and the charge separation rate is very fast.

On increasing the scan rate, the ions do not get much time to interact with the electrode material hence the current density increases with increasing the scan rate mainly dominated by the diffusion-controlled process. However, the rectangular and symmetric shape of the cyclic voltammetry curves is observed for the MXene deposited on the graphite sheet indicating superior capacitive performance. The electrodes of 0.025 V-MXene on glass substrate at different scan rates show a specific capacitance of 258.07, 254.15, 203.25, 170, 128.5 mF/cm^2 with a current density of 39, 30, 25, 15 and 9 mA/cm^2 at a scan rate of 10, 20, 40, 60, 100 mV/s respectively.

Whereas, the value of capacitance in graphite sheet at a scan rate of 10,20,40,60,100mV/s are 1107, 813, 582.75, 481.16, 368.07 mF/cm^2 with a current density of 70,50,40,30 and 20 mA/cm^2. Moreover, the comparison of various DMSO-treated vanadium doped MXene and undoped DMSO MXene on glass and graphite sheet is illustrated and compared individually in figure 5.7 (a) and 5.7 (b) at a scan rate of 20mV/s. The values corresponding to the graph in figure 5.7 are illustrated in Table 5.1. It can be seen that for both rigid and flexible substrates, 0.025 V-doped MXene provides the maximum capacitance. On further increasing the V-doping the capacitance value decreases which is because the greater vanadium doping has covered the

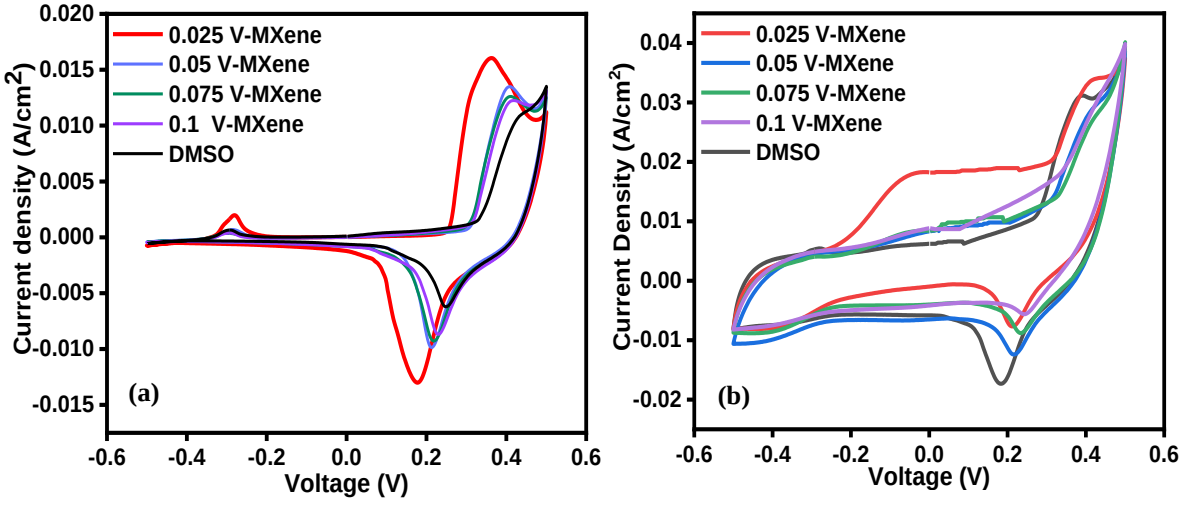

Figure 5.7: (a) Comparison of different MXene treated samples at 20mV/s on glass, (b) comparison of different MXene treated samples at 20 mV/s on graphite sheet.

entire surface of MXene layers thus, reducing the surface area available for the electrolyte ions to penetrate. Further, decrease in the value of capacitance in 0.075 and 0.1 V-MXene is because of the increased contact resistance as also depicted through EIS. Also, the value of capacitance shown by the graphite sheet is larger glass substrate value for any of the samples which is because of the greater conductivity of the graphite sheet.

Table 5.2: Values of areal capacitance obtained for different samples synthesized on the glass substrate and graphite sheet substrate at a scan rate of 20 mV/s.

S.No.	Sample	Glass Substrate	Graphite Substrate
1.	0.025 V-MXene	254.15 mF/cm^2	813 mF/cm^2
2.	0.05 V-MXene	158 mF/cm^2	735 mF/cm^2
3.	0.075 V-MXene	154 mF/cm^2	639 mF/cm^2
4.	0.1 V-MXene	153 mF/cm^2	634 mF/cm^2
5.	DMSO	121 mF/cm^2	740 mF/cm^2

Afterward, the capacitance versus scan rate for the MXene deposited on a glass substrate and graphite substrate is plotted in figures 5.8 (a) and 5.8 (b). From the graph, it can also be observed that with the increase in scan rate, the value of capacitance decreases.

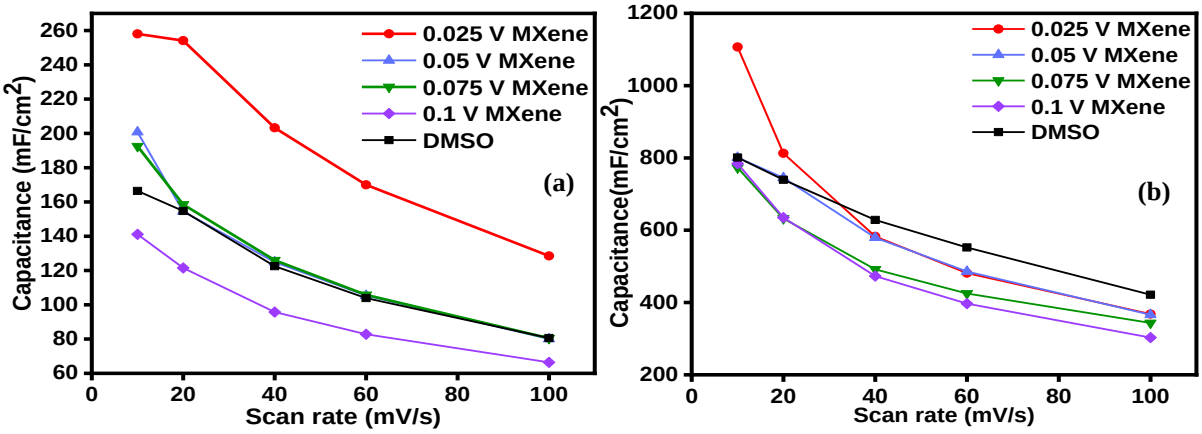

Figure 5.8: (a) Capacitance vs scan rate on the glass substrate, (b) graphite sheet.

To further understand the increased capacitive properties of vanadium doped MXene, the processes involving charge transfer and mass transport are investigated by performing (EIS) [146]. The equivalent series resistance (R_s) and charge transfer resistance (R_{ct}) caused due to electrolyte resistance and electrode resistance, adsorption, faradaic reactions are calculated by fitting the EIS spectra to an equivalent circuit. Figure 5.9 (a) shows the EIS behavior of the

supercapacitor device on a rigid substrate and figure 5.9 (b) shows the EIS behavior of the device on a flexible graphite sheet in the frequency range of 100 kHz to 0.01 Hz. In the high-frequency region (low impedance), the equivalent series resistance (R_s) is represented from the intercept of the Nyquist plot at the real axis (Z'), which arises from the ionic resistance of the electrolyte, intrinsic resistance of the electrode, and contact resistance at the active material-electrode substrate interface[147].

In figure 5.9 (a) the value of series resistance of all the samples made on a glass substrate is around 1.6 ohms whereas, in figure 5.9 (b), the respective value of series resistance (R_e) for DMSO, 0.025 V-MXene, 0.05 V-MXene, 0.075 V-MXene and 0.1 V-MXene on graphite sheet are 0.82, 0.70, 0.58, 0.67, 0.77 ohms which indicate an improved conductivity of MXene on V- doping. This is because the doping of a foreign metal atom into the material is known to increase their charge carrier density and result in better accessibility of ions to the surface of the electrodes [159]. However, an interesting behavior is seen that as V-doping has been increased to 0.075 and 0.1, the R_s increases which is because greater vanadium doping leads to the rough surface of the MXene which is also confirmed by the SEM image from figure 5.6 e-f) where the thread-like structure starts appearing on the surface of MXene. In the medium frequency region, the charge transfer resistance is indicated from the diameter of the semicircle also known as the Faraday resistance of the electrode. It has been seen clearly that at medium frequencies, no semicircles are observed on glass substrate for all of the MXene samples

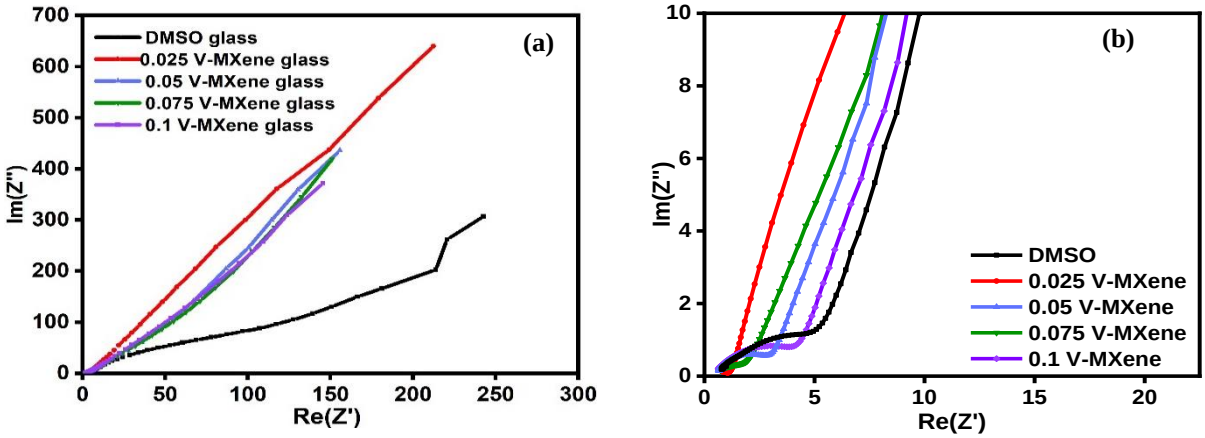

Figure 5.9: (a) EIS behavior of different V-doped MXene deposited over a glass substrate, (b) graphite sheet

illustrating excellent pseudo capacitance with significantly low charge transfer resistance. This is because the film on the glass substrate is crack-free as compared to the film on the flexible graphite substrate. In the low-frequency region (high impedance), the diffusion resistance is

represented from the sloped portion of the Nyquist plots which results from the diffusion/transport of electrolyte ions in electrolyte and electrode material. With a decrease in frequency (increased impedance), change in impedance line occurs from a semicircle to 45˚ to nearly vertical, which implies the movement of electrolyte ions within electrode interphases. This change in impedance is named as Warburg diffusion (Z_w). At low frequencies, the diffusion-controlled region is represented from the tail of the EIS plot. In figure 5.9 (a) with the glass substrate, it can be seen that various V-doped MXene have low values of Z_w as compared to the value of Z_w in DMSO which indicates the capacitive nature of the charge storage mechanism. Moreover, in figure 5.9 (b), the nearly vertical increase in the impedance line indicates the pseudocapacitive charging of the electrodes which attributes to more accessibility of ions in the electrode material. Also, the arc radii of every vanadium doped electrodes on the EIS plot of graphite sheet are smaller than that of undoped DMSO electrode suggesting that the vanadium particles are attached successfully on the surface of MXene layers. The radius on the EIS plot of V-MXene is smaller than that of the undoped DMSO MXene, which indicates that the V-doping made the charge transfer easier.

The inset of figure 5.10 (a) and 5.10 (b) shows the galvanostatic charge-discharge behavior of 0.025 V-MXene on a glass substrate as well as on a graphite sheet at a current density of 0.02A/g. The triangular shape of the graph illustrates that charge-discharge occurs very fast. It shows the capacitance of 107.6 mF/g and 201 mF/g at a current density of 0.02 A/g. Moreover,

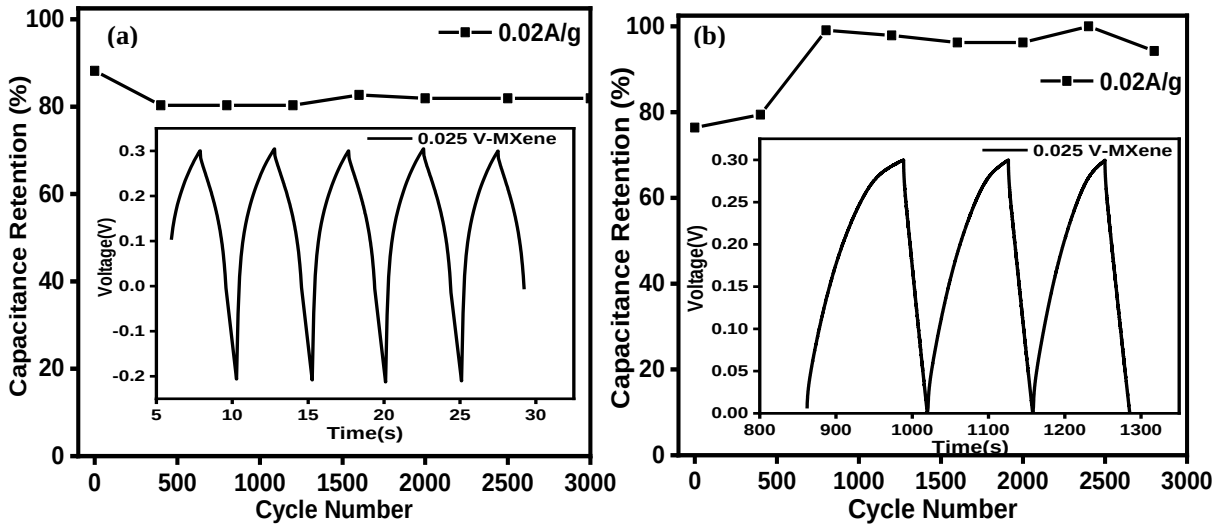

Figure 5.10: Variation of capacitance retention vs cycle number for 0.025 V-MXene, the inset shows galvanostatic charge-discharge plot at the current density of 0.02 A/g on (a) glass substrate, (b) graphite sheet.

the synthesized vanadium doped 0.025 V-MXene exhibits excellent stability with the capacitance retention of 82.2% and 92.7% respectively on the glass substrate as well as graphite sheet after 3000 cycles.

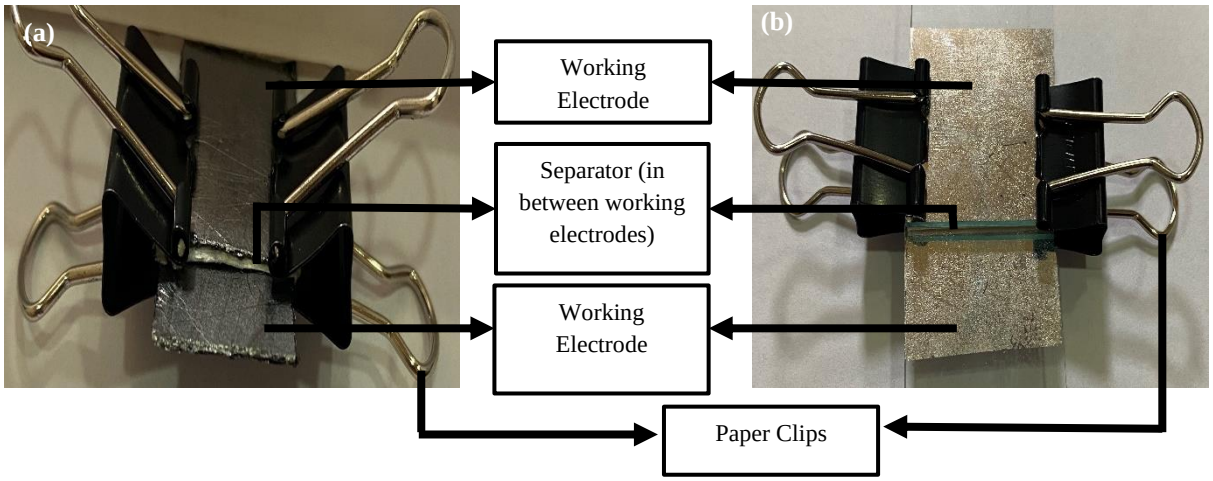

Figure 5.11: Fabricated images of the supercapacitor device on (a) graphite sheet and (b) glass substrate.

The fabricated images of the supercapacitor device on the glass as well as flexible graphite sheet substrate are shown in figure 5.11 (a) and 5.11 (b). In figure 5.11 (a) the symmetrical the supercapacitor is formed by depositing 0.025 V-doped MXene over two graphite sheets and in between the sheets a filter paper as a separator is present dipped in an electrolyte solution. Moreover, to hold the device, paper clips are attached. Similarly, in figure 5.11 (b) symmetrical supercapacitor is made by depositing V-doped MXene over two glass slides and in between the two slides a separator (filter paper) is present. Again to hold the device, paper clips are attached. The device exhibits an energy density of 37.36Wh/Kg, 69.7Wh/Kg on the glass substrate and graphite sheet, respectively. It shows the power density of 53.79KW/Kg and 8.1KW/Kg on glass substrates and graphite sheet, respectively.

CHAPTER 6

CONCLUSION AND FUTURE SCOPE

6.1. CONCLUSION

The comparison of the process parameters with the electrical properties is important for using an electrode material in energy storage devices or any other application. It is observed that decreasing the HF concentration though decreases the resistance but does not etch the aluminium. Whereas, increasing the etching time increases the aluminium etching as well as decreases the resistance. Hence optimum value of etching time has to be provided to obtain the best MXene properties. Moreover, increasing the HF quantity with reduced HF concentration (20%) neither etch the aluminium completely nor affects the resistance. However, increasing the HF quantity with HF concentration of (40%) leads to the accumulation of small particles on the surface of MXene.

The supercapacitor device is then fabricated using these optimised process parameters to obtain the capacitance results. It is seen that the maximum capacitance obtained with glass substrate is maximum as compared to the capacitance obtained on flexible substrates. The slope of the current *vs.* scan rate provides information regarding the storage mechanism. It is seen that the CV curves do not show any detectable change in the shape of the graph on increasing scan rate which shows that electron transport and the charge separation rate is very fast. The electrodes of MXene on glass, PET and PP substrates show a maximum specific capacitance of 70mF/cm^2, 66.8 mF/cm^2 and 54.44 mF/cm^2, respectively at a scan rate of 50mV/s.

Further, the Cu_2S hollow rods are synthesized through a simple chemical reaction that occurs between copper sulphate and ascorbic acid in presence of sodium thiosulphate solution. It is observed that Cu_2S-1:1 shows a high specific capacitance value of 587mF/cm^2 on glass, 128.5 mF/cm^2 on PET and 30 mF/cm^2 on PP at a scan rate of 80mV/s in 6M KOH electrolyte. The three-electrode cell is formed to measure the capacitance of the device using (Cu_2S) as a working electrode with a potential range applied between -0.5 to 0.5V. The excellent properties of Cu_2S as an electrode material made it a potential candidate for serving as electrode material for supercapacitors. Moreover, the excellent cycle stability with the capacitance retention of 85.7%, 91.1%, 86.18%, and 92.8%, respectively of Cu_2S-1:1 on the PP, Glass, and PET substrates is obtained after 3500 cycles.

To observe the effect of doping, the few-layered MXene structure is treated with different amounts of ammonium vanadate. It is observed that as the doping is increased, the different MX layers start contracting and delivers the increased series and charge transfer resistance. It is also seen that greater capacitance is achieved with the graphite sheet as compared to the glass substrate. This is because graphite sheet has greater conductivity.

The electrochemical performance of the supercapacitor device is investigated through cyclic voltammetry, galvanostatic charge-discharge and electrochemical impedance spectroscopy. It is found that in cyclic voltammetry no detectable change is observed in the shape of the graph on increasing scan rate which shows that electron transport and the charge separation rate are very fast. The slight change in the rectangular shape is due to the current overloading with respect to the voltage. The appearance of a couple of redox peaks in glass and graphite sheet is because of the deviation in the cyclic voltammetry curves from the ideal rectangular shape which signifies their pseudocapacitive behavior. The electrodes of MXene on glass substrate at different scan rates show a specific capacitance of 258.07, 254.15, 203.25, 170, 128.5 mF/cm^2 with a current density of 39, 30, 25, 15 and 9 mA/cm^2 at a scan rate of 10,20,40,60,100 mV/s, respectively. Whereas, the value of capacitance in graphite sheet at a scan rate of 10,20,40,60,100mV/s are 1107, 813, 582.75, 481.16, 368.07 mF/cm^2 with a current density of 70,50,40,30 and 20 mA/cm^2. Moreover, the synthesized vanadium doped 0.025 V-MXene exhibits excellent stability with the capacitance retention of 82.2% and 92.7% respectively on the glass as well as graphite sheet after 3000 cycles.

In this era, when electronic devices are becoming compact and flexible, smaller energy storage devices *e.g.,* supercapacitors are catching up with the trend. As compared to the predecessor 2D graphene, there is a rapid progress in the volumetric capacitance performance shown by 2D MXene by optimizing both physical and chemical aspects. Hence, the optimisation in the synthesis parameters would lead to a useful path for further investigations towards energy storage applications. Thus, it is hoped that MXene will recognise its true capability by showing its potential in industrial application. Moreover, the results on doping in MXene suggests that it is also a new pathway for enhancing the device performance.

6.2. FUTURE SCOPE

Since, a large number of elements in the periodic table are still available and need to be explored

for doping into the MXene to know their influence on the performance of the device. Moreover, the fabrication of copper sulfide electrodes has mainly been carried on metal substrates which open various new ways to fabricate copper sulfide over other substrates. Since, the outstanding results of MXene and copper sulfide can open the possibility of designing the hybrid of copper sulfide and MXene as an asymmetric supercapacitor to obtain the benefits of both copper sulfide and MXene in single device.

LIST OF PUBLICATIONS

P1: Garg, Ruby, Alpana Agarwal, and Mohit Agarwal. "A review on MXene for energy storage application: effect of interlayer distance." *Materials Research Express*, Vol. 7, No. 2, pp. 022001, 2020.

DOI: 10.1088/2053-1591/ab750d.

P2: Garg, R., A. Agarwal, and M. Agarwal. "Synthesis and optimisation of MXene for supercapacitor application." *Journal of Materials Science: Materials in Electronics, Vol* 31, No.21, pp. 18614-18626, 2020.

DOI: 10.1007/s10854-020-04404-5.

P3: Garg, R., A. Agarwal, and M. Agarwal. "Effect of vanadium doping on MXene-based supercapacitor." *Journal of Materials Science: Materials in Electronics, Vol. 32, No. 17, pp. 22046-22059*, 2021.

DOI: 10.1007/s10854-021-06668-x.

P4: Garg, R., A. Agarwal, and M. Agarwal. " Performance of Copper Sulfide Hollow Rods in Supercapacitor based on Flexible Substrates." *Journal of Electronic Materials*, Vol. 50, No. 12, pp. 6974-6980, 2021.

DOI: 10.1007/s11664-021-09162-6

P5: Garg, Ruby, Alpana Agarwal, and Mohit Agarwal. "Synthesis and characterization of solution processed MXene." *AIP Conference Proceedings*., Jodhpur, India, 2020, Vol. 2265. No. 1, pp. 030665.

DOI: 10.1063/5.0016599.

REFERENCES

[1] D. Ahuja and M. Tatsutani, "Sustainable energy for developing countries," *SAPI EN. S. Surv. Perspect. Integr. Environ. Soc.*, vol. 2, no. 1, 2009.

[2] S. Baskar and R. Baskar, *Environmental Studies For Undergraduate Courses*. Unicorn Books, 2007.

[3] R. Kötz and M. Carlen, "Principles and applications of electrochemical capacitors," *Electrochim. Acta*, vol. 45, no. 15–16, pp. 2483–2498, 2000.

[4] M. Aneke and M. Wang, "Energy storage technologies and real life applications–A state of the art review," *Appl. Energy*, vol. 179, pp. 350–377, 2016.

[5] R. Carnegie, D. Gotham, D. Nderitu *et al.*, "Utility scale energy storage systems," *State Util. Forecast. Group. Purdue Univ.*, vol. 1, 2013.

[6] H. D. Abruna, Y. Kiya, and J. C. Henderson, "Batteries and electrochemical capacitors," *Phys. Today*, vol. 61, no. 12, pp. 43–47, 2008.

[7] M. M. Biswas, M. S. Azim, T. K. Saha, *et al.*, "Towards implementation of smart grid: an updated review on electrical energy storage systems," vol. 4, no. 1, 2013.

[8] J. P. Zheng and T. R. Jow, "High energy and high power density electrochemical capacitors," *J. Power Sources*, vol. 62, no. 2, pp. 155–159, 1996.

[9] T. T. Grove, M. F. Masters, and R. E. Miers, "Determining dielectric constants using a parallel plate capacitor," *Am. J. Phys.*, vol. 73, no. 1, pp. 52–56, 2005.

[10] M. S. Halper and J. C. Ellenbogen, "Supercapacitors: A brief overview," *MITRE Corp. McLean, Virginia, USA*, pp. 1–34, 2006.

[11] W. Schmickler, "Electronic effects in the electric double layer," *Chem. Rev.*, vol. 96, no. 8, pp. 3177–3200, 1996.

[12] B. K. Kim, S. Sy, A. Yu, and J. Zhang, "Electrochemical supercapacitors for energy storage

and conversion," *Handb. clean energy Syst.*, pp. 1–25, 2015.

[13] S. Y. Attia, S. G. Mohamed, Y. F. Barakat, *et al.*, "Supercapacitor electrode materials: addressing challenges in mechanism and charge storage," *Rev. Inorg. Chem.*, 2021.

[14] A. Yu, V. Chabot, and J. Zhang, *Electrochemical supercapacitors for energy storage and delivery: fundamentals and applications*. Taylor & Francis, 2013.

[15] Y. Wang, Y. Song, and Y. Xia, "Electrochemical capacitors: mechanism, materials, systems, characterization and applications," *Chem. Soc. Rev.*, vol. 45, no. 21, pp. 5925–5950, 2016.

[16] G. G. Prasad, N. Shetty, S. Thakur *et al.*, "Supercapacitor technology and its applications: a review," in *IOP Conference Series: Materials Science and Engineering*, 2019, vol. 561, no. 1, p. 12105.

[17] T. Chen and L. Dai, "Carbon nanomaterials for high-performance supercapacitors," *Mater. Today*, vol. 16, no. 7–8, pp. 272–280, 2013.

[18] M. Conte, "Supercapacitors technical requirements for new applications," *Fuel cells*, vol. 10, no. 5, pp. 806–818, 2010.

[19] W. Choi, I. Lahiri, R. Seelaboyina *et al.*, "Synthesis of graphene and its applications: a review," *Crit. Rev. Solid State Mater. Sci.*, vol. 35, no. 1, pp. 52–71, 2010.

[20] P. Simon and Y. Gogotsi, "Materials for electrochemical capacitors," *Nanosci. Technol. a Collect. Rev. from Nat. journals*, pp. 320–329, 2010.

[21] Y. M. Vol'fkovich and T. M. Serdyuk, "Electrochemical capacitors," *Russ. J. Electrochem.*, vol. 38, no. 9, pp. 935–959, 2002.

[22] J. Garthwaite, "How ultracapacitors work (and why they fall short)," *Earth2Tech. GigaOM Netw.*, 2011.

[23] J. P. Zheng, P. J. Cygan, and T. R. Jow, "Hydrous ruthenium oxide as an electrode material

for electrochemical capacitors," *J. Electrochem. Soc.*, vol. 142, no. 8, pp. 2699–2703, 1995.

[24] W. Chen, Z. Fan, L. Gu *et al.*, "Enhanced capacitance of manganese oxide via confinement inside carbon nanotubes," *Chem. Commun.*, vol. 46, no. 22, pp. 3905–3907, 2010.

[25] Z. Cai, L. Li, J. Ren *et al.*, "Flexible, weavable and efficient microsupercapacitor wires based on polyaniline composite fibers incorporated with aligned carbon nanotubes," *J. Mater. Chem. A*, vol. 1, no. 2, pp. 258–261, 2013.

[26] M. Liang, M. Zhao, H. Wang *et al.*, "Enhanced cycling stability of hierarchical $NiCo_2S_4$@$Ni(OH)_2$@PPy core-shell nanotube arrays for aqueous asymmetric supercapacitors," *J. Mater. Chem. A*, vol. 6, no. 6, pp. 2482–2493, 2018.

[27] Q. Zhang, X. Wang, Z. Pan, *et al.*, "Wrapping aligned carbon nanotube composite sheets around vanadium nitride nanowire arrays for asymmetric coaxial fiber-shaped supercapacitors with ultrahigh energy density," *Nano Lett.*, vol. 17, no. 4, pp. 2719–2726, 2017.

[28] B. E. Conway, *Electrochemical supercapacitors: scientific fundamentals and technological applications*. Springer Science & Business Media, 2013.

[29] B. S. Pali and S. Vadhera, "Renewable energy systems for generating electric power: A review," in *2016 IEEE 1st International Conference on Power Electronics, Intelligent Control and Energy Systems (ICPEICES)*, 2016, pp. 1–6.

[30] K. V. Singh, H. O. Bansal, and D. Singh, "A comprehensive review on hybrid electric vehicles: architectures and components," *J. Mod. Transp.*, vol. 27, no. 2, pp. 77–107, 2019.

[31] P. Jain, A. Das, and T. Jain, "Aggregated electric vehicle resource modelling for regulation services commitment in power grid," *Sustain. cities Soc.*, vol. 45, pp. 439–450, 2019.

[32] S. Deb, A. Goswami, P. Harsh *et al.*, "Charging coordination of plug-in electric vehicle for congestion management in distribution system integrated with renewable energy sources,"

IEEE Trans. Ind. Appl., vol. 56, no. 5, pp. 5452–5462, 2020.

[33] S. Gilligan, H. Ahmed, S. Chandra *et al.*, "Optimization and Photostability Studies of Luminescent Organic Dyes for Solar Devices."

[34] S. P. Bremner, G. M. Liu, N. Faleev *et al.*, "Growth and characterization of Ga $As_{1-x}Sb_x$ barrier layers for advanced concept solar cells," *J. Vac. Sci. Technol. B Microelectron. Nanom. Struct. Process. Meas. Phenom.*, vol. 26, no. 3, pp. 1149–1152, 2008.

[35] S. Chu and A. Majumdar, "Opportunities and challenges for a sustainable energy future," *Nature*, vol. 488, no. 7411, p. 294, 2012.

[36] B. Dunn, H. Kamath, and J.-M. Tarascon, "Electrical Energy Storage for the Grid: A Battery of Choices (Supporting Online Material)," *Science (80-.).*, vol. 334, no. 6058, pp. 928–935, 2011.

[37] S. Westerlund, "Capacitor Theory," *IEEE Trans. Dielectr. Electr. Insul.*, vol. 1, no. 5, pp. 1–3, 1994, Accessed: Jun. 25, 2019.

[38] A. G. Pandolfo and A. F. Hollenkamp, "Carbon properties and their role in supercapacitors," *J. Power Sources*, vol. 157, no. 1, pp. 11–27, Jun. 2006.

[39] J. F. Manwell and J. G. McGowan, "Lead acid battery storage model for hybrid energy systems," *Sol. energy*, vol. 50, no. 5, pp. 399–405, 1993.

[40] B. Y. Liaw, R. G. Jungst, G. Nagasubramanian *et al.*, "Modeling capacity fade in lithium-ion cells," *J. Power Sources*, vol. 140, no. 1, pp. 157–161, 2005.

[41] X. Sui, M. Świerczyński, R. Teodorescu *et al.*, "The Degradation Behavior of $LiFePO_4$/C Batteries during Long-Term Calendar Aging," *Energies*, vol. 14, no. 6, p. 1732, 2021.

[42] Z. Zhu, M. Wang, Y. Meng *et al.*, "A high-rate lithium manganese oxide-hydrogen battery," *Nano Lett.*, vol. 20, no. 5, pp. 3278–3283, 2020.

[43] X. Han, L. Lu, Y. Zheng *et al.*, "A review on the key issues of the lithium ion battery

degradation among the whole life cycle," *ETransportation*, vol. 1, pp. 100005, 2019.

[44] A. Kobayashi, T. Kishimoto, Y. Hino *et al*, "Development of a high performance Ni-MH battery for smaller electric vehicles," 2000.

[45] X. Shen, Z. Tian, R. Fan *et al.*, "Research progress on silicon/carbon composite anode materials for lithium-ion battery," *J. Energy Chem.*, vol. 27, no. 4, pp. 1067–1090, 2018.

[46] J. Ho, T. R. Jow, and S. Boggs, "Historical introduction to capacitor technology," *IEEE Electr. Insul. Mag.*, vol. 26, no. 1, pp. 20–25, 2010.

[47] M. Jayalakshmi and K. Balasubramanian, "Simple capacitors to supercapacitors-an overview," *Int. J. Electrochem. Sci*, vol. 3, no. 11, pp. 1196–1217, 2008.

[48] V. Lehmann, W. Hönlein, H. Reisinger *et al.*, "A novel capacitor technology based on porous silicon," *Thin Solid Films*, vol. 276, no. 1–2, pp. 138–142, 1996.

[49] A. Nishino, "Capacitors: operating principles, current market and technical trends," *J. Power Sources*, vol. 60, no. 2, pp. 137–147, 1996.

[50] S. Niwa and Y. Taketani, "Development of new series of aluminium solid capacitors with organic semiconductive electrolyte (OS-CON)," *J. Power Sources*, vol. 60, no. 2, pp. 165–171, 1996.

[51] M. Liu, L. Chang, Z. Le *et al.*, "Emerging Potassium-ion Hybrid Capacitors," ChemSusChem, vol. 13, no. 22, pp. 5837–5862, 2020.

[52] V. A. Boicea, "Energy storage technologies: The past and the present," *Proc. IEEE*, vol. 102, no. 11, pp. 1777–1794, 2014.

[53] H. Tang, J. Wang, H. Yin *et al.*, "Growth of polypyrrole ultrathin films on MoS2 monolayers as high-performance supercapacitor electrodes," *Adv. Mater.*, vol. 27, no. 6, pp. 1117–1123, 2015.

[54] Z. Ma, Z. Zhang, Y. Qu *et al.*, "Yeast protein derived hierarchical mesoporous carbon for

symmetrical capacitor with excellent electrochemical performances," *Microporous Mesoporous Mater.*, vol. 281, pp. 50–56, 2019.

[55] P. Delahay, "Double layer studies," *J. Electrochem. Soc.*, vol. 113, no. 10, p. 967, 1966.

[56] M. A. V Devanathan and B. Tilak, "The structure of the electrical double layer at the metal-solution interface," *Chem. Rev.*, vol. 65, no. 6, pp. 635–684, 1965.

[57] H. I. Becker, "Low voltage electrolytic capacitor,(1957)," *Google Patents*, 1957.

[58] M. Endo, T. Takeda, Y. J. Kim *et al*. "High power electric double layer capacitor (EDLC's); from operating principle to pore size control in advanced activated carbons," *Carbon Lett.*, vol. 1, no. 3_4, pp. 117–128, 2001.

[59] D. L. Boos, "Electrolytic capacitor having carbon paste electrodes." Google Patents, Oct. 27, 1970.

[60] S. Huang, X. Zhu, S. Sarkar, and Y. Zhao, "Challenges and opportunities for supercapacitors," *APL Mater.*, vol. 7, no. 10, p. 100901, 2019.

[61] J. Gamby, P. L. Taberna, P. Simon, J. F. Fauvarque, and M. Chesneau, "Studies and characterisations of various activated carbons used for carbon/carbon supercapacitors," *J. Power Sources*, vol. 101, no. 1, pp. 109–116, 2001.

[62] K.H. An, W.S. Kim, Y.S. Park *et al.*, "Supercapacitors Using Single-Walled Carbon Nanotube Electrodes," *Adv. Mater.*, vol. 13, no. 7, pp. 497–500, Apr. 2001.

[63] L.L. Zhang, X.S. Zhao, "Carbon-based materials as supercapacitor electrodes," *pubs.rsc.org*, vol. 38, no. 9, pp. 2520–31, 2009.

[64] C. Liu, Z. Yu, D. Neff *et al.*, "Graphene-Based Supercapacitor with an Ultrahigh Energy Density," *Nano Lett.*, vol. 10, no. 12, pp. 4863–4868, Dec. 2010.

[65] A. Pandey, V. K. Singh, H.Mishra *et al.*, "WS_2 quantum dot graphene nanocomposite film for UV photodetection," *ACS Appl. Nano Mater.*, vol. 2, no. 6, pp. 3934–3942, 2019.

[66] H. Xia, Y.S. Meng, G. Yuan *et al.*, "A symmetric RuO_2/RuO_2 supercapacitor operating at 1.6 V by using a neutral aqueous electrolyte," *Electrochemical and Solid State Letters*, vol. 15, no. 4, pp A60, 2012.

[67] Demarconnay, E. Raymundo-Pinero, F.Beguin, "Adjustment of electrodes potential window in an asymmetric carbon/MnO_2 supercapacitor," *Elsevier*, vol. 1, no. 196, pp. 580–586, 2011.

[68] B. E. Conway, "Transition from 'supercapacitor' to 'battery' behavior in electrochemical energy storage," *J. Electrochem. Soc.*, vol. 138, no. 6, pp. 1539–1548, 1991.

[69] D. Punnoose, S. S. Rao, S.-K. Kim *et al.*, "Exploring the effect of manganese in lead sulfide quantum dot sensitized solar cell to enhance the photovoltaic performance," *RSC Adv.*, vol. 5, no. 42, pp. 33136–33145, 2015.

[70] G. Tian, Z. Zhao, C.Das *et al.*, "Understanding the Li-ion storage mechanism in a carbon composited zinc sulfide electrode," *J. Mater. Chem. A*, vol. 7, no. 26, pp. 15640–15653, 2019.

[71] M. Gautam, Z. Shi, and A. H. Jayatissa, "Graphene films as transparent electrodes for photovoltaic devices based on cadmium sulfide thin films," *Sol. Energy Mater. Sol. Cells*, vol. 163, pp. 1–8, 2017.

[72] K.-J. Huang, J.-Z. Zhang, Y. Liu *et al.*, "Synthesis of reduced graphene oxide wrapped-copper sulfide hollow spheres as electrode material for supercapacitor," *Int. J. Hydrogen Energy*, vol. 40, no. 32, pp. 10158–10167, 2015.

[73] E. Miniach and G. Gryglewicz, "Solvent-controlled morphology of bismuth sulfide for supercapacitor applications," *J. Mater. Sci.*, vol. 53, no. 24, pp. 16511–16523, 2018.

[74] W. Wei, L. Mi, Y. Gao *et al.*, "Partial ion-exchange of nickel-sulfide-derived electrodes for high performance supercapacitors," *Chem. Mater.*, vol. 26, no. 11, pp. 3418–3426, 2014.

[75] A. G. Pandolfo and A. F. Hollenkamp, “Carbon properties and their role in supercapacitors,” *J. Power Sources*, vol. 157, no. 1, pp. 11–27, 2006.

[76] M. Noked, A. Soffer, and D. Aurbach, “The electrochemistry of activated carbonaceous materials: past, present, and future,” *J. Solid State Electrochem.*, vol. 15, no. 7–8, p. 1563, 2011.

[77] M. Noked, A. Soffer, and D. Aurbach, “The electrochemistry of activated carbonaceous materials: past, present, and future,” *J. Solid State Electrochem.*, vol. 15, no. 7–8, p. 1563, 2011.

[78] E. Frackowiak and F. Beguin, “Carbon materials for the electrochemical storage of energy in capacitors,” *Carbon N. Y.*, vol. 39, no. 6, pp. 937–950, 2001.

[79] T. Cottineau, M. Toupin, T. Delahaye *et al.*, “Nanostructured transition metal oxides for aqueous hybrid electrochemical supercapacitors,” *Appl. Phys. A*, vol. 82, no. 4, pp. 599–606, 2006.

[80] T. Otowa, R. Tanibata, and M. Itoh, “Production and adsorption characteristics of MAXSORB: high-surface-area active carbon,” *Gas Sep. Purif.*, vol. 7, no. 4, pp. 241–245, 1993.

[81] J. Laine and S. Yunes, “Effect of preperation method on the pore size distribution of AC from coconut shell,” *Carbon N. Y.*, vol. 30, no. 4, pp. 601–604, 1992.

[82] Z. Weng, Y. Su, D. Wang *et al.*, “Graphene–cellulose paper flexible supercapacitors,” *Adv. Energy Mater.*, vol. 1, no. 5, pp. 917–922, 2011.

[83] D. Yu and L. Dai, “Self-assembled graphene/carbon nanotube hybrid films for supercapacitors,” *J. Phys. Chem. Lett.*, vol. 1, no. 2, pp. 467–470, 2010.

[84] T. Brousse, D. Bélanger, and J. W. Long, “To be or not to be pseudocapacitive?,” *J. Electrochem. Soc.*, vol. 162, no. 5, p. A5185, 2015.

[85] X. Lang, A. Hirata, T. Fujita *et al.*, "Nanoporous metal/oxide hybrid electrodes for electrochemical supercapacitors," *Nat. Nanotechnol.*, vol. 6, no. 4, pp. 232–236, 2011.

[86] J. Du, G. Zhou, H. Zhang *et al.*, "Ultrathin porous NiCo2O4 nanosheet arrays on flexible carbon fabric for high-performance supercapacitors," *ACS Appl. Mater. Interfaces*, vol. 5, no. 15, pp. 7405–7409, 2013.

[87] J. Chen, J. Xu, S. Zhou *et al.*, "Facile and scalable fabrication of three-dimensional $Cu(OH)_2$ nanoporous nanorods for solid-state supercapacitors," *J. Mater. Chem. A*, vol. 3, no. 33, pp. 17385–17391, 2015.

[88] K. S. Ryu, K. M. Kim, N.-G. Park *et al.*, "Symmetric redox supercapacitor with conducting polyaniline electrodes," *J. Power Sources*, vol. 103, no. 2, pp. 305–309, 2002.

[89] E. Kemnitz, U. Groß, S. Rüdiger *et al.*, "Amorphous metal fluorides with extraordinary high surface areas," *Angew. Chemie Int. Ed.*, vol. 42, no. 35, pp. 4251–4254, 2003.

[90] C. N. R. Rao and K. P. R. Pisharody, "Transition metal sulfides," *Prog. Solid State Chem.*, vol. 10, pp. 207–270, 1976.

[91] R. Prins and M. E. Bussell, "Metal phosphides: preparation, characterization and catalytic reactivity," *Catal. Letters*, vol. 142, no. 12, pp. 1413–1436, 2012.

[92] A. F. Young, C. Sanloup, E. Gregoryanz *et al.*, "Synthesis of novel transition metal nitrides IrN_2 and OsN_2," *Phys. Rev. Lett.*, vol. 96, no. 15, p. 155501, 2006.

[93] T. Zhao, X. Peng, X. Zhao *et al.*, "Facile preparation and high capacitance performance of copper sulfide microspheres as supercapacitor electrode material," *Compos. Part B Eng.*, vol. 163, pp. 26–35, 2019.

[94] C. Shi, H. Dong, R. Zhu *et al.*, "An 'all-in-one' mesh-typed integrated energy unit for both photoelectric conversion and energy storage in uniform electrochemical system," *Nano Energy*, vol. 13, pp. 670–678, 2015.

[95] R. Mas-Balleste, C. Gomez-Navarro, J. Gomez-Herrero *et al.*, "2D materials: to graphene and beyond," *Nanoscale*, vol. 3, no. 1, pp. 20–30, 2011.

[96] M. Naguib, M. Kurtoglu, V. Presser *et al.*, "Two-dimensional nanocrystals produced by exfoliation of Ti_3AlC_2," *Adv. Mater.*, vol. 23, no. 37, pp. 4248–4253, 2011.

[97] M. Naguib, O. Mashtalir, J. Carle *et al.*, "Two-Dimensional Transition Metal Carbides," *ACS Nano*, vol. 6, no. 2, pp. 1322–1331, 2012.

[98] M. Naguib, V. N. Mochalin, M. W. Barsoum et al., "25th Anniversary Article: MXenes: A New Family of Two-Dimensional Materials," *Adv. Mater.*, vol. 26, no. 7, pp. 992–1005, 2014.

[99] M. Naguib, M. Kurtoglu, V. Presser *et al.* "Two-Dimensional Nanocrystals Produced by Exfoliation of Ti_3AlC_2," *Adv. Mater.*, vol. 23, no. 37, pp. 4248–4253, Oct. 2011.

[100] O. Mashtalir, M. Naguib, V.N. Mochalin *et al.*, "Intercalation and delamination of layered carbides and carbonitrides," *Nat. Commun.*, vol. 4, p. 1716, 2013.

[101] J. Come, P.Rozier, M.Naguib *et al.*, "A non-aqueous asymmetric cell with a Ti2C-based two-dimensional negative electrode," *J. Electrochem. Soc.*, vol. 159, no. 8, pp. A1368–A1373, 2012.

[102] M. Naguib, J.Come, B.Dyatkin *et al.*, "MXene: a promising transition metal carbide anode for lithium-ion batteries," *Electrochem. commun.*, vol. 16, no. 1, pp. 61–64, 2012.

[103] M. Lukatskaya, O. Mashtalir, C. Ren *et al.*, "Cation intercalation and high volumetric capacitance of two-dimensional titanium carbide," *science.sciencemag.org*, vol. 341, no. 6153, pp. 1502–5, 2013.

[104] Y. Guan, S.Jiang, Y.Cong *et al.*, "A hydrofluoric acid-free synthesis of 2D vanadium carbide (V_2C) MXene for supercapacitor electrodes," *2D Mater.*, vol. 7, no. 2, p. 25010, 2020.

[105] J. Xuan, Z.Wang, D.Liang *et al.*, "Organic-base-driven intercalation and delamination for the production of functionalized titanium carbide nanosheets with superior photothermal therapeutic performance," *Angew. Chemie*, vol. 128, no. 47, pp. 14789–14794, 2016.

[106] Y. Gogotsi, M. W. Barsoum, M. Ghidiu *et al.*, "Conductive two-dimensional titanium carbide 'clay' with high volumetric capacitance," *Nature*, vol. 516, no. 7529, pp. 1–9, 2014.

[107] Q. Jiang, N. Kurra, M. Alhabeb *et al.*, "All pseudocapacitive MXene-Ruo_2 asymmetric supercapacitors," *Adv. Energy Mater.*, vol. 8, no. 13, pp. 1703043, 2018.

[108] R. Syamsai and A. N. Grace, "Synthesis, properties and performance evaluation of vanadium carbide MXene as supercapacitor electrodes," *Ceram. Int.*, vol. 46, no. 4, pp. 5323–5330, 2020.

[109] Q. X. Xia, J. Fu, J. M. Yun *et al.*, "High volumetric energy density annealed-MXene-nickel oxide/MXene asymmetric supercapacitor," *Rsc Adv.*, vol. 7, no. 18, pp. 11000–11011, 2017.

[110] M. Fatima, J. Fatheema J, N. Monir *et al.*, "Nb-doped MXene with enhanced energy storage capacity and stability," *Front. Chem.*, vol. 8, pp. 168, 2020.

[111] L. Zhang, G. Yang, Z. Chen *et al.*, "MXene coupled with molybdenum dioxide nanoparticles as 2D-0D pseudocapacitive electrode for high performance flexible asymmetric micro-supercapacitors," *J. Mater.*, vol. 6, no. 1, pp. 138–144, 2020.

[112] J. Li, X. Cheng, J. Sun *et al.*, "based ultracapacitors with carbon nanotubes-graphene composites," *J. Appl. Phys.*, vol. 115, no. 16, pp. 164301, 2014.

[113] H. Xia, J. Feng, H. Wang et al., "MnO_2 nanotube and nanowire arrays by electrochemical deposition for supercapacitors," *J. Power Sources*, vol. 195, no. 13, pp. 4410–4413, 2010.

[114] Z. Lei, J. Zhang, and X. S. Zhao, "Ultrathin MnO_2 nanofibers grown on graphitic carbon spheres as high-performance asymmetric supercapacitor electrodes," *J. Mater. Chem.*, vol. 22, no. 1, pp. 153–160, 2012.

[115] Z. Lei, Z. Chen, and X. S. Zhao, "Growth of polyaniline on hollow carbon spheres for enhancing electrocapacitance," *J. Phys. Chem. C*, vol. 114, no. 46, pp. 19867–19874, 2010.

[116] L. Kou, T. Huang, B. Zheng *et al.*, "Coaxial wet-spun yarn supercapacitors for high-energy density and safe wearable electronics," *Nat. Commun.*, vol. 5, no. 1, pp. 1–10, 2014.

[117] K. Chi, J. Zhang, J. Xi *et al.*, "Freestanding graphene paper supported three-dimensional porous graphene–polyaniline nanocomposite synthesized by inkjet printing and in flexible all-solid-state supercapacitor," *ACS Appl. Mater. Interfaces*, vol. 6, no. 18, pp. 16312–16319, 2014.

[118] C. Zhang, B. Anasori, A. Seral-Ascaso *et al.*, "Transparent, flexible, and conductive 2D titanium carbide (MXene) films with high volumetric capacitance," *Adv. Mater.*, vol. 29, no. 36, pp. 1702678, 2017.

[119] N. Wang, J. Liu, Y. Zhao *et al.*, "Laser-cutting fabrication of MXene-based flexible micro-supercapacitors with high areal capacitance," *ChemNanoMat*, vol. 5, no. 5, pp. 658–665, 2019.

[120] L. Yu, Z. Fan, Y. Shao *et al.*, "Versatile N-doped MXene ink for printed electrochemical energy storage application," *Adv. Energy Mater.*, vol. 9, no. 34, pp. 1901839, 2019.

[121] C.-H. Mun, C. V. V. M. Gopi, R. Vinodh *et al.*, "Microflower-like nickel sulfide-lead sulfide hierarchical composites as binder-free electrodes for high-performance supercapacitors," *J. Energy Storage*, vol. 26, pp. 100925, 2019.

[122] P. Xu, J. Liu, P. Yan *et al.*, "Preparation of porous cadmium sulphide on nickel foam: a novel electrode material with excellent supercapacitor performance," *J. Mater. Chem. A*, vol. 4, no. 13, pp. 4920–4928, 2016.

[123] A. Moyseowicz, "Scalable one-pot synthesis of bismuth sulfide nanorods as an electrode active material for energy storage applications," *J. Solid State Electrochem.*, vol. 23, no. 4,

pp. 1191–1199, 2019.

[124] J. Zhu, Y. Xu, J. Wang *et al.*, "The effect of various electrolyte cations on electrochemical performance of polypyrrole/RGO based supercapacitors," *Phys. Chem. Chem. Phys.*, vol. 17, no. 43, pp. 28666–28673, 2015.

[125] H. Wu, X. Wang, L. Jiang *et al.*, "The effects of electrolyte on the supercapacitive performance of activated calcium carbide-derived carbon," *J. Power Sources*, vol. 226, pp. 202–209, 2013.

[126] Y. Wen, T.E. Rufford, X. Chen *et al.*, "Nitrogen-doped $Ti_3C_2T_x$ MXene electrodes for high-performance supercapacitors," *Nano Energy*, vol. 38, no. 17, pp. 368–376, 2017.

[127] J. K. McDonough, A.L. Frolov, V. Presser *et al.*, "Influence of the structure of carbon onions on their electrochemical performance in supercapacitor electrodes," *Carbon N. Y.*, vol. 50, no. 9, pp. 3298–3309, 2012.

[128] V. L. Pushparaj, M.M. Shaijumon, A. Kumar *et al.*, "Flexible energy storage devices based on nanocomposite paper," *Proc. Natl. Acad. Sci.*, vol. 104, no. 34, pp. 13574–13577, 2007.

[129] Q. Chen, X. Li, X. Zang *et al.*, "Effect of different gel electrolytes on graphene-based solid-state supercapacitors," *RSC Adv.*, vol. 4, no. 68, pp. 36253–36256, 2014.

[130] R. Paul and A. K. Roy, "BN-codoped CNT based nanoporous brushes for all-solid-state flexible supercapacitors at elevated temperatures," *Electrochim. Acta*, vol. 365, pp. 137345, 2021.

[131] Y. Li, Z. Kang, X. Yan *et al.*, "A three-dimensional reticulate CNT-aerogel for a high mechanical flexibility fiber supercapacitor," *Nanoscale*, vol. 10, no. 19, pp. 9360–9368, 2018.

[132] W. Zhou, K. Zhou, X. Liu *et al.*, "Flexible wire-like all-carbon supercapacitors based on porous core–shell carbon fibers," *J. Mater. Chem. A*, vol. 2, no. 20, pp. 7250–7255, 2014.

[133] J. Wang, Q. Zhang, X. Li *et al.*, “Smart construction of three-dimensional hierarchical tubular transition metal oxide core/shell heterostructures with high-capacity and long-cycle-life lithium storage,” *Nano Energy*, vol. 12, pp. 437–446, 2015.

[134] S.-L. Chou, J.-Z. Wang, H.-K. Liu *et al.*, “Electrochemical deposition of porous $Co(OH)_2$ nanoflake films on stainless steel mesh for flexible supercapacitors,” *J. Electrochem. Soc.*, vol. 155, no. 12, pp. A926, 2008.

[135] X. He, Y. Hu, H. Tian *et al.*, “In-situ growth of flexible 3D hollow tubular Cu_2S nanorods on Cu foam for high electrochemical performance supercapacitor,” *J. Mater.*, vol. 6, no. 1, pp. 192–199, 2020.

[136] R. N. Bulakhe, S. Sahoo, T. Nguyen *et al.*, “Chemical synthesis of 3D copper sulfide with different morphologies for high performance supercapacitors application,” *RSC Adv.*, vol. 6, no. 18, pp. 14844–14851, 2016.

[137] S. Jiang, X. Zhou, H. Xiao *et al.*, “Robust and durable flexible micro-supercapacitors enabled by graphene nanoscrolls,” *Chem. Eng. J.*, vol. 405, pp. 127009, 2021.

[138] Z. Niu, H. Dong, B. Zhu *et al.*, “Highly stretchable, integrated supercapacitors based on single-walled carbon nanotube films with continuous reticulate architecture,” *Adv. Mater.*, vol. 25, no. 7, pp. 1058–1064, 2013.

[139] H. Hu and T. Hua, “An easily manipulated protocol for patterning of MXenes on paper for planar micro-supercapacitors,” *J. Mater. Chem. A*, vol. 5, no. 37, pp. 19639–19648, 2017.

[140] M. Magnuson, J. Halim, and L.-Å. Näslund, “Chemical bonding in carbide MXene nanosheets,” *J. Electron Spectros. Relat. Phenomena*, vol. 224, pp. 27–32, 2018.

[141] M. Alhabeb, K. Maleski, B. Anasori *et al.*, “Guidelines for synthesis and processing of two-dimensional titanium carbide ($Ti_3C_2T_x$ MXene),” *Chem. Mater.*, vol. 29, no. 18, pp. 7633–7644, 2017.

[142] T. Hou, Z. Jia, B. Wang *et al.*, "MXene-based accordion 2D hybrid structure with Co_9S_8/C/$Ti_3C_2T_x$ as efficient electromagnetic wave absorber," *Chem. Eng. J.*, vol. 414, pp. 128875, 2021.

[143] Z. Li, L. Wang, D. Sun *et al.*, "Synthesis and thermal stability of two-dimensional carbide MXene Ti_3C_2," *Mater. Sci. Eng. B*, vol. 191, pp. 33–40, 2015.

[144] F. Zhuge, X. Li, X. Gao *et al.*, "Synthesis of stable amorphous Cu2S thin film by successive ion layer adsorption and reaction method," *Mater. Lett.*, vol. 63, no. 8, pp. 652–654, 2009.

[145] J. Kundu and D. Pradhan, "Controlled synthesis and catalytic activity of copper sulfide nanostructured assemblies with different morphologies," *ACS Appl. Mater. Interfaces*, vol. 6, no. 3, pp. 1823–1834, 2014.

[146] A. Lasia, "Electrochemical impedance spectroscopy and its applications," in *Modern aspects of electrochemistry*, Springer, 2002, pp. 143–248.

[147] U. Retter and H. Lohse, "Electrochemical impedance spectroscopy," in *Electroanalytical Methods*, Springer, 2010, pp. 159–177.

[148] R. Garg, A. Agarwal, and M. Agarwal, "A review on MXene for energy storage application: effect of interlayer distance," *Mater. Res. Express*, vol. 7, no. 2, pp. 22001, 2020.

[149] N. K. Chaudhari, H. Jin, B. Kim, D. S. Baek, S. H. Joo, and K. Lee, "MXene : An Emerging Two-Dimensional Material for Future Energy," *J. Mater. Chem. A Mater. energy Sustain.*, vol. 00, no. November, pp. 1–16, 2017.

[150] M. Okubo, A. Sugahara, S. Kajiyama *et al.*, "MXene as a Charge Storage Host," *Acc. Chem. Res.*, vol. 51, no. 3, pp. 591, 2018.

[151] C. Zhan, M. Naguib, M. Lukatskaya *et al.*, "Understanding the MXene pseudocapacitance," *J. Phys. Chem. Lett.*, vol. 9, no. 6, pp. 1223–1228, 2018.

[152] W. Jiang, X. Zou, H. Du *et al.*, "Universal descriptor for large-scale screening of high-

performance mxene-based materials for energy storage and conversion," *Chem. Mater.*, vol. 30, no. 8, pp. 2687–2693, 2018.

[153] Y. Xie, M. Naguib, V.N. Mochalin *et al.*, "Role of Surface Structure on Li-Ion Energy Storage Capacity of Two-Dimensional Transition-Metal Carbides," *J. Am. Chem. Soc.*, vol. 136, no. 17, pp. 6385–6394, 2014.

[154] W. Bao, L. Liu, C. Wang *et al.*, "Facile synthesis of crumpled nitrogen-doped MXene nanosheets as a new sulfur host for lithium–sulfur batteries," *Adv. Energy Mater.*, vol. 8, no. 13, pp. 1702485, 2018.

[155] X. Wang, S. Lin, H. Tong *et al.*, "Two-dimensional V_4C_3 MXene as high performance electrode materials for supercapacitors," *Electrochim. Acta*, vol. 307, pp. 414–421, 2019.

[156] A. R. Marlinda, N. Yusoff, A. Pandikumar *et al.*, "Tailoring morphological characteristics of zinc oxide using a one-step hydrothermal method for photoelectrochemical water splitting application," *Int. J. Hydrogen Energy*, vol. 44, no. 33, pp. 17535–17543, 2019.

[157] J. L. Hart, K. Hantanasirisakul, A. Lang *et al.*, "Control of MXenes' electronic properties through termination and intercalation," *Nat. Commun.*, vol. 10, no. 1, pp. 1–10, 2019.

[158] C. Eames and M. S. Islam, "Ion Intercalation into Two-Dimensional Transition-Metal Carbides: Global Screening for New High-Capacity Battery Materials," *J. Am. Chem. Soc.*, vol. 136, pp. 16270, 2014.

[159] G. Liang, X. Chen, D. Ren *et al.*, "Ion doping simultaneously increased the carrier density and modified the conduction type of Sb_2Se_3 thin films towards quasi-homojunction solar cell," *J. Mater.*, vol. 7, no. 6, pp. 1324-1334, 2021.